Titre: Title:	Development of Electrospun Mat for Antibacterial and Antiviral Air Filtration Mask Based on Cellulose Acetate
Auteur: Author:	Sheyda Kordjazi
Date:	2025
Type:	Mémoire ou thèse / Dissertation or Thesis
Référence: Citation:	Kordjazi, S. (2025). Development of Electrospun Mat for Antibacterial and Antiviral Air Filtration Mask Based on Cellulose Acetate [Thèse de doctorat, Polytechnique Montréal]. PolyPublie. https://publications.polymtl.ca/71458/

POLYTECHNIQUE MONTRÉAL

affiliée à l'Université de Montréal

Development of Electrospun Mat for Antibacterial and Antiviral Air Filtration Mask Based on Cellulose Acetate

SHEYDA KORDJAZI

Département de génie chimique

Thèse présentée en vue de l'obtention du diplôme de *Philosophiæ Doctor*

Génie chimique

Décembre 2025

POLYTECHNIQUE MONTRÉAL

affiliée à l'Université de Montréal

Cette thèse intitulée :

Development of Electrospun Mat for Antibacterial and Antiviral Air Filtration Mask Based on Cellulose Acetate

présentée par **Sheyda KORDJAZI**

en vue de l'obtention du diplôme de *Philosophiæ Doctor*

a été dûment acceptée par le jury d'examen constitué de :

Marie-Claude HEUZEY, présidente
Abdellah AJJI, membre et directeur de recherche
Nick VIRGILIO, membre
Hani NAGUIB, membre externe

DEDICATION

To the glory of God,

my beloved parents,

my beloved

husband, my

beloved sisters.

ACKNOWLEDGEMENTS

I would like to extend my deepest gratitude to my supervisor, Professor Abdellah Ajji, for his support and invaluable guidance throughout my research. It has been a true privilege to carry out my Ph.D. studies under his mentorship at Polytechnique Montréal. His expertise and insightful advice were crucial at every step of this work.

I also wish to express my gratitude to the members of my thesis committee, including Prof. Heuzey, Prof. Virgilio, and Prof. Naguib, for their thoughtful feedback and contributions, which significantly enhanced my research.

I would also like to thank to Mrs. Claire Cerclé and Mr. Matthieu Gautier, our lab managers, their assistance and dedication created a productive and motivating laboratory environment. Their commitment ensured I had all the resources needed to conduct my experiments efficiently.

I am especially thankful to my friends and colleagues Anahita, Mina, Aida, Emad, Mahdi, and Maryam. Their companionship, encouragement, and collaboration added great value to this journey and made it truly rewarding experience.

To my parents, I owe my deepest gratitude. Their unwavering love, sacrifices, and belief in me have been my greatest sources of strength and motivation.

Finally, I want to extend my deepest appreciation to my husband. His encouragement, and boundless support have been my anchors. This achievement would not have been possible without his enduring love and understanding.

RÉSUMÉ

Au cours de la dernière décennie, la demande en équipements de protection individuelle (EPI) s'est accrue de manière considérable, particulièrement à la suite des pandémies mondiales, en raison de leur rôle clé dans la limitation de la propagation des micro-organismes pathogènes. Parmi la diversité des EPI disponibles, gants, cagoules, visières ou encore combinaisons intégrales, le masque facial occupe une place de choix. Il constitue la première barrière face aux agents aéroportés et se trouve en contact direct avec le système respiratoire et la peau de l'utilisateur. Cette importance accrue s'accompagne d'un besoin urgent d'optimiser les matériaux de fabrication, afin qu'ils soient à la fois respectueux de l'environnement et efficaces contre bactéries et virus, même lors de temps de contact très courts. Par ailleurs, ces matériaux doivent préserver leurs performances physiques et fonctionnelles en conditions de forte humidité, garantissant ainsi une protection continue sur de longues périodes d'utilisation.

Cette présente étude vise à concevoir un système de filtration performant à partir de polymères biodégradables intégrant des agents antimicrobiens, dans le but de conférer une double activité antibactérienne et antivirale. L'objectif est de mettre au point des membranes hydrophiles mais résistantes à l'humidité, obtenues par électrofilage coaxial afin de produire des fibres à structure cœur/gaine. Deux agents antimicrobiens ont été associés pour générer un effet synergique, renforçant ainsi les propriétés protectrices et assurant une inactivation microbienne marquée dès les premiers instants de contact. Afin de prolonger l'efficacité et améliorer la stabilité, une huile essentielle a été encapsulée au cœur des fibres ainsi qu'au sein de nanotubes, permettant une libération progressive et maîtrisée. Cette stratégie ouvre des perspectives prometteuses pour la mise au point de membranes électrofilées de nouvelle génération destinées aux masques faciaux.

Dans un premier volet expérimental, l'électrofilage coaxial a permis de fabriquer des fibres cœur/gaine composées d'acétate de cellulose (CA) en gaine et de polycaprolactone (PCL) en cœur. Les paramètres clés, nature et proportion des solvants, concentration des polymères, débit d'injection et distance buse-collecteur, ont été étudiés pour optimiser la structure finale. Les observations au microscope électronique à transmission (MET) ont confirmé la formation de fibres homogènes et exemptes de perles dans certaines conditions précises, alors que d'autres paramètres menaient à des défauts. Le chlorure de cétylpyridinium (CPC), un ammonium quaternaire à propriétés antimicrobiennes, a été incorporé dans la fibre. Bien que la membrane ait démontré une

activité antibactérienne et antivirale, ses performances à très court temps de contact restaient perfectibles.

La seconde phase a consisté à intégrer l'huile essentielle d'eucalyptus (EEO) dans le cœur des fibres via électrofilage coaxial, tout en ajoutant le CPC dans la gaine. L'étude du profil de libération a montré que la structure cœur/gaine permettait de limiter le relargage initial et d'assurer une diffusion prolongée de l'EEO, l'enveloppe jouant un rôle de barrière. Les essais antimicrobiens ont mis en évidence qu'une combinaison EEO/CPC offrait une action plus rapide et plus efficace grâce à des mécanismes d'action complémentaires, confirmant l'intérêt d'une approche synergique.

Enfin, la troisième phase a exploité des nanotubes d'halloysite (HNTs) comme support d'encapsulation de l'EEO, afin de renforcer le contrôle de libération et d'allonger la durée de conservation. Une modification de surface par tensioactif anionique a permis d'augmenter la capacité de chargement. Les HNTs chargés en EEO ont ensuite été incorporés dans la solution d'électrofilage, donnant naissance à des fibres aux propriétés antimicrobiennes optimisées.

Dans l'ensemble, cette recherche propose une approche intégrée pour surmonter les principaux défis liés aux membranes antimicrobiennes pour masques faciaux : gonflement excessif en milieu humide, efficacité antimicrobienne lente, faibles performances mécaniques et libération brutale d'agents actifs comme les huiles essentielles. L'association de fibres cœur/gaine, de l'effet synergique de plusieurs agents antimicrobiens et de l'encapsulation d'huiles essentielles constitue une piste solide pour développer la prochaine génération de matériaux filtrants durables, réactifs et hautement protecteurs pour les EPI.

ABSTRACT

The demand for personal protective equipment (PPE) has increased in the recent decade, especially during and after global pandemics, as it is an effective means of preventing the spread of harmful microorganisms. Among different types of PPE, including gloves, hoods, eye shields, and full-body suits, face masks have received specific importance. Face masks act as the primary barrier against airborne pathogens and are in direct contact with the respiratory system and the skin of mask wearers. With the growing demand for face masks, there is a vital need to use materials in mask fabrication that are not only environmentally friendly but also active against bacteria and viruses within short contact times. Additionally, these products should maintain their physical and functional performance under high moisture conditions to ensure thoroughly protection during long term usage.

This study aims to develop an effective filtration system using biodegradable polymers incorporated with antimicrobial agents to provide both antibacterial and antiviral activity. The goal is to produce hydrophilic mats with resistance to moisture, employing coaxial electrospinning to fabricate core/shell fiber structures. Two antimicrobial agents were used to create a synergistic effect, thereby improving the protective properties of the material and ensuring significant microbial inactivation within short contact times. To further enhance stability and prolong antimicrobial activity, the essential oil was encapsulated within the core of the fiber and inside of nanotubes, creating controlled and sustained release of the agent. This strategy, suggest a promising approach to develop advanced electrospun mat for face mask applications.

In the first phase of this research, coaxial electrospinning method was employed to fabricate core/shell fibers by cellulose acetate (CA) as the shell and polycaprolactone (PCL) as the core. Different factors, including solvents, ratio of solvents, polymer concentrations, electrospinning parameter like flow rate and tip distance to collector were assessed to provide proper fabrication of the core/shell structure. Transmission Electron Microscope (TEM) analysis showed the successful fabrication of uniform and bead-free fibers using specific conditions, whereas alternative factors resulted in formation of defects or beaded fiber. Additionally, Cetylpyridinium chloride (CPC), a quaternary ammonium compound, was incorporated in the fiber as an antimicrobial agent. While the mat demonstrated antibacterial and antiviral activity, its activity under short contact times was not fully acceptable.

In the second phase of the study, eucalyptus essential oil (EEO) was incorporated into the fiber core via coaxial electrospinning, while CPC was embedded in the shell. The release behavior of EEO was evaluated in both single and coaxial fiber. The core/shell structure provided a more controllable release, effectively limiting the initial burst and ensuring sustained EEO release over an extended period. This behavior was attributed to the presence of shell as barrier in the structure of fibre. Moreover, antimicrobial testing confirmed that the combination of EEO and CPC resulted in rapid and more effective antibacterial and antiviral activity of the mat, owing to their different mechanisms of action against harmful microorganisms. This revealed the importance of synergistic effect for advanced protection.

In the third phase, halloysite nanotubes (HNTs) were employed as carrier for encapsulation of EEO to further controllable release and also prolonging storage time of final product. An anionic surfactant was used for surface modification of HNTs to enhance the EEO loading efficiency. EO-loaded HNTs were integrated into the electrospinning solution, resulting in fibers with antibacterial and antiviral activities.

Overall, this study demonstrates a comprehensive strategy to overcome obstacles in antimicrobial mat for face mask applications, including excessive swelling of fibers in high moisture condition, not rapid antimicrobial activity, poor mechanical properties of mat, and burst release of active agents such as EO. Core/shell fiber engineering, in combination with the synergistic activity of diverse antimicrobial agents and the encapsulation of EO, offers a promising approach to advance sustainable, fast-acting antimicrobial filtration materials for next-generation PPE.

TABLE OF CONTENTS

LIST OF TABLES

LIST OF FIGURES

LIST OF SYMBOLS AND ABBREVIATIONS

AC	Acetone
CA	Cellulose Acetate
CFU	Colony Forming Units
CPC	Cetylpyridinium Chloride
CTAB	Cetyltrimethylammonium Bromide
DMAc	Dimethylacetamide
DMF	Dimethylformamide
DSC	Differential Scanning Calorimetry
E. coli	Escherichia coli
EEO	Eucalyptus Essential Oil
EDX	Energy Dispersive X-ray Spectroscopy
EMEM	Eagle's Minimum Essential Medium
EO	Essential Oil
EtOH	Ethanol
FTIR	Fourier Transform Infrared Spectroscopy
HCoV-229E	Human Coronavirus 229E
HNT	Halloysite Nanotube
HCW	Healthcare workers
ISO	International Organization for Standardization
log CFU/disk	Logarithmic Colony-Forming Units per Disk
MRC-5	Medical Research Council cell strain 5
nm	Nanometer
PCL	Polycaprolactone
PBS	Phosphate Buffered Saline
PPE	Personal Protective Equipment
RH	Relative Humidity

S. aureus	Staphylococcus aureus
SDS	Sodium Dodecyl Sulfate
SEM	Scanning Electron Microscopy
$TCID_{50}$	Tissue Culture Infectious Dose (50%)
TGA	Thermogravimetric Analysis
UV	Ultraviolet

CHAPTER 1 INTRODUCTION

The demand for protective face masks has significantly increased in recent years, as they are recognized as an effective means of controlling infectious diseases transmitted through airborne particles, droplets, or microorganism-containing aerosols [1]. However, the massive fabrication of face masks increases concerns in three main aspects.

First, their environmental issues are significant, as face mask waste has negative impact on daily life of humans, animals, and aquatic organisms. Most facemasks are manufactured from synthetic polymers such as polyethylene (PE), polypropylene (PP), polyurethane (PU), polyacrylonitrile (PAN), polycarbonate (PC), polystyrene (PS), and polyester, which contributes substantially to plastic waste that is difficult to recycle and poses a significant environmental burden [1]. Second, the process for the fabrication of face masks consumes energy and release greenhouse gases into atmosphere. Additional energy is also needed for collecting, sorting, treating, and disposing of used face masks. Third, there is a socioeconomic issue, with increased costs and resources needed to manage PPE waste [2].

Face mask production in China increased to 110 million units per day in 2020 to provide rising demand [3, 4]. Therefor, the development of face masks requires strategic selection of materials and fabrication methods to achieve environmentally sustainable, highly effective protection against harmful microorganisms, while also enabling extended usage to decrease consumption and minimize waste. In general, face masks specifically surgical mask, consist of three layers [5], among these layers, the middle layer plays the most critical role in protective performance [6]. This layer is responsible for capturing particles and droplets containing microorganisms and preventing their transmission. Consequently, designing a middle layer with suitable hydrophilic properties can facilitate droplet absorption and improve filtration efficiency. In this study, particular attention is given to the development of an advanced middle filtration electrospun mat.

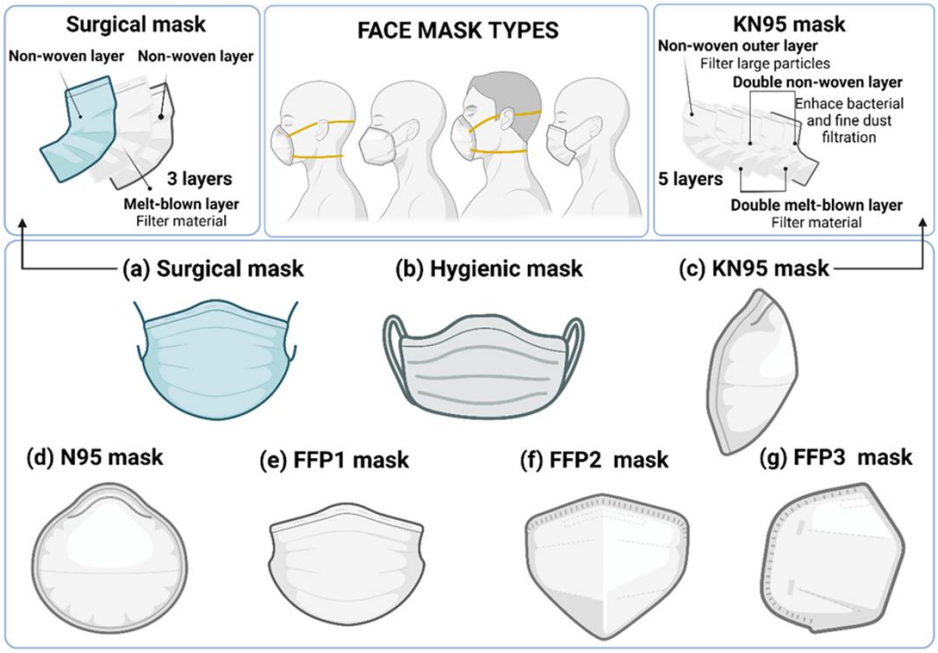

Figure 1.1 Different types of face masks commercially available worldwide: (a) surgical mask (three-layer structure depicted in upper left panel); (b) hygienic mask; (c) KN95 mask (five-layer structure depicted in upper right panel); (d) N95 mask; (e) FFP1 mask; (f) FFP2 mask; (g) FFP3 mask. Adapted with permission from [5].

Among the various fabrication methods used for face mask production, such as melt-blowing, spunbonding, and needleless processes [5], electrospinning has emerged as a promising technique for producing fibrous mats with high filtration performance. Nevertheless, few studies have investigated the deformation of fine hydrophilic fibers under high-humidity conditions, as encountered in face mask applications, where such deformation can reduce filtration performance. Furthermore, many studies have overlooked the integration of antimicrobial agents in the final products. For face mask applications, there is a crucial need to achieve rapid antimicrobial activity within short contact times, while maintaining prolonged effectiveness throughout use.

The aim of this study is to develop an electrospun mat based on biodegradable polymers that combines good mechanical strength, controlled swelling under high-humidity conditions similar to exhalation, maintained hydrophilicity, and high filtration performance. This study seeks to extend the functional lifespan of the product while achieving both rapid onset and sustained antimicrobial performance.

The first phase of the study focused on assessing the electrospinning of cellulose acetate (CA) and poly(ε-caprolactone) (PCL) through two methods of electrospinning, single and coaxial. Results

showed that incorporating PCL as a hydrophobic polymer in the fiber core was effective in controlling fiber swelling under high humidity, while simultaneously maintaining hydrophilic properties and enhancing the mechanical performance of the electrospun mat.

The second part of the study evaluated the antibacterial and antiviral properties of the mats by incorporating different antimicrobial agents, including quaternary ammonium compounds (QACs) and essential oils (EOs), and by examining the synergistic effects of combining both types of agents. In addition, the release behavior of EO from single and core/shell fibers was investigated.

The third part of the study focused on employing halloysite clay nanotubes (HNTs) as carriers for EEO, with emphasis on evaluating the influence of surface modification on enhancing loading efficiency. This approach aimed to maximize EEO encapsulation, promote supplementary release under high-moisture conditions, and achieve improved controlled release alongside extended storage stability.

This dissertation is structured as follows. Chapter 2 reviews the literature on mat fabrication methods for filtration, fiber swelling control, effective antibacterial and antiviral agents, and encapsulation techniques for sustained release. Chapter 3 outlines the main and specific research objectives, as well as the organization of the included research articles. Chapter 4 focuses on the fabrication of core–shell fibers using cellulose acetate as the shell and PCL as the core, along with an analysis of fiber formation parameters and the antimicrobial performance of QAC-incorporated mats. Chapter 5 investigates the synergistic effects of combining different antimicrobial agents, their release behavior in single and coaxial fiber configurations, and their overall performance. Chapter 6 describes the EO loading into HNTs, optimization of loading capacity, incorporation into electrospun fibers, and evaluation of release and antimicrobial activity. Chapter 7 presents a comprehensive discussion of all findings, highlights the originality of the work, and provides recommendations for future research.

CHAPTER 2 LITERATURE REVIEW

2.1 Protective Face Mask

The use of personal protective equipment (PPE) has been an important factor in preventing the spread of infectious diseases, particularly during global pandemics. During the initial stages of the COVID-19 pandemic, global shortages of personal protective equipment (PPE) contributed to elevated infection rates among healthcare workers Among the different kind of PPE, face masks have been determined as one of the most effective tools in controlling the transmission of airborne pathogens [7, 8]. Wearing face masks provides promising protection against respiratory viruses, including influenza and other aerosol-transmitted pathogens that threaten healthcare workers (HCWs) and the public [8-10].

2.1.1 Mechanisms of Particle Arrest and Filtration Spectrum

Air filtration happens through several mechanisms. Larger particles are effectively captured when their size exceeds the pore size of the filter. However, in the other scenario, where the particle size is less than the pore size, fibers can prevent particle movement through different ways. Here are the most important mechanisms for particle capture through fibers [11-13]:

(a) Direct interception: when particles approach the fiber, natural forces such as Van der Waal's forces cause them to adhere if the distance to the fiber surface is smaller than the particle radius.

The capture efficiency due to interception for $R < 0.2$ and $\alpha < 0.5$ is given by [12, 14]:

$$\eta_R = \frac{1-\alpha}{K}\left(\frac{R^2}{1+R}\right) \qquad Equation: (2.1)$$

where, α present the packing density or solidity, R is the interception parameter and K is the Kuwabara hydrodyna factor which is given by:

$$K = -\frac{1}{2}ln(\alpha) - 0.75 + \alpha - 41\alpha^2 \qquad Equation: (2.2)$$

(b) Inertial deposition: When suspended particles carried by the fluid are unable to follow airflow streamlines around stationary cylindrical fibers, they are deposited on the fibers as a result of their high momentum (c) Diffusion: Brownian motion of fluid results small particles under 0.5 μm to diffuse into fibers because of random collisions with other particles. Low flow velocity, fine particles, and high temperature are important for this phenomenon.

(d) Electrostatic deposition: according to electrostatic attraction, fibers and particles with different charges are attracted to each other. Particles ranging from 0.1 μm to 1 μm can be attached to the fiber by electrostatic force.

(e) Gravitational forces: without any interaction between fiber and particle, large particles can be easily filtered by gravity.

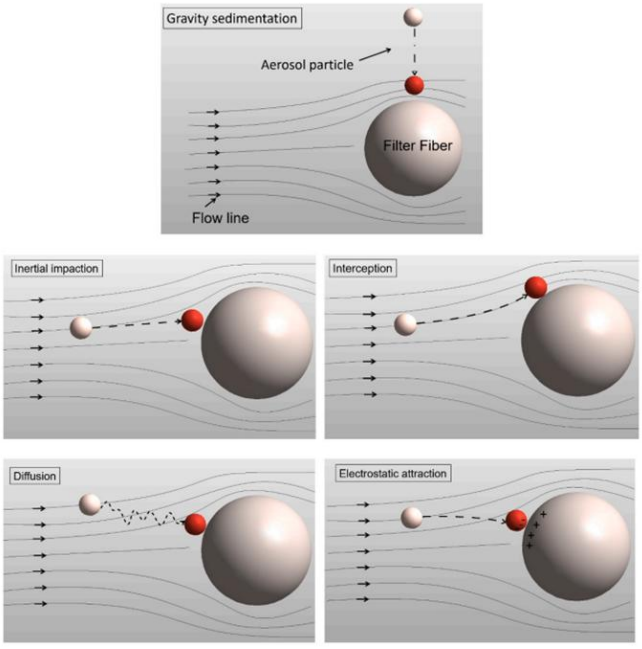

Figure 2.1 Particle arrest mechanisms. Adapted with permission from [13]

It is noticeable that in nonwoven fibrous filter mat, there is an opposite relationship between fiber diameter and total filtration efficiency. This relationship is shown by the following equation [15, 16]:

$$E = 1 - \exp\left(-4\eta \frac{\alpha}{1-\alpha} . \frac{Z}{\pi d_f}\right) \qquad Equation: (2.3)$$

where E demonstrates the total filtration efficiency, η is the single fiber efficiency, Z is the filter thickness, α is the packing density, and d_f is the fiber diameter. According to this equation, decreasing the fiber diameter increases the magnitude of the exponential term, as a result it enhances the filtration efficiency.

Additionally, smaller fiber diameters result in a greater surface area-to-volume ratio and reduced pore size, while fiber packing density is maintained, which significantly improves particle capture through mechanical mechanisms such as diffusion and direct interception. These effects are particularly important for the filtration of submicron and nanoscale particles. As a result, fabricating filters with finer fibers is an effective strategy to enhance performance.

2.2 Manufacturing Methods of Mask Filters

Non-woven mats generally provide higher filtration efficiencies compared to woven or knit fabrics because of their randomness and three-dimensional structure which provides larger thickness that increases the distance for the particle to travel. there is also the chance to have layered nonwoven structures [12, 17].

Melt blowing, spunbonding, and electrospinning are the major nonwoven fabrication method used to produce fine fibers that can be used for filter mat, barrier protection, and other applications.

In the melt-blowing process, a polymer or resin is melted and extruded through hundreds of fine nozzles [5]. A high-velocity air stream is used to collect fibers onto a moving conveyor, producing a nonwoven mat with randomly oriented fibers. This technique fabricates fine fibers with diameters of approximately 1–5 μm, providing to the formation of smaller pore sizes. [1, 12]. Materials such as polystyrene (PS), polycarbonate (PC), polyester, and polyethylene (PE) are suitable for this method [18].

In the spunbonding process, molten polymer is extruded and deposited onto a moving conveyor belt. The deposited fibers are subsequently bonded through thermal, chemical, or mechanical methods to fabricate a nonwoven fabric, which is then collected onto a reel [12]. This group of

nonwoven mat is composed of fibers in the range from 1 to 50 μm. Polymers like polypropylene (PP), polyester (PES), polyethylene (PE), and polyurethane (PU) can be processed using this technique, with isotactic polypropylene being the most commonly used material [1, 12].

In electrospinning an applied electric field, draw a polymer solution from a nozzle toward a grounded collector or plate. During this process, the polymer jet undergoes extensive stretching, providing the formation of nanofibrous nonwoven structures [19]. Specifically, in solution electrospinning method, polymers are dissolved in solvents before feeding to the syringe. When the polymer solution is exposed to an electric field, it creates a charged jet, causing the solvent to evaporate and electrospun fibres are formed [20]. This technique can be conducted at ambient temperature and standard atmospheric conditions, but humidity is an importance factor in this process [21]. Although solution electrospinning is a versatile fabrication technique, it is often not considered environmentally friendly because of using organic solvents that may be flammable, toxic, difficult to dispose of, or energy-intensive to produce. Consequently, the limited availability of acceptable solvents represents a key challenge for the industrial implementation of electrospun materials. To increase the environmental compatibility and scalability of electrospinning, significant efforts have considered for developing greener approaches, including the use of safer and more sustainable solvents. Most explored alternatives are water, ethanol, methanol, acetic acid, acetone, and dimethyl sulfoxide. Additionally, solvent-free methodologies, such as suspension electrospinning, provide fiber formation from polymer dispersions instead of dissolving polymers. These advances demonstrate ongoing progress toward more sustainable electrospinning processes suitable for applications such as filtration, drug delivery, and functional membranes [22].

Another important limitation of electrospinning associated to the process and scalability constraints. The technique needs high operating voltages, often affected by needle clogging, and offers limited control over fiber alignment and morphology [23, 24]. In addition, electrospinning method is largely dependent on the polymer solutions with specific electrical conductivity, as low conductivity can cause charge accumulation, causing jet instability and fiber breakage [25]. Moreover, the inherently low production rate of conventional electrospinning restricts its ability for large-scale industrial manufacturing. Although multi-needle systems can increase throughput, interactions between adjacent jets arising from non-uniform electric fields may adversely affect nanofiber quality [25].

Regarding fiber diameters produced by electrospinning, they are generally in the range of nanometer [1]. In this method, polymers which commonly used include poly(vinylpyrrolidone), poly (vinyl alcohol), polyacrylonitrile, and polystyrene, as well as biodegradable materials such as polycaprolactone (PCL) [5, 26].

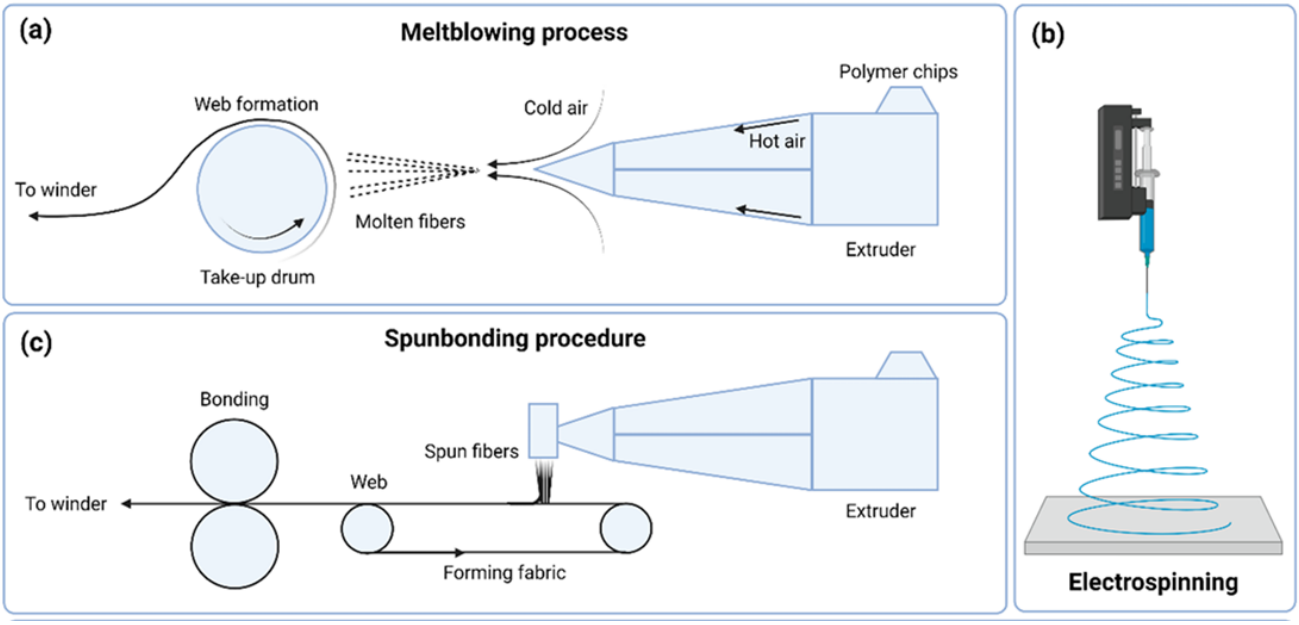

Figure 2.2 Schematic of the meltblowing (a), spunbonding, (b), electrospinning (c) Adapted with permission from [6]

Table 2.1 provides a list of fiber production methods that includes melt spinning, spunbonding, and electrospinning. These methods provide a wide range of fiber diameter, from the nanometer to micrometer range [12].

Table 2.1 Fiber production by melt blowing, spunbonding, and electrospinning methods

Factors	Meltblowing	Spunbonding	Electrospinning
Method	Molten thermoplastic resin blown through hundreds of small nozzles by high-velocity air from an extruder die [27]	Transmission of extruded molten polymer through spinneret via heated barrel and conveyor belt with rotating screw	Electrostatic force pulls charged polymer jet through nozzle during extrusion [28]
Bonding	Self-bonding of fabric web in an airborne state	Bonding via mechanical, chemical, or thermal processes	Post-processing thermal bonding for enhanced fiber strength [29]
Fiber diameter	Usually ranging from 1-5 µm	Usually ranging from 15- 50 µm	Usually ranging from 100 - 500 nm
Application	Applications of face masks and filters in Surgery, filtration, and clean rooms	Applications of disposable diapers and textiles in hygiene, filtration, and construction industries [30]	drug delivery, face masks, tissue engineering, protective textiles, and filtration. [31]

Among different methods of fiber fabrication, electrospinning is the preferred process for the fabrication of fine fiber for filtration mat due to several advantages. Firstly, the smaller fiber diameter of electrospun nanofibers provides a smaller pore size resulting in higher filtration efficiency for submicron particles. Secondly, because of low fiber diameter in electrospinning process, the minimum resistance to air occurs which leads to lower pressure drop and increased breathability of the face mask. Finally, the higher surface area of nanofibers fabricated in electrospinning, increases the chance of particle capture, making it a more effective choice for face mask filtration mat [32].

2.2.1 Electrospinning Materials Characteristics

Face masks are usually fabricated from plastic materials such as polyethylene and polypropylene, which are not biodegradable. This can lead to masks ending up in landfills or oceans, where they negatively affect the environment and human health by harming aquatic life and entering the food chain [32, 33].

In order to tackle the negative impact of masks made from non-biodegradable materials on the environment, scientists have investigated several eco-friendly alternatives. These options comprise both natural biodegradable materials, such as chitin, chitosan, cellulose, gelatin, silk fibroin, and synthetic biodegradable polymers, such as polyglycolide (PGA), poly(ε-caprolactone) (PCL), polyvinyl alcohol(PVA), PLA, and their copolymers P(LLA-CL). Developing masks using these biodegradable materials has been suggested as a viable solution to the problem of waste accumulation caused by non-biodegradable masks [34, 35].

The following table presents a brief overview of the latest studies on the production of air filter membrane using biodegradable polymers and the characteristics of these materials:

Table 2.2 Biodegradable polymers for filtration applications

Polymer	Method	Application	Ref
Cellulose acetate (CA)	Electrospinning	Suggesting as disposable masks	[36]
Gelatin (Gel)	Electrospinning	Filter media for aerosols and volatile organic	[37]
Silk Fibroin (SF)	Electrospinning	Filtration membrane	[38]
Polycaprolactone (PCL)	Electrospinning	Advanced face mask filters	[39]
Polyvinyl pyrrolidone (PVP) and polyvinyl alcohol (PVA)	Electrospinning	Antimicrobial face masks	[40]
Poly (lactic acid) (PLA)	Electrospinning	Mask filter	[41]
PolyvinylAlcohol/Water-Soluble Chitosan (PVA/WS-CS)	Needleless electrospinning	Antibacterial air filter	[42]
Quaternary ammonium chitosan/polyvinyl alcohol (HTCC/PVA)	Electrospinning	Antibacterial nanofiber membranes	[43]

2.2.2 Cellulose Acetate (CA)

Cellulose acetate (CA) is created through replacing some of the hydroxyl groups that exist in cellulose (Figure 2.3) [44]. This polymer has been specifically chosen for the filtration system due to its chemical resistance, stability, and ability to dissolve in organic solvents [45]. Moreover, CA shows strong hydrophilicity, biodegradability, and a high capacity for water absorption, making it

an appropriate polymer that can be used in various applications [46, 47]. The CA nanofibers produced by electrospinning method have a narrow distribution range, a fine fiber diameter, and a large surface area, which makes them an ideal material for efficient filtration [48]. However, pure CA nanofibers exhibit low tensile strength and Young's modulus, which can be significantly improved by blending with other polymers [49, 50].

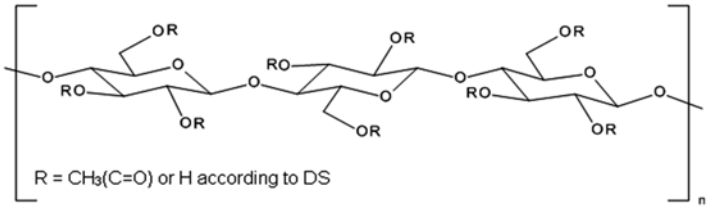

Figure 2.3 General structure of cellulose acetate (CA) [44]

In this study, in addition to the appropriate and desirable properties of cellulose acetate (CA), such as sustainability, cost-effective, biodegradability, and excellent electrospinnability with uniform fiber formation, CA was selected because of its intrinsic hydrophilicity. This characteristic makes CA a suitable option for fabricating hydrophilic electrospun mats with final application in the middle layer of facemasks, where efficient absorption of pathogen-containing droplets is needed to prevent microbial transmission. Furthermore, CA can be dissolved in a wide range of solvents, which desire for solution electrospinning method specifically coaxial electrospinnig. In fact, this solvent versatility facilitates matching solvent systems between the core and shell solutions, allowing stable formation of core–shell fiber structures.

2.2.3 Poly-ε-caprolactone (PCL)

PCL is a type of polyester which offers a partially crystalline structure. Its formation through Ring-Opening Polymerization (ROP) using "ε-caprolactone" as the monomer makes it an attractive material because of its affordability [51, 52]. It is highly versatile in processing methods because it can dissolve in a wide range of organic solvents PCL and its copolymers have exhibited their versatility through their effective utilization in various techniques such as electrospinning [53]. It has been approved by the Food and Drug Administration (FDA) and is widely used as a drug

delivery system. However, hydrophobicity of PCL can cause issues such as poor wettability. Despite this limitation, electrospun PCL fibers show excellent flexibility and mechanical strength, offering them highly appropriate for tissue engineering and regenerative medicine applications [54].

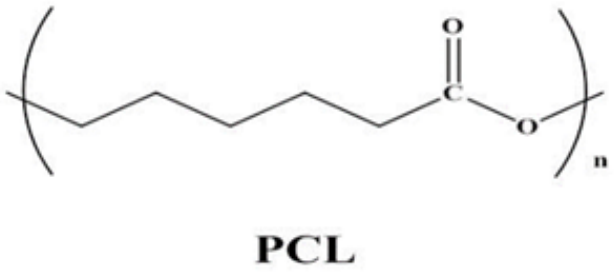

Figure 2.4 Figure 2.4 PCL polymer chemical structure [52]

As mentioned, PCL is a hydrophobic polymer; therefore, it can provide as an effective complementary material when combined with hydrophilic polymers such as CA to control excessive swelling under high-humidity conditions, specifically in facemask applications. During exhalation, humidity inside a face mask increases significantly; therefore, it is vital to provide conditions that control excessive swelling under such conditions. In addition, PCL exhibits good mechanical properties, including flexibility and tensile strength. This mechanical reinforcement improves structural integrity during handling and prolonged use, decreasing deformation and damage because of repeated mask contact and movement.

2.2.4 Swelling in Electrospun Structures

The selection of materials used in the production of air filtration membranes is significantly important. In some cases, the application of filtration mat is hindered due to the high hydrophilicity of the polymer, which decrease its performance in humid conditions. To solve this problem, different methods have been used to increase the moisture resistance of electrospun mats. These methods includes crosslinking with additives [55], incorporating far-infrared nanoparticles on the

surface of electrospun fibers to decrease moisture adsorption [56], and mixing hydrophobic and hydrophilic fibers and electrospinning these materials at the same time to maintain low pressure drop in high humidity conditions [57].

In a study by Wang et al., zein, a biopolymer derived from plant, was used to fabricate electrospun mats for air filtration systems [58]. The researchers understood that pure zein nanofibers showed poor moisture resistance in high humidity over prolonged time. As a result, the mat structure was clearly damaged because of swelling, causing a significant reduction in filtration performance. To resolve this issue, they applied a citric acid crosslinking system, which effectively decreased fiber swelling and promoted the structural integrity of the electrospun mat. This method significantly developed the stability of the filter under humid conditions to maintain filtration efficiency during longer period [58]. Figure 2.2 exhibits that in humid conditions, the particle filtration efficiency (PFE) of non-crosslinked fibers reduced to less than 20%, while the crosslinked mat showed around 10% reduction in filtration efficiency.

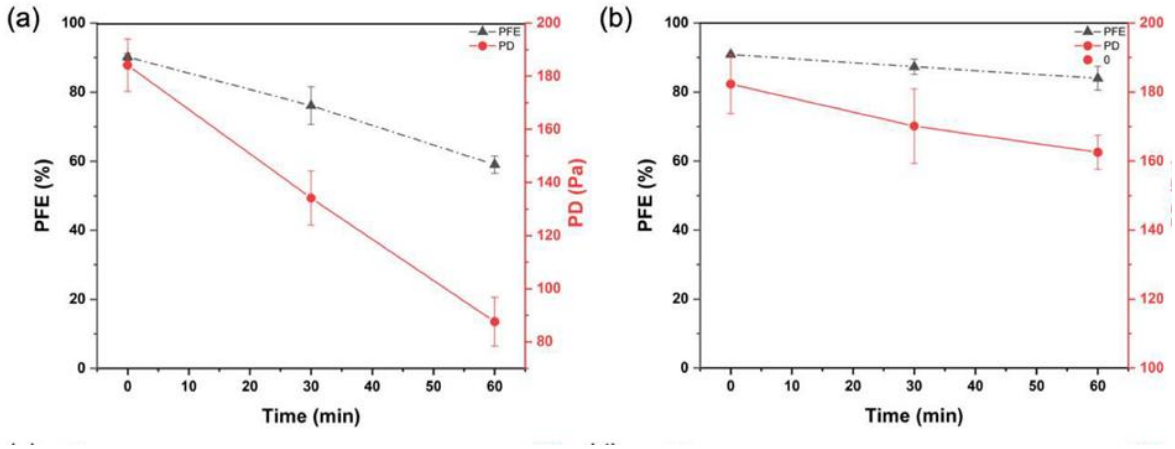

Figure 2.5 Particle filtration efficiency (PFE) and pressure drop (PD) of zein filters at 85% RH: (a) Non-crosslinked filter; (b) Crosslinked filter [58]

2.3 Antibacterial and Viral Activity

The air filters, particularly those fabricated through electrospinning, are highly effective in capturing specific types of particulate matter (PM). However, microorganisms such as bacteria,

viruses, and fungi present in the air can attach to the filter surface, remain alive, and even can replicate on the filtration mat. This issue causes a risk of secondary airborne contamination. This highlights the importance of fabricating air filter mats that have antimicrobial properties, particularly for safeguarding respiratory health using masks and indoor air filtration systems. In this field, various antimicrobial agents have been investigated for biocidal filters, including cationic ammonium compounds (QACs), natural products such as essential oils, metal–organic frameworks (MOFs), metal and metal oxide nanoparticles, as well as graphene and its derivatives [59]

.

2.4 Safety Considerations of Antiviral and Antibacterial Agents

The incorporation of antiviral and antibacterial agents, as well as nanoparticles, into materials has attracted significant attention because of the ability to improve protective performance. However, beyond providing antimicrobial efficacy, it is vital to consider the regulatory requirements and safety constraints related to these additives. This section discusses risk considerations associated with different antimicrobial agents and nanoparticles.

Among the antimicrobial agents one of the most commonly used in consumer and industrial products are quaternary ammonium compounds (QACs). This large group of chemicals has been widely applied for decades due to their antimicrobial, preservative, antistatic, and related functional properties. QACs are frequently found in cleaning and disinfection products, personal care formulations, and various durable consumer goods. The regulatory oversight of these compounds varies depending on their intended application, such as use in disinfectants, pesticides, or cosmetic products. Consequently, the same QAC may be evaluated under different regulatory frameworks and subjected to varying levels of scrutiny depending on the responsible authority [60]. For instance, in the European Union, certain QACs such as cetylpyridinium chloride (CPC) are regulated under the Cosmetics Regulation (EC). According to assessments by the Scientific Committee on Consumer Safety (SCCS), CPC is considered safe for use in cosmetic products at concentrations of up to 0.1 % in mouthwashes, up to 0.5 % in other oral hygiene cosmetic products, and up to 0.2 % in skin lotions and creams, reflecting regulatory measures designed to protect consumer health [61]. Despite their extensive use and documented release into the environment, many QACs have not been subject to comprehensive regulatory evaluation regarding their potential adverse effects on human health or ecosystems. Furthermore, key data required for robust risk

assessment, including information on production volumes, physicochemical characteristics, exposure pathways, and toxicity remain limited or unavailable for a significant number of these compounds [62].

Essential oils (EOs) represent another class of anti microbial agent that can be absorbed through different routes, such as inhalation, ingestion, massage, and topical application [63-65]. EOs have been used to relieve stress and in treatments for sleep disorders, Alzheimer's disease, cardiovascular conditions, cancer, and labor pain during pregnancy [64, 66-68]. However most essential oils are considered safe, some adverse effects have been reported, including pregnancy loss and abnormalities, neurotoxicity, bronchial hyperactivity, hepatotoxicity, prepubertal gynecomastia, and premature thelarche [64, 69, 70]. It is noticeable that cases of serious poisoning from essential oils are generally associated with oral ingestion of undiluted oil at doses much higher than therapeutic use. For example, wintergreen oil poisoning has been documented in adults, where survival was reported following ingestion of 6-24 mL, while fatal outcomes occurred after ingestion of 15-80 mL. Based on reported cases, average non-fatal doses were estimated at approximately 15.3 mL, whereas average fatal doses reached 41.7 mL, corresponding to an estimated median lethal dose of 0.2–0.6 mL kg^{-1} for adults of average body weight. In addition, eucalyptus oil ingestion has been reported to cause severe toxicity and is considered potentially fatal in humans at oral doses between 30 and 60 mL [71].

Within antimicrobial research, metallic nanoparticles represent one of the most extensively studied classes of nanoantimicrobial agents. In particular, metals such as silver (Ag), gold (Au), copper (Cu), zinc (Zn), and titanium (Ti) have attracted significant attention due to their intrinsic antimicrobial activity and their potential for use in a wide range of therapeutic and biomedical applications [72]. However, available reports indicate that the use of nanoparticles raises important safety concerns, as exposure has been associated with potential neurological and respiratory effects, circulatory disturbances, and other toxicological outcomes [73]. Nanoparticles of sufficiently small size can penetrate deeply into the pulmonary system and reach the alveolar region, where they interact closely with the alveolar epithelium. After deposition, these particles may traverse the air–blood–tissue barrier and gain access to the systemic circulation, allowing them to be transported to other organs throughout the body [74]. The toxicological behavior of nanoparticles is strongly influenced by their physicochemical characteristics, including particle size and surface area,

morphology and aspect ratio, surface coatings, crystalline structure, dissolution behavior, and their tendency to agglomerate [75]. For example, one study reported that the most pronounced cellular alterations occurred following exposure to 15 nm silver nanoparticles, which induced cell shrinkage and the presence of cellular debris in the culture medium. Cells treated with 30 nm silver nanoparticles exhibited abnormal morphology, with agglomerated particles observed both within and surrounding the cells. In contrast, exposure to 55 nm silver nanoparticles resulted in only minor morphological changes, indicating a clear size-dependent effect on cellular toxicity [76, 77]. Exposure thresholds for nanoparticles vary depending on particle size and other physicochemical factors. For example, to account for inhalation exposure, the U.S. National Institute for Occupational Safety and Health (NIOSH) has established size-dependent exposure limits for silver. For silver nanomaterials with primary particle sizes below 100 nm, NIOSH recommends an airborne respirable 8-hour time-weighted average (TWA) exposure limit of 0.9 µg m^{-3}. In contrast, a higher 8-hour TWA limit of 10 µg m^{-3} is maintained for total silver, including metallic dusts, fumes, and soluble silver compounds [78].

2.4.1 Quaternary Ammonium Compounds

Quaternary ammonium compounds (QAC) are positively charged surface-active chemicals commonly used in textile products for various purposes, including use as biocides, color treatment agents, conditioning agents, and finishing agents [79, 80]. The cationic sector of QACs includes a central nitrogen atom that is attached to four groups, which can have different structures. The negatively charged anionic part (X) is usually chlorine or bromine which forms a QAC salt when it is attached to nitrogen (Figure 2.4).

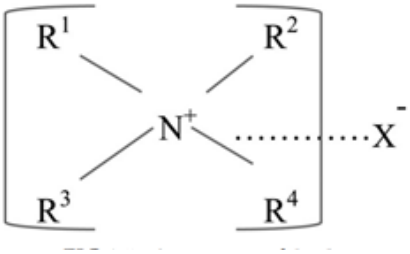

Figure 2.6 Basic structure of QACs [81]

QACs can be categorized according to the number of positively charged nitrogen centers in their molecular structure, including mono-QACs with a single nitrogen atom, bis-QACs with two, and multi- or poly-QACs containing multiple charged sites (Figure 2.5). These nitrogen parts may be incorporated into heterocyclic frameworks such as piperidine, pyridine, or imidazole. QAC molecules generally include one or more long hydrophobic alkyl chains, often including of ten or more carbon atoms. In bis-QAC, multi-QAC, and poly-QAC systems, the charged nitrogen groups are connected by a molecular spacer or linker, while the alkyl chains extending from the charged centers are identified as hydrophobic tails [82].

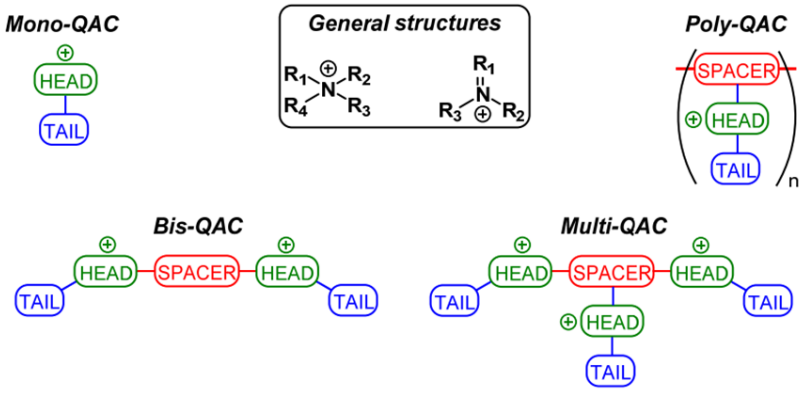

Figure 2.7 General structures and types of QACs [82]

In general, QACs containing two or more positively charged nitrogen parts (bis-QACs, multi-QACs, and poly-QACs) often provide stronger biocidal activity compared to the mono-QACs. Having an additional charged nitrogen can improve antimicrobial performance because of

increased electrostatic interactions with microbial membranes. However, increasing the number of positive charges is also increase the level of toxicity, particularly when additional alkyl chains are present [82]. Therefore, considering that low toxicity and safety are critical factors for applications involving direct human contact such as face mask, cetylpyridinium chloride (CPC) which is mono-QAC was selected in this study. Among pyridine-based quaternary ammonium compounds, CPC represents the simplest mono-QAC structure, featuring one pyridinium head group and a single C16 alkyl chain. CPC has been widely used in oral hygiene products, especially mouthwashes [83].

QACs are agents that affect membranes by interacting with the cytoplasmic membrane of bacteria and the plasma membrane of yeast. They can also attach to DNA and intracellular targets. QACs are effective against lipid-containing viruses, non-lipid-containing viruses, and spores, but this depends on how they are formulated. At low concentrations, they can prevent the growth of algae, bacteria, tuberculosis, spores, and fungi, but at higher concentrations, they can kill these microorganisms, depending on the particular organism and formulation [84]. At the first step of activity, the quaternary ammonium cation (QA^+), with Cl^- or Br^- as counterions, is electrostatically attracted to the negatively charged phospholipid components of the microbial cell membrane. This interaction disrupts the membrane's electrical balance, providing a net positive charge and causing structural alterations in the membrane of depolarized cells [85, 86]. The QA molecules displace stabilizing cations such as calcium and magnesium, which normally maintain membrane integrity, reducing membrane fluidity. Subsequently, the hydrophobic tails of the QA compounds penetrate the lipid bilayer and integrate into the membrane because of their favorable affinity for the hydrophobic interior. This insertion provides temporary pores or channels, rising membrane permeability and changing its physical structure. As a result, intracellular components which includes potassium ions, proteins, and nucleic acids, start to leak out, therefore disrupting the cell's biochemical activities and ultimately compromising cell viability [87-89]. In a research conducted by Chun-Chieh Tseng and colleagues, they investigated the role of GS5, a quaternary ammonium compound, as an antimicrobial agent when used in surgical mask filters [90]. The study showed that when the agent was coated onto the filter, GS5 provided prolonged protection against bacteria that settle or penetrate the mask filter. The results suggest that GS5 has potential to apply in surgical masks as a solution for combating infections caused by harmful organisms [90]. It is noticeable

that QAC also can be used as disinfectants in the food and medical industries, as well as in pharmaceutical products [91-93].

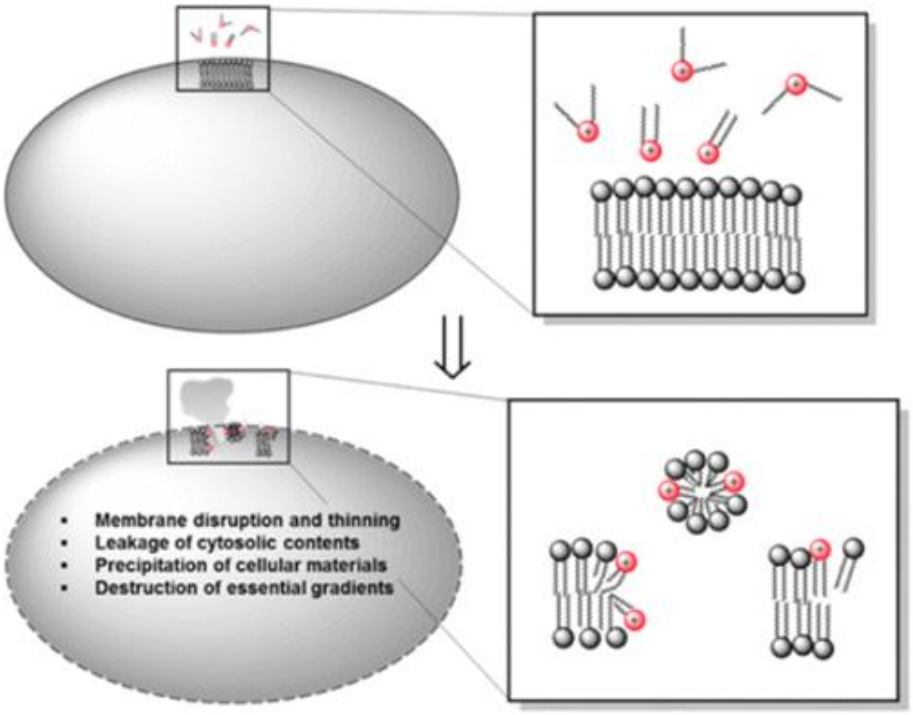

Figure 2.8 Mechanism of QAC action: Disrupts membrane integrity, causing leakage, content precipitation, and loss of essential gradients. Adapted with permission from [94]

QACs are valued for their low volatility and mild odor [95] which are suitable properties for a range of disinfection applications. QACs are also cost effective and easily accessible disinfectants material [96]. However, they require a longer contact time to effectively inactivate bacteria and viruses. The table below compares the key properties of various antimicrobial agents [1].

Table 2.3 Comparison of key properties of various antimicrobial agents (AMAs) for potential use in face masks

Antimicrobial Agent Group	Key Points
QAC	- Less effective and requires > 60 min contact time - Slightly corrosive and can induce skin irritation - Very few studies reported
N-halamine	- Broad-spectrum antimicrobial activity - 5 to 30 min contact time - Danger of leaching and biotoxicity - Potential AMA for face mask
Metal and metal oxides	- More popular and matured - Broad-spectrum antimicrobial activity - Leaching and nanotoxicity
Organic groups	- PEI, PPy → biocompatible - PEI → effective against airborne fungi and virus, potential AMA for face mask - BP → not evaluated for biocompatibility
HDP and Natural compound	- Higher contact time requires (1 to 24 h) - Biocompatible and eco-friendly face mask - No reported cytotoxicity and ecotoxicity
Miscellaneous	- Saline coatings → stable, biocompatible - Iodine → Commercialised but less antimicrobial activity - LIG → Excellent antimicrobial activity (in 10 min), potential AMA for face mask

In a study by Mona El-Deeb et al. [97], QAC was incorporated into the primer of a commercially available adhesive (OptiBond XTR), and its time-kill kinetics profile was investigated. The results demonstrated a reduction in the number of viable bacteria after 2 hours at all tested concentrations. The graph below confirms the low antimicrobial activity of QAC compounds when exposed to short contact times. additionally, a complete bacterial death was achieved after 10 h at QAC

concentrations equal to 3×MIC, and 4×MIC. Regarding 2×MIC, QAC demonstrated complete death at 12 h. (MIC: Minimum Inhibitory Concentration).

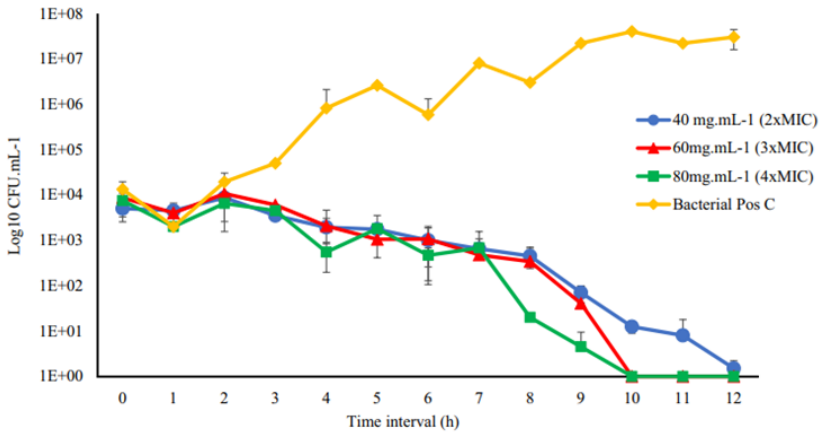

Figure 2.9 Kill kinetics of S. mutans treated with QAC at different concentrations [97]

2.4.2 Natural Extracts

Antimicrobial extracts derived from natural material have been widely investigated as potential antimicrobial agents for biomedical application. This is due to their high efficacy in combating with harmful microorganisms, being cost effective, and environmentally-friendly properties [98, 99]. In a study, Andrade et al. evaluated the antimicrobial activity of 27 essential oils through the agar dilution method and analyzed the minimal inhibitory concentrations ($MIC_{50\%}$ and $MIC_{90\%}$) against Staphylococcus aureus, Escherichia coli, and Pseudomonas aeruginosa strains [100]. The MIC was determined as $MIC_{90\%}$ for the tested bacterial strains (Table 2.4). The results demonstrated that Staphylococcus aureus strains were susceptible to a large number of essential oils. Among the 27 oils tested, eight showed considerable inhibitory activity, with MIC_{90} values below 0.30 mg/mL, such as eucalyptus, lemongrass, patchouli, black pepper, clary sage, tea tree, vetiver, and ylang-ylang [100].

Table 2.4 Minimal inhibitory concentration 50%(MIC50%) and 90%(MIC90%) (mg/mL) [100].

Essential oil	**S. aureus (n=11), CIM50%–CIM90%**	**E. coli (n=11), CIM50%–CIM90%**	**P. aeruginosa (n=10), CIM50%–CIM90%**
Bergamot (Citrus aurantium bergamia)	10.50–19.81	>26.13–>26.13	>26.13–>26.13
Black pepper (Piper nigrum)	0.21–0.21	>25.38–>25.38	>25.38–>25.38
Brazil's spearmint (Mentha arvensis)	1.90–2.26	5.52 -5.52	>25.47–>25.47
Cardamom (Elettaria cardamomum)	7.58–7.58	>26.07–>26.07	>26.07- >26.07
Cedar (Cedrus atlantica)	1.78–2.76	22.27–26.73	>26.73–>26.73
Cinnamon (Cinnamomum cassia)	1.00–1.14	2.00–2.00	25.00 – 30.0
Clary sage (Salvia sclarea)	0.29–0.29	>25.71–>25.71	>25.71–>25.71
Clove (Syzygium aromaticum)	0.67 -1.21	1.11–2.00	4.60–8.29
Copaiba (Copaifera officinalis)	24.07–26.52	>26.52–>26.52	>26.52–>26.52
Cypress (Cupressus sempervirens)	>25.2–>25.2	>25.20–>25.20	>25.20–>25.20
Eucalyptus (Eucalyptus globulus)	0.22–0.22	11.00–14.35	>26.49–>26.49
Fennel (Foeniculum vulgare)	7.81–7.81	13.08–20.22	>27.57–>27.57
Geranium (Pelargonium graveolens)	0.20- 0.31	3.90–4.24	>25.40–>25.40
Ginger (Zingiber officinalis)	3.23–4.93	>25.5–>25.5	>25.50–>25.50
Lavender (Lavandula officinalis officinalis)	2.37–4.27	21.3–25.59	>25.59–>25.59
Lemongrass (Cymbopogon schoenanthus)	0.15–0.22	1,98–2.10	>25.74–>25.74
Marjoram (Origanum majorana)	4.21–4.21	4.21–4.21	>25.23 ->25.23

Table 2.4 (continued) Minimal inhibitory concentration 50%(MIC50%) and 90%(MIC90%) (mg/mL) [100]

Essential oil	**S. aureus (n=11), CIM50%–CIM90%**	**E. coli (n=11), CIM50%–CIM90%**	**P. aeruginosa (n=10), CIM50%–CIM90%**
Nutmeg (Myristica fragans)	13.96–13.96	18.52–18.52	>26.67- >26.67
Orange (Citrus aurantium dulcis)	12.50–16.5	>24.63–>24.63	>24.63–>24.63
Palmarosa (Cymbopogon martinii)	0.48–0.59	1.90–2.09	>26.22- >26.22
Patchouli (Pogostemon patchouli)	0.25–0.25	>30.27–>30.27	>30.27–>30.27
Pine (Pinus sylvestris)	2.58–2.58	>26.22–>26.22	>26.22–>26.22
Rosemary (Rosmarinus officinallis)	6.40–7.26	17.70–22.12	>26.55–>26.55
Tahiti lime (Citrus limonum)	10.0–14.91	>25.2–>25.2	>25.2–>25.2
Tea tree (Melaleuca alternifolia)	0.21–0.21	4.29–4.29	>25.74–>25.74
Vetiver (Vetiveria zizanioides)	0.24–0.24	>29.31–>29.31	>29.31–>29.31
Ylang ylang (Cananga odorata)	0.23–0.23	>27.12–>27.12	>27.12–>27.12

Due to their hydrophobic nature, essential oils can interact with the lipid components of bacterial plasma membranes or mitochondrial membranes. This interaction damages membrane integrity and impairs function through increasing permeability, a phenomenon usually assessed by membrane electrical conductivity measurements [101, 102]. The antiviral effects of essential oils are commonly related to their capacity to disrupt the viral envelope and degrade the capsid or block the attachment of viruses to host cell receptors. Moreover, essential oils can promote their activity by interfering with the replication process of the virus [102].

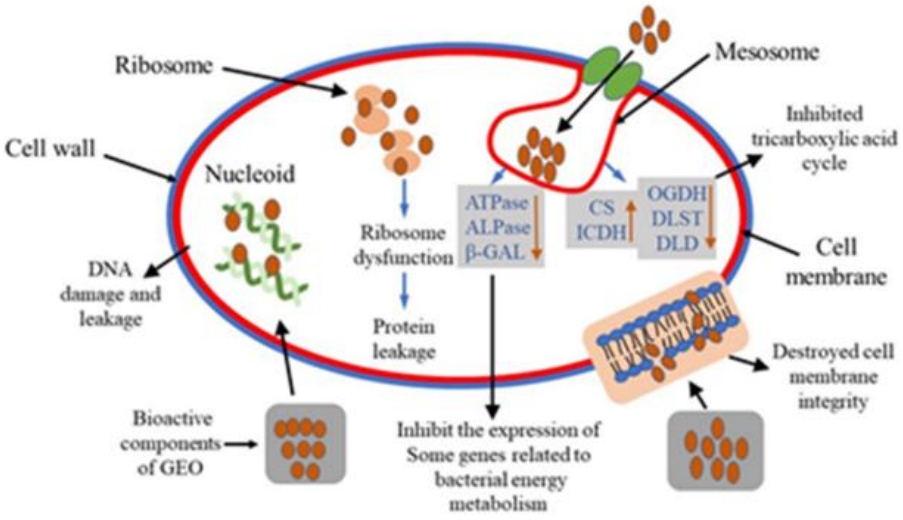

Figure 2.10 Possible antibacterial mechanism of action of essential oil [103]

2.5 Encapsulation of EO for Protection and Control Release

Essential oils (EOs) and some other bioactive compounds often show limited applicability because of their inherent instability. They usually degrade by oxidative reactions, hydrolysis, crystallization, and enzymatic activity, particularly during storage time or processing under specific conditions such as exposure to oxygen, light, or elevated temperatures [104, 105]. To overcome this issue, encapsulation techniques have been used to preserve and stabilize sensitive active agents. These systems are particularly designed to protect the chemical, physical, and biological integrity of the encapsulated materials and enabling their controlled release. Encapsulation not only improve the bioavailability of active compounds but also develop their functional performance in various applications [106].

2.5.1 Core-Shell Structure

Coaxial electrospinning is a method that differs from traditional electrospinning and involves the use of two nozzles attached to a high-voltage power supply [107]. This technique simultaneously pumps two distinct solutions, known as core and shell materials, to produce fibers that have a core-sheath structure. The core and shell solutions are kept separate until the final moment to prevent contact [108]. Many researchers use co-electrospinning for various applications because it enables

the encapsulation of non-spinnable materials such as powders, nanoparticle suspensions, proteins, essential oils, gelatin, and monomers within the nanofiber core or as a shell [109-112]. Core–shell nanofibers are designed to enclose one material within another. In fact, the inner core is surrounded by an outer shell layer. An important aim of this structure is its capability to ensure controlled release of encapsulated active agents [113].

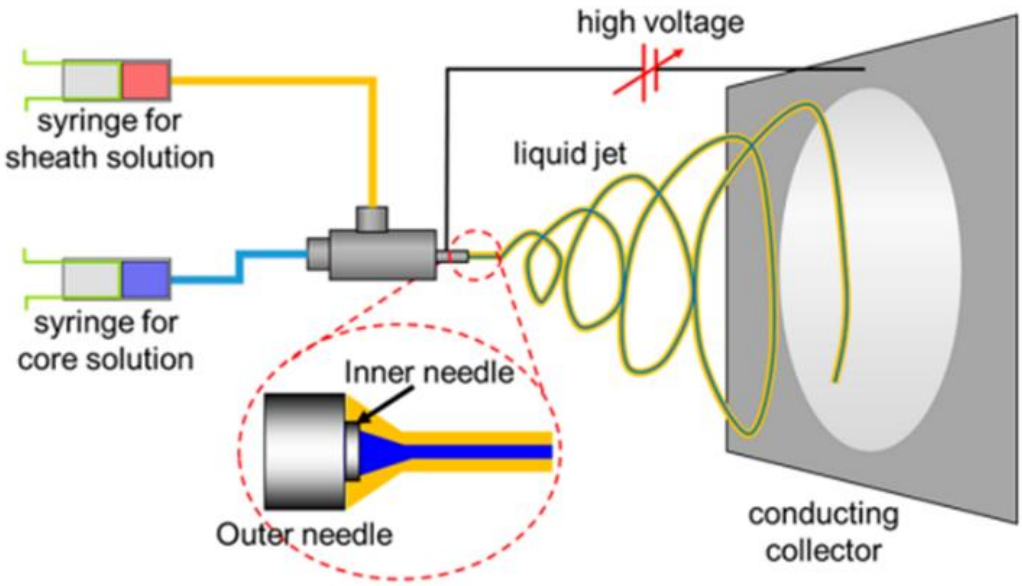

Figure 2.11 Diagram of coaxial electrospinning and resulting core- sheath fibers. Adapted with permission from [107]

Table 2.5 summarizes some studies that coaxial electrospinning has been used to fabricate core-shell nanofibers for the encapsulation of different cargos in biomedical applications. These studies highlight the importance of coaxial electrospinning in controlling release profile, ranging from burst-free to biphasic and triphasic profiles, by right selection of shell and core materials, providing applications such as drug delivery, tissue engineering, wound healing, and antimicrobial systems.

Table 2.5 examples of core–shell nanofibers fabricated by coaxial electrospinning for control release of cargo

Sheath material (shell)	**Core material (cargo)**	**Release behavior**	**Application**
poly-(3-hydroxy butyrate) (PHB)	Poly(DL-lacticacid) (PDLLA)/ dimethyloxalylglycine (DMOG)	Two-stage release kinetics	Drug delivery [114]
Polycaprolactone (PCL)	Lavender essentialoil (LO)	Long-term release	Air filtration [115]
Poly(L-lacticacid)(PLLA)	Tricalcium/phosphate nanoparticles/PLLA	Sustained, no burst	Bone tissue engineering [116]
Poly(lactic-co-glycolicacid)(PLGA)/ Metronidazole (MNA)	Naringin(NAR)/ polyvinylpyrrolidone(PVP)	Burst release	Tissue regeneration [117]
Gelatin	MNA/PCL	Biphasic	Tissue regeneration [118]
Cellulose acetate/ gelatin	Amoxicillin/Polyethylene glycol (PEG)	Controlled, prolonged release	Gastrointestinal delivery [119]
Nylon-6	Ampicillin/ Poly(methylmethacrylate)(PMMA)	Three-stage release	Antibacterial membranes [120]

Several studies have investigated the impact of processing parameters in coaxial electrospinning. For successful core-shell fiber formation, both core and shell polymer solutions should exceed the entanglement concentration (Ce) and provide minimum viscosity requirements. In fact, the viscosity of a solution is a critical factor that determines the size and shape of polymeric fibers during electrospinning. Studies indicate that if the viscosity is too low, fibers will not form continuously, while if it is too high, ejecting the polymer solution from the jets becomes challenging. Therefore, an ideal viscosity level is vital to optimize the electrospinning process. According to a study conducted by J.M. Deitzel and their colleagues, highly viscous polymer solutions have longer stress relaxation times, which may block jet fracturing in the process of electrospinning. Additionally, increasing the viscosity or concentration of the solution leads to the creation of larger and more uniformly sized fibers [121]. A stable coaxial electrospinning also

depends on an appropriate viscosity ratio (η core/η shell) to form a consistent Taylor cone and uniform fibers [122-124].

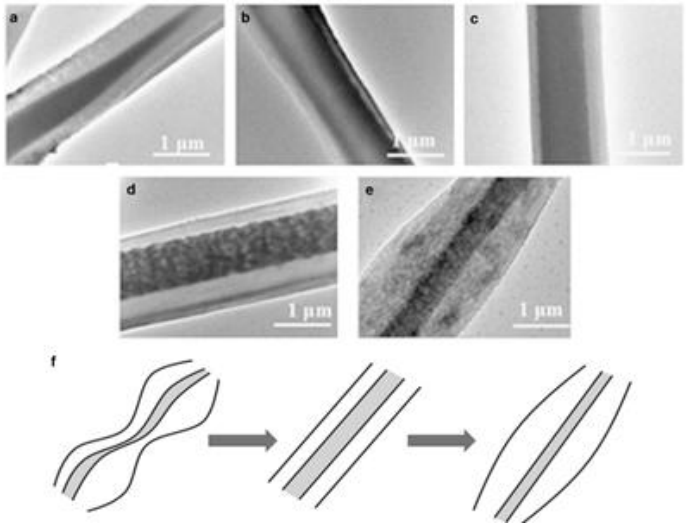

Figure 2.12 Transmission electron microscopy (TEM) images of electrospun PMMA/PAN core–shell nanofibers prepared with various viscosity ratios of shell/core: a) 0.67, b) 1.22, c) 1.81, d) 2.82, and e) 4.21. f) Schematic diagram of the core–shell morphology as the viscosity ratio increases. Adapted with permission from [125]

Moreover, solvent evaporation rate plays an important role in jet stability and fiber morphology. When solvent evaporation is too rapid, drying of the polymer solution can occur at the nozzle tip, destabilizing the Taylor cone and resulting in jet breakage or the formation of beaded fibers. In contrast, slow evaporation can prevent sufficient solidification before the fibers collection at the drum, resulting in wet or flattened fibers. Also, significant difference between the evaporation rates of the core and shell solutions can cause fiber collapse due to pressure imbalances. Therefore, investigating solvent evaporation is necessary for fabricating stable, high-quality core–shell nanofibers [126, 127].

Another method for encapsulation is emulsion-based systems that can effectively encapsulate, protect, and release a variety of valuable ingredients. This method generally composed of oil, surfactant/co-surfactant, and water, and can be categorized into two main types: oil in water (O/W) and water in oil (W/O) emulsions. In an O/W emulsion, the oil droplets are dispersed in the continuous water phase, while in a W/O emulsion, the aqueous droplets are dispersed in the oil

phase. The dispersed phase in an emulsion refers to the substance that makes up the droplets, while the continuous phase refers to the surrounding liquid substance [128]. A detailed mechanism is outlined to describe the impact of an emulsion on the electrospinning process, which involves several steps, such as stabilizing the droplet at the spinneret, deforming droplets caused by leaky dielectrics, and phase separation during jet thinning. The distribution of bioactive molecules within the fibers can be different based on the molecular weight of the molecules. For low molecular-weight applications, the molecules can be dispersed within the fibers, while for high molecular-weight applications, they can create a fibrous structure with a core-shell morphology [129-131].

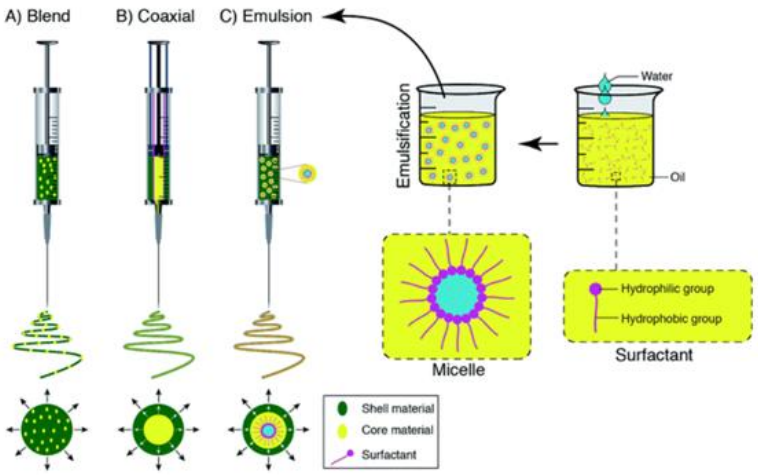

Figure 2.13 Schematic displays of the spinneret loaded with a bioactive agent for (A) blend, (B) coaxial, and (C) emulsion electrospinning [128].

2.5.2 Encapsulation Using Clay Nanotubes

Clay nanotubes have unique properties and wide range application due to their low cost, excellent physical and chemical characteristics, as well as availability in large quantities [132-134]. Halloysite structure is one of the most widely used kinds of clay nanotubes. Halloysite nanotubes (HNT) are cylindrical structures with a diameter of approximately 50 nanometers. They occur naturally and possess a hollow structure with both an outer surface and an inner lumen. The chemical composition of the outer surface and inner lumen is different, with common compositions including SiO_2 and Al_2O_3. Halloysite nanotubes can act as carriers for sensitive agents, which can be transported both internally and externally because of heir unique configuration [135].

As the use of halloysite nanotubes (HNTs) in biomedical applications is growing, investigating their nanotoxicity toward living systems has become significantly important. Most recent studies have focused on in vitro evaluations. For example, In a study, toxicity on human cells have demonstrated that cell viability remains relatively high, at approximately 70%, even after exposure to a high HNT concentrations (0.075 mg mL^{-1}) [136, 137]. In another study, Long et al. assessed cytotoxicity and demonstrated that HNTs, at concentrations up to 200 μg mL^{-1}, exhibited good biocompatibility and did not induce significant apoptosis in human umbilical vein endothelial cells (HUVECs) or human breast adenocarcinoma (MCF-7) cells. Furthermore, in vivo experiments using a zebrafish model revealed that HNTs at concentrations up to 25 mg mL^{-1} caused no significant acute toxicity or sublethal effects, including changes in survival rate [137].

In addition to halloysite nanotubes, other porous inorganic materials such as metal–organic frameworks (MOFs) and mesoporous silica nanoparticles have also been widely studied for encapsulation and drug delivery applications [138]. However, each of these materials presents specific benefits and limitations.

Metal–organic frameworks (MOFs) are an emerging group of hybrid porous materials including metal ions or clusters which is connected to organic linkers. Key properties of MOFs are well-defined pore structures, tunable composition and size, versatile surface functionality, high loading capacity, make them desirable candidates for drug delivery applications [139]. However, for biomedical and related uses, important challenges such as toxicological compatibility, biodegradability, and structural stability should be carefully considered and addressed [140].

Mesoporous silica nanoparticles (MSNs) are another promising candidate for encapsulation, recognized for their high surface area, large pore volume, and controllable particle size. However, more comprehensive toxicological investigations, specifically regarding toxicity associated with different particle sizes, are still required. Such studies are necessary to ensure the development of MSNs appropriate for biomedical applications without undesirable side effects [141].

2.5.3 Maximizing Guest Chemical Loading in Halloysite Lumen

Surface modification of halloysite nanotubes is generally used to improve their loading capacity, and can be achieved through different methods, including thermal calcination, acid etching, and organic decoration. Calcination can modify both the exterior wall and interior lumen of halloysite nanotubes, whereas selective modification of the lumen can be achieved through acid etching and organic decoration techniques [142].

The process of calcination on halloysite has been thoroughly investigated in research studies [143, 144]. Generally, as the temperature of calcination increases, there will be a sequence of changes in the structure and appearance of halloysite clay nanotubes. Below 400°C, the primary transformation of clay nanotubes is the elimination of interlayer/adsorbed water. Subsequently, calcination in temperature ranges of approximately 450-900°C leads to dehydroxylation and the creation of amorphous meta-halloysite, in which amorphous SiO_2 and Al_2O_3 are phase-separated [142].

A different approach to modify halloysite's surface involves acid etching, where medium-concentration sulfuric or hydrochloric acid is used at moderate temperatures (50-100°C) [145, 146]. The acid targets the alumina octahedron inside the lumen and dissolves Al^{3+} cations because the outer silica wall of the clay nanotubes is less reactive than alumina under acidic conditions. As Al^{3+} cations leach from the lumen, halloysite nanotubes can be converted into silicon-rich nanotubes while retaining their tubular shape [147, 148]. When the alumina octahedron is completely removed from the lumen, halloysite nanotubes can be converted into amorphous silica nanotubes. It has been found in some studies that complete removal of the alumina octahedron can cause the outer silica wall of clay nanotubes to break and collapse, producing porous amorphous silica nanorods [142, 146, 149].

Another method is grafting organic molecules with active hydroxyl groups to the surface of the clay lumen, resulting in the formation of organolumened clay nanotubes. Covalent bonds, such as Al-O-Si, Al-O-P, Al-O-C, or Al-O-B bonds, can be established between the organic molecules and the aluminum alcohol sites within the halloysite clay lumen through dehydration condensation [150, 151]. In addition to covalent bonding, the lumen of halloysite can also be decorated with organic molecules through non-covalent adsorption, for instance, the positively charged lumen of halloysite can electrostatically attract and adsorb anionic organic molecules [142].

In order to promote loading, Xing Xuteng investigated the potential of Halloysite nanotubes (HNTs) as a nanocontainer for 2-Mercaptobenzothiazole (MBT) by acid-treating the HNTs with H_2SO_4. The acid treatment caused the HNTs to expand in diameter and increased their specific surface area, making them more efficient at loading MBT. The loading capacity of acid-treated HNTs was about three times higher than that of untreated HNTs, while the release behavior was minimally affected. Overall, the study suggests that acid-treated HNTs have the potential to be used as effective nanocontainers for certain chemicals [152].

Another method to increase loading efficiency in halloysite nanotubes is by changing the surface functional groups of the lumen. This approach has been shown to tackle problems such as inefficient loading for hydrophobic or hydrophilic guest chemicals. By modifying the surface chemistry of the lumen, the affinity of halloysite nanotubes can be increased, improving their loading capacity. In addition, surface modification can also alter the release behavior of the loaded compound, allowing for more controlled and sustained release. Some of the techniques used for modifying the lumen surface of halloysite nanotubes include grafting organic molecules the lumen with organic molecules with anionic surfactants or cationic surfactants due to increasing loading efficiency for hydrophobic or hydrophilic guest chemicals respectively [142, 153, 154]. This method can increase loading for hydrophobic or hydrophilic guest chemicals. By modifying the surface chemistry of the lumen, the affinity of halloysite nanotubes can be increased which leads to improving their loading capacity [142, 153, 154].

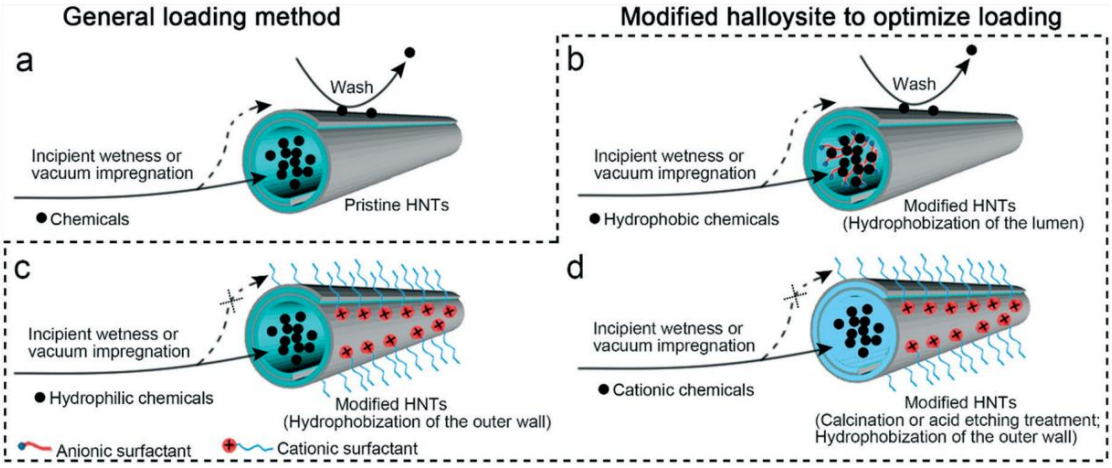

Figure 2.14 (a) The general method of loading the guest chemicals into the halloysite lumen. The optimized methods involve: (b) the hydrophobization of the lumen promotes the loading of hydrophobic chemicals; (c) the hydrophobization of the nanotube outer wall of the nanotubes ensures the site-oriented loading of hydrophilic chemicals; (d) the co-modification of the nanotube lumen and outer wall ensures the site-oriented loading of cationic chemicals. Adapted with permission from [155].

2.6 Problem Identification

As discussed in the previous sections, one of the limitations of current air filtration materials with hydrophilic properties is swelling of the mat under high humidity conditions, especially in face mask applications, where the filter is exposed to high levels of moisture because of exhalation. This issue causes significant filter ineffectiveness. To provide optimal air filtration, it is necessary that fiber swelling under moist conditions be controlled, and the mat maintain its structure.

Another critical challenge in developing effective mat for face mask is having active antimicrobial agents during usage of face mask. These agents must be active from the first minute of use and remain active throughout the duration of mask wear to prolong its protective function. While many studies focus only on the physical properties of filtration, the addition of antimicrobial agents is also necessary for pathogen inactivation, especially within a short contact time.

Quaternary ammonium compounds (QACs) are commonly used as antimicrobial agents. They are highly promising because of their wide antibacterial spectrum and low toxicity, making them appropriate agents for use in biomedical application [156]. For example, cetylpyridinium chloride

(CPC), a quaternary ammonium compound with surfactant properties, is considered safe for human use over a wide range of concentrations. It is commonly used in products such as mouthwashes, toothpastes, oral tablets, deodorants, and treatments in low concentrations ranging from 0.05 to 0.1% (0.5–1 mg/mL) [157, 158]. However, according to literature, they usually need prolonged contact times to be effective. In fact, this factor is a limitation for face mask applications where fast antimicrobial action is crucial to decrease the risk of transmission of harmful microorganisms to the wearer or surrounding individuals. Another candidate antimicrobial agent is essential oils (EOs), as natural antimicrobial agents, but they also have limitations since they are highly volatile and evaporate quickly from the product. Therefore, in order to have effective EOs, their release should be controlled during the entire period of mask use. Encapsulation techniques are a promising method to control EO release profiles in products.

A further research gap is the limited investigation into synergistic effects of incorporating two different types of antimicrobial agents with distinct structures and mechanisms against bacteria and virus. This approach can help achieving both fast and prolonged antimicrobial activity within the same filter material.

To address these issues, this study proposes the development of electrospun fiber mats with a specific structure that keeps hydrophilic properties to absorb user-generated droplets containing bacteria and viruses while controlling fiber swelling and improving mechanical properties. As a result, by absorbing droplets, the electrospun mat helps prevent the transmission of pathogenic microorganisms. Also, controlling fiber swelling provides the filtration efficiency and breathability to be maintained during use, as the structural integrity and pore size of the mat are not compromised by fiber swelling.

Additionally, the study aims to provide mats with sustained EO release and investigate the synergistic effect of QAC and EO incorporation in the mat to produce a filter that remains antimicrobial throughout its entire usage period.

CHAPTER 3 OBJECTIVES AND ORGANIZATION OF THE ARTICLES

3.1 General Objective

The main purpose of this study is:

To design a biodegradable electrospun mat exhibiting low fiber swelling, improved mechanical strength, and controllable release of active agents with synergistic antibacterial and antiviral effects for use in face mask applications

3.2 Specific Objectives

The three main objectives of this study were addressed through the following specific objectives:

- To develop and modify a core–shell biodegradable poly(ε-caprolactone) (PCL)/cellulose acetate (CA) mat using the coaxial electrospinning set up, with the goal of enhancing moisture resistance and mechanical properties.
- To incorporate antimicrobial agents into the electrospun fibers by adding quaternary ammonium compounds (QACs) and essential oils (EOs), and to assess their synergistic effects under different contact time as well as providing controllable release of EO through coaxial electrospinnig.
- To investigate the loading of essential oil into halloysite clay nanotubes (HNTs) to improve the controlled release performance of the active agent and to modify the HNTs using anionic surfactant to maximize loading efficiency.

3.3 Organization of Articles

This thesis comprises three research papers, which are presented as scientific contributions in Chapters 4, 5, and 6.

Chapter 4 presents the first study, titled “Biodegradable Electrospun Core–Sheath Nanofibers with Moisture Resistance Performance, Antibacterial and Antiviral Properties for Face Mask Application.” In this work, a biodegradable electrospun mat was developed using cellulose acetate

(CA) and poly(ε-caprolactone) (PCL) by coaxial electrospinning method. Core-shell fiber formation was characterized under different solvent systems, polymer concentrations, and processing conditions. The mechanical properties, wettability, and swelling behavior under high relative humidity (RH) were evaluated for different mats, including pure CA, pure PCL, a blend of CA and PCL, and a core–shell structure with CA as the shell and PCL as the core. Moreover, the antimicrobial activity of mat evaluated before and after adding CPC as antimicrobial agent.

Chapter 5 includes the second study, titled "Development of Electrospun Fibers Embedding Antimicrobial Compounds with Synergistic Effects for Rapid Action and Controlled Release." This research focused on incorporating two kinds of antibacterial and antiviral agents: quaternary ammonium compounds (QACs) and essential oils (EOs), into electrospun fibers. Their antibacterial and antiviral activity were assessed in different contact times. The study investigated how the core-shell fiber structure affects the release behavior of EOs in comparison to single electrospinning fibers (CA, PCL) and CA/PCL blends. Results demonstrated that combining EO with QAC significantly decreased the required contact time for effective antimicrobial action against both Gram-positive and Gram-negative bacteria, as well as viruses. Moreover, core–shell fibers showed better control over EO release compared to other fiber configurations.

Chapter 6 focuses on the third study, titled "Enhanced Stability and Controlled Release of Eucalyptus Essential Oil via Halloysite Nanotube Encapsulation in Electrospun Mats." This article investigated the loading of essential oil into halloysite clay nanotubes (HNTs) and explored surface modification approach to improve loading efficiency and increase dispersion stability of HNT in the solution by limiting sedimentation. The release behavior of the encapsulated EO was assessed after incorporation into nanotube in normal condition and high relative humidity.

CHAPTER 4 ARTICLE 1: BIODEGRADABLE ELECTROSPUN CORE-SHEATH NANOFIBERS WITH MOISTURE RESISTANCE PERFORMANCE, ANTIBACTERIAL AND ANTIVIRAL PROPERTIES FOR FACE MASK APPLICATION

Sheyda Kordjazi [a], Abdellah Ajji [a], Zahra Kordjazi [a]

[a] Department of Chemical Engineering, École Polytechnique de Montréal, Montréal, Québec H3T 1J4, Canada.

Submitted to Carbohydrate Polymers on October 6, 2025

4.1 Abstract

Growing use of personal protective equipment (PPE), particularly after the prevalence of pandemics in recent years, have had a negative impact on the environment. Biodegradable materials provide a promising approach to address these environmental issues. In this study, a biodegradable electrospun mat was developed using cellulose acetate (CA) and poly(ε-caprolactone) (PCL) polymers. To fabricate the mat, a coaxial electrospinning set up was used, and cetylpyridinium chloride (CPC) was incorporated to provide antibacterial and antiviral activity. The fabricated mats were characterized using SEM, TEM, TGA, tensile testing, contact angle measurements, etc. The results demonstrated that the core–shell structure of fibers provides enhanced mechanical properties for the mat and allows for more controlled fiber swelling under high-humidity conditions. The antibacterial properties were characterized against both Gram-positive and Gram-negative strains, showing antibacterial activity in the mats containing CPC. Antiviral test also confirmed that the mat can prevent the activity of the human coronavirus, however contact time is an important factor in the antimicrobial activity of the mats. Overall, the results demonstrated CA-PCL mat loaded CPC has the potential to be used as an efficient barrier for face mask application.

Keywords: Electrospun Mats, Biodegradable Polymers, Cetylpyridinium Chloride (CPC), Core–Shell Electrospinning, Antimicrobial Activity, Personal Protective Equipment (PPE)

4.2 Introduction

Over the last few decades, the emergence of pandemics has highlighted the importance role of Personal Protective Equipment (PPE), particularly face masks, as highly effective product to prevent and control infectious diseases [159]. However, the widespread use of face masks has caused an environmental concern because face masks are mainly produced using non-biodegradable materials [160]. As a result, research groups around the world are studied on design and material selection with the aim of fabricating masks that offer better performance than existing masks while reducing their detrimental environmental impact.

Recently, there has been a growing emphasis on using the electrospinning technique to create filters with high performance. This method make it easier to fabricate fibers with smaller diameters and higher surface areas, resulting in smaller pore sizes, which ensure more opportunities to trap particles, enhance filtration efficiency for submicron particles, and increase the ability to capture contaminants [161]. In addition, the fabricated mats through electrospinning show minimal air resistance because of the low fiber diameter and high porosity, resulting in a reduction in pressure drop and improvement in mask breathability. In addition, electrospun mats have low weight and high flexibility, providing more comfort for individual [32, 160, 162].

To resolve the negative environmental issue of non-biodegradable masks, scientists have investigated several alternatives. One way is using natural biodegradable materials, such as chitin, chitosan, cellulose, gelatin and silk fibroin, or synthetic biodegradable polymers like poly(ε-caprolactone) (PCL), polyvinyl alcohol(PVA), PLA and their copolymers P(LLA-CL) [34, 35, 163]. Ferreira and her colleagues, developed antibacterial face-mask filters by electrospinning method, using polycaprolactone (PCL) incorporated with magnesium oxide (MgO) and copper oxide (CuO) nanoparticles. The fabricated mat showed effective respiratory protection and enhanced antibacterial activity against E. coli and S. aureus [39]. İrem Yağmur Mol et al. fabricated antibacterial cellulose acetate (CA) nanofibers in their study [164]. They fabricated CA/zinc oxide (ZnO) composite nanofibers via electrospinning, resulting in thin, uniform and beadless fibers in the range of 354–464 nm. Their results confirmed that fiber diameter, air permeability, and water vapor permeability increased with increasing ZnO concentration. In another study, K. Geetha and colleagues employed two types of biodegradable polymers, PVP and PVA, along with ZnO

nanoparticles, to create cost-effective and highly durable nanofibers ZnO/PVA/PVP composite mats through electrospinning [40]. These mats were developed to use as an effective face masks filtering both particulate matter and microbial contaminants.

Among these various biodegradable polymers, cellulose acetate (CA) is a potential candidate for face mask applications due to water resistance, non-toxicity, stability, high water absorption capacity, and ability to dissolve well in organic solvents, which is preferable for solution electrospinning [46, 48, 50]. In addition, The nanofibers produced from CA have a narrow distribution range, a fine fiber diameter, and a large surface area, which makes them an ideal material for effective filtration [48]. However, there are some issues that limit the use of cellulose acetate for the desire face mask applications. One of them is the limited mechanical properties of electrospun CA mats restricts their potential use in various fields, particularly for face masks [165, 166]. Pure CA nanofibers have low tensile strength and Young's modulus, but these limitations can be developed by combining them with another polymer [49, 50]. Additionally, the high hydrophilicity of CA can cause high swelling in the electrospun fiber during the usage of face masks because of the high humidity from exhalation. This swelling effect on pore size in the mat and can impact negatively in the breathability of the mask [167].

Another promising candidate polymer for filtration applications is synthetic PCL. This is mainly because of its cost-effectiveness, biocompatibility, biodegradability, wide accessibility, good mechanical properties, and its effective application in various fabrication methods, such as electrospinning [26, 168, 169]. However, the semi-crystalline and hydrophobic nature of PCL causing in poor wettability and can lead to issues in face mask applications. It has been shown that absorbent materials (not in the outer layer) that can capture mucosal or salivary droplets from the user can reduce microbial transmission and increase the efficiency of the face mask [170].

For the fabrication of mat, the coaxial electrospinning method has obtained considerable attention due to the ability of combining different materials in the fiber to modify and develop the fiber properties [109]. Coaxial electrospinning is a method that is similar to the traditional electrospinning in basic roles but including two nozzles connected to to a high-voltage power supply. This method simultaneously pumps two different solutions (core and shell materials) to fabricate fibers that have a core-shell configuration [171]. There are different factors that can impact the development and optimization of coaxial electrospinning such as nozzle geometry [124,

172], viscosity ratio of the solutions [122, 124], solvent evaporation rates [126, 127], and electrical properties of the solution [124, 173].

In addition to inherent filtration capacity of the face masks that effectively block and trap microorganism, small particles and salivary droplets, incorporating antimicrobial agents can significantly improve its overall effectiveness. Various antimicrobial agents have been employed to provide antimicrobial activity for the mat such as cationic ammonium compounds [90], natural products [174], metal-organic frameworks (MOFs) [175], metal and metal oxide nanoparticles [176], graphene [177], and its derivatives [170]. Quaternary ammonium compounds (QAC) are a kind of positively charged surface-active material which the cationic component consists of a central nitrogen atom attached to four groups, each of which can exhibit distinct structures [178]. The negatively charged anionic portion is usually chlorine or bromine, creating a QAC salt upon bonding with nitrogen. The categorization of QACs is determined by the characteristics of their alkyl groups such as the number of nitrogen atoms, the presence of aromatic groups, and the number of carbon chain branching [81]. QACs are substances that affect membranes by interacting with the cytoplasmic membrane of bacteria [84, 179]. In fact, the positively charged QAC interacts with the bacterial membrane, which carries a natural negative charge due to its composition of lipoteichoic acid (LTA) in Gram-positive and lipopolysaccharides (LPS) in Gram-negative bacteria. Subsequently, the hydrophobic tail integrates into the lipid membrane and disrupts its structure [83, 179, 180].

Cetylpyridinium chloride (CPC) is a type of the quaternary ammonium compounds with antibactericidal effects, known for its surfactant properties that are safe for human use across a wide range of concentrations [83, 90, 181].

The main objective of this study is to develop a biodegradable electrospun mat through the coaxial electrospinning method for face mask applications, with the ability to absorb saliva droplets containing contaminants to prevent microbial transmission, while also able to control high swelling under high-humidity conditions.

The initial phase of the article related to producing PCL-CA (core-sheath fibers) with the incorporation of CPC in the shell layer, along with fabricating single PCL and CA electrospun fibers, and a blend of CA and PCL. Consequently, the morphology of the produced fibers was

investigated by SEM and TEM. The mechanical performance, wettability, degree of swelling, and antibacterial and antiviral properties of the electrospun mat also were assessed.

4.3 Experimental

4.3.1 Materials

CA with average molecular weight of 30,000 g/mol and PCL (molecular weight of 80,000 g/mol), chloroform (CHL), dimethyl formamide (DMF), acetone 99.9 %, N,N-Dimethylacetamide (DMAC), methanol, dioxene and Cetylpyridinium chloride (CPC powder) were provided by Sigma Aldrich. Beef extract powder, peptone powder, minimum essential medium eagle (EMEM), and fetal bovine serum (FBS) were all purchased from Sigma (Canada, ON).

4.3.2 Preparation of Polymer Solutions for Single and Blend Electrospinning

The PCL polymer solution was prepared using a mix of CHF/DMF in a 4:1 (v:v) ratio. Initially, PCL was dissolved in CHF solvent and stirred at 35°C. After 3 hours, DMF was added to the solution, and stirring overnight continuously. Regarding the cellulose acetate (CA) solution, it was dissolved in a mixture of acetone and DMAC in a 2:1 (v:v) ratio. This mixture was placed at laboratory magnetic stirrer in room temperature. The concentrations of PCL and CA in single electrospinning method were in the range of 10-15% w/v and 14-20% w/v, respectively. To prepare the blend of CA and PCL, PCL was dissolved in a DMF/CHF mixture (1:9 (v:v)), while CA was dissolved in an acetone/DMF mixture (2:1 (v:v)). The final blend ratio of CA to PCL was fixed to 1:1 (v:v).

4.3.3 Preparation of Polymer Solutions for Coaxial Electrospinning

All polymer solutions were freshly prepared within 24 hours before electrospinning process. In coaxial electrospinning method, the concentration range considered for CA was 14-20% w/v, and for PCL polymer was 10-20% w/v. The type of solvent and solvent content in this study is summarized in Table 4.1. The incorporation of CPC into the mats was achieved by adding it into the CA solution (shell solution) at a concentration of 0.5% respect to polymer.

Table 4.1 Summary of core and shell solution compositions

Solvent mixtures	Volume ratio (v:v)	Concentration (w/v)	Polymer	Core/Shell Assignment
Acetone:DMAC	3:2	14-18%	CA	Shell
Acetone:DMAC	7:3	10-20%	PCL	Core
Chloroform:methanol	9:1	10-20%	PCL	Core
Aceton:dioxane	1:2	14-18%	CA	Shell

4.3.4 Electrospinning

Electrospinning was conducted by a vertical electrospinning setup (Tong Li Tech Co., Ltd., Shenzhen, China) which was equipped with an adjustable high-voltage DC power supply and a programmable syringe pump. CA and PCL solutions were transferred into 10 mL plastic syringes and placed on the pump. For coaxial electrospinning the syringes were connected by plastic tubes to the inlets of a coaxial spinneret. Solutions for electrospinning were injected at controlled flow rates and conditions as outlined in Table 4.2.

Table 4.2 Processing parameters used to produce electrospun membranes

Operating parameters	Parameter Operation value
CA solution concentration	14-18% w/v
PCL solution concentration	10-20% w/v
Single solution flow rate	0.8-1.5 ml/h
Shell flow rate	0.5-1 ml/h
Core flow rate	0.5-1 ml/h
Spinning distance	12-25 cm
Voltage applied	15-25 kV
needle gauge	15-22

4.3.5 Morphology Characterization

To characterize the surface morphology of the electrospun nanofibers, a high-resolution microscope (Hitachi TM3030Plus) was employed, operated at 15 kV. Samples were prepared through cutting co-electrospun mats collected on aluminum foil for 2 hours and then the mat was attached to carbon tape. The determination of fiber diameters was conducted using ImageJ processing software. At least 200 fibers from three images of each electrospun mat were assessed to assess the average diameter.

The core-shell structure of the fabricated fiber was characterized using JEOL JEM-F200 transmission electron microscope (TEM). To prepare the TEM samples, electrospun fibers were directly fabricated to a TEM copper mesh during around 3-second electrospinning process.

4.3.6 Solvent Extraction Analysis

To assess fiber configuration, CA/PCL (mixed) and CA-PCL (core-shell) mats were placed in acetone container for 10 hours. The remaining fibers after exposure were then characterized using

Scanning Electron Microscopy (SEM) to assess the breakdown or structural integrity of the fiber structure.

4.3.7 Rheological Measurements

To gain knowledge of their flow behavior in the needles during the electrospinning process, the dynamic and steady shear rheological behavior of the solutions were measured at 25 °C at shear rates ranging from 0.01 to 700 s^{-1} using a stress-controlled rheometer Physica MCR 501 rheometer (Anton Paar, Canada) equipped with a concentric cylinder geometry. To limit solvent evaporation at the sample surface, a small amount of acetone was applied, this amount was negligible compared with the sample volume.

4.3.8 Solvents Properties and Boiling Point Determinations

To determine the evaporation rate, the boiling points of the solvent mixtures were measured using reference tables [182] and Raoult's law. Based on simple Raoult's Law, the total vapor pressure of each solvent combination was calculated. According to Raoult's law, the partial pressure of a component in a vapor mixture at equilibrium with its liquid mixture is assessed by multiplying the vapor pressure of the pure component by its mole fraction in the liquid phase [183].

$$P_{mix} = (P_A X_A + P_B X_B) \qquad Equation(4.1)$$

Where P_{mix} is the total vapour pressure of solvent combination, P_A and P_B show the vapour pressures of the individual components, and X indicate the molar fraction of the respective components [184]. Based on the formula, the boiling point of the mixture was estimated for each corresponding volume fraction.

4.3.9 Thermal Analysis

For the determination of polymer percentage in the fiber, the thermal degradation behavior of the electrospun fiber mats was investigated using a thermogravimetric analyzer (TGA Instruments Q-500, USA) under a nitrogen atmosphere with a flow rate of 50 mL/min. Samples of electrospun mats were weighed (typically more than 5 mg) and subjected to heating from room temperature to 600°C at a consistent heating rate of 20 °C/min. The weight loss of pure CA and PCL, as well as PCL-CA (core-shell) and CA/CPC in the nanofibers, was determined through the first-order derivative from the weight loss thermograms.

4.3.10 Mechanical Properties

The tensile strength and elongation at break of CA, PCL, CA/PCL (blend), and CA-PCL (core-shell) mats were characterized using an Instron Model 3000 (UK). Mats were cut into rectangular strips with the dimension of 4 cm in length and 2 cm in width, and average thickness was approximately ≈ 0.11 mm. These strips were loaded into the tensile test instrument. Stiffness was determined from the slope of the tensile strength (N) versus extension (%) in the linear region of the curve. The breaking point was determined on the load-extension results. Each experiment was conducted three times for each mat, and the average values were considered.

4.3.11 Wettability and Degree of Swelling

To evaluate surface hydrophilicity or hydrophobicity of mat surface, water contact angle measurements were done using an FDS Contact Angle System OCA. For assessing the mat's wettability through sessile drop measurement, droplets of 10 μL of deionized water (H_2O) were used. Deionized water was chosen rather than the other solvents to better represent the high-humidity conditions during face mask use.

Each type of sample underwent 5 tests, with recording angles immediately after contact of the drop with the surface of mats.

The degree of swelling (DS) in the mats was assessed by measuring the sample weights before and after exposure to 95% relative humidity (RH) and a temperature of 35°C (defined as the average temperature of exhaled air) [185]. For the DS calculation, based on the weight change over a 4-hour period (recommended maximum time for mask use) [174], was performed using Equation (1) and reported as a percentage:

$$DS = \frac{(Wwet - W\ dry)}{W\ dry} * 100\% \qquad Equation\ (4.2)$$

4.3.12 Antibacterial Activity

The antibacterial test was carried out based on the ISO 20743:2021 guidelines (Textiles-Determination of the antibacterial activity of textile products). This ISO standard evaluates the antibacterial activity of textile-like fibrous materials in direct contact with bacteria, which aligns withassessing the antibacterial performance of the electrospun mat for face mask applications.

Two types of bacteria, gram-positive (S. aureus) and gram-negative (E. coli), were employed to assess the antibacterial activity of the CA-CPC mat. The electrospun mats, both containing CPC and without CPC, were placed under vacuum condition to provide complete solvent evaporation. The mats were then cut into rectangular shape and before starting the test, the samples were sterilized through UV light and immersed in bacterial solution.

To prepare the bacterial solution (S. aureus and E. coli), 5 µL of bacteria, which had been kept at -80°C, were added to 5 mL of LB medium and incubated at 200 rpm and 37°C for 18 hours. The bacterial solution was adjusted to a concentration of 3-5 × 10^8 CFU/mL by a spectrophotometer instrument. Nutrient broth (NB), according to ISO instructions, was used for dilution to achieve final concentrations of 10^5 CFU/mL. Then, 5 µL of the prepared bacterial inoculum was placed onto the sample surface at various points, and 5 mL of NB (involved dissolving 3.0 g of meat extract and 5.0 g of peptone in 1000 ml of Milli-Q water and then adjusting the pH to range between

6.8 and 7.2) was added to the vials containing the CA and CA-CPC samples. Both vials, along with control samples, were incubated for 24 hours at 37°C and 90% relative humidity.

After the incubation period, 500 µL of the solutions in the vials were mixed with 9.5 mL of Neutralizing Broth (D/E). The vials were then thoroughly shaken using a vortex mixer. Serial dilutions were conducted by adding 100 µL of the solution from previous steps into 900 µL of phosphate-buffered saline (PBS). finally, 100 µL of the diluted solution disperse on agar plate and incubated for 24 h at 37 °C. Antibacterial values were calculated by counting bacterial colonies in Petri dishes.

The bacterial viability was determined by spreading and incubating 100 µl of the diluted samples on solid agar plates, allowing them to incubate overnight at 37°C, and counting the resulting colony formations [186]. The experiment was repeated three times, and the average values were reported.

4.3.13 Antiviral Tests

The antiviral test was conducted with following the ISO 18184:2019 protocol entitled “Textiles-Determination of the Antiviral Activity of Textile Products”. The method used in this study is the Median Tissue Culture Infectious Dose ($TCID_{50}$) technique [187]. The antiviral activity of the samples was characterized using the human coronavirus 229E and the human MRC-5 cell line. Each sample was cut into 3×3 cm dimensions and put into a tube. Then, 100 µl of virus with a concentration of 3×10^5 $TCID_{50}$/ml was poured onto the sample. The samples were incubated in two different contact time, for 30 minutes and 2 hours at 25°C. At the end of the incubation time, 5 ml of neutralizing solution was added to the tube and vortexed for 5 seconds. The resulting solution was performed serially diluted with EMEM by a factor of 10. From each diluted sample, 100 µl was added to a 96-well plate. The 96-well plate contained MRC-5 cells with a confluency of around 60% and was repeated 4 times. After a 1-hour incubation at 35°C under 5% CO2, the virus solution was removed, and the cells were washed with PBS. At the end, 100 µl of EMEM supplemented with 2% FBS was added to the infected cells. The cells were incubated at 37°C for 5 days until cytopathic effects were observed using a microscope. The $TCID_{50}$ values were calculated [186].

According to the standard 18184:2019 [187], the antiviral activity (Mv) is the reduction in infectivity titer value and is calculated as follows:

$$Mv = Log\frac{Va}{Vc} = Log\ Va - Log\ Vc \qquad Equation\ (4.3)$$

Where log (Va) represents the common logarithmic average of three infectivity titer values right after the control sample inoculation. Log (Vc) refers to the common logarithmic average of three infectivity titer values after a 2-hour contact with the tested samples. Strong antiviral activity is indicated by a value of $3.0 > Mv \geq 2.0$.

The experiment was repeated three times, and the average values were reported.

4.4 Results and Discussion

Samples from each experimental run were assessed using SEM (Fig 4.1) and characterize based on their fiber morphology and spinnability.

Figure 4.1 shows SEM images, and Figure 4.2 indicates diameter histograms of optimum condition for bead-free nanofibers produced by single electrospinning of CA and PCL and mix of CA and PCL (CA/PCL), as well as coaxial electrospinning (CA-PCL).

For single electrospinning, successful formation of CA fibers was achieved using a 20% CA solution in an Acetone:DMAC (2:1) solvent mixture (run 3), with a high voltage of 18 kV and a 12 cm distance between the needle and the collector. The mean diameter of the CA nanofibers produced under these optimal conditions was 748 nm. Results demonstrated that, in 17 % and 15% CA concentration (run 2 and 1, respectively), the entanglement of polymer chains during spinning was insufficient. This finding was qualitatively identified from electrospinning behavior and fiber morphology, since insufficient chain entanglement caused unstable jets and the formation of highly beaded mat with very fine fibers connecting the beads.

The electro spinnability and fiber structure of the single PCL, were evaluated at two concentrations (run 4,5), 10% and 15%, of PCL in a DMF: CHF mixture (1:9), using a voltage of 15 kV and a 20 cm distance between the needle and collector. In this case, a greater distance between the needle and the collector was required to ensure complete solvent evaporation and proper fiber formation. PCL fibers fabricated at the 15% (w/v) concentration were more uniform, with an average diameter of 880 nm. At lower concentration, the unstable and non-uniform jet formation resulted in the formation of beaded fibers on the collector.

For the coaxial electrospinning, the solvent and concentration that used for the single CA and PCL were (run 6) in the first attempt. However, no fiber formation happened in this case. So, in the next try (run 7), the same polymer concentrations were used, using different solvents, Aceton:dioxane (1:2) for CA and CHF: methanol (9:1) for PCL. In this condition, solution jets exhibited blocking and clogging behavior at the tip of the spinneret, limiting fiber formation. The lower boiling point of the core solution compared to the shell solution caused clogging, as further explained in the boiling point characterization section.

In runs 8, 9, and 10, the same solvent, Acetone:DMAC (3:2), was used for both core and shell solutions, and the effect of the core-shell solution concentration was assessed. According to the results, in runs 8 and 10, no fibers were fabricated due to insufficient viscosity in the shell solution compared to the core solution. In run 9, the observed bubbling structures in the fiber occurred by the fact that the shell material allowed the core PCL to flow out of the spinneret in larger amounts periodically. The viscosity of the shell solution was not sufficient to overcome the viscosity of the core solution. This will be discussed further in the viscosity measurement section.

Optimum condition in the coaxial setup happened in run 11 and CA-PCL structure revealed a uniform distribution of fibers by using 17% CA in Aceton:DMAC (3:2) and 14% PCL in Acetone:DMAC (7:3), with an applied voltage of 15 kV. The average diameter was 792 nm.

For the CA/PCL blend with a 1:1 ratio, the optimal conditions for fabricating uniform, bead-free fibers were found to be 14% PCL in a DMF:CHF (1:9) mixture and 17% CA in an acetone:DMF (1:1) mixture (run 13). These conditions were achieved by applying a 12 kV voltage and maintaining a 12 cm distance between the tip and the collector in the electrospinning setup. The average diameter was 932 nm. The lower concentration of polymer in this blend (run 12, with 15% for CA and 10% for PCL) was insufficient for the entanglement required for fiber fabrication.

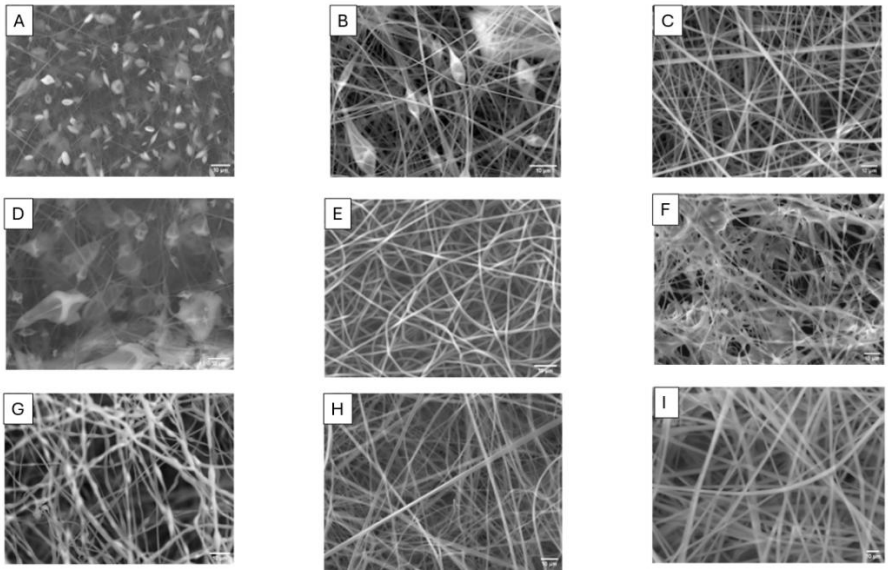

Figure 4.1 Scanning electron micrographs of single and coaxial fibers based on table 3: (A) run order 1, (B) run order 2, (c) run order 3, (D) run order 4, (E) run order 5, (F) run order8, (G) run order 9, (H) run order 11, (I) run order 13

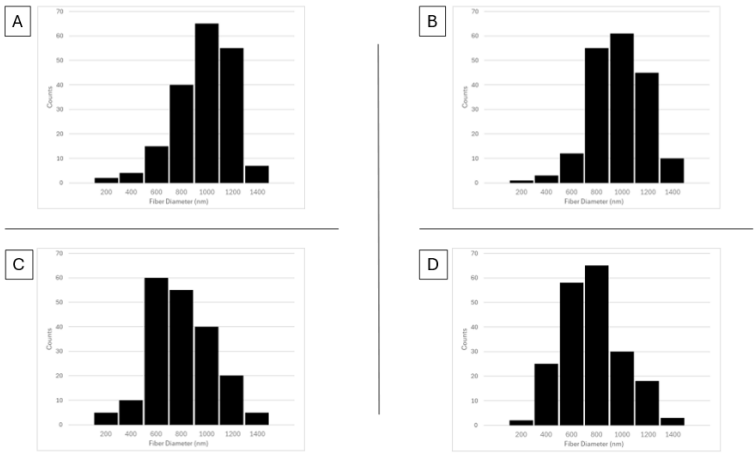

Figure 4.2 Diameter histogram of fibers: (A) run order 3, (B) run order 5, (C) run order 11, (D) run order 13

The condition of each runs are summarised in the table below:

Table 4.3 Summary of core and shell fluid compositions utilized. Fiber as bead-less fibers (++), fiber with beads (+-), and poor fibers (--)

Run order	Polymer	Concentration of polymer w(g) /v (ml)	Solvent (v/v)	Fiber evaluation
1	CA	15%	Acetone:DMAC (2:1)	--
2	CA	17%	Acetone:DMAC (2:1)	+ -
3	CA	20%	Acetone:DMAC (2:1)	++
4	PCL	10%	CHF:DMF (4:1)	--
5	PCL	15%	CHF:DMF (4:1)	++
6	CA PCL(Core-shell)	17% 14%	Acetone:DMAC (2:1) CHF:DMF (4:1)	- -
7	CA PCL(Core-shell)	17% 14%	Acetone:dioxane (1:2) CHF:methanol (9:1)	--
8	CA PCL(Core-shell)	15% 14%	Acetone:DMAC (3:2) Acetone:DMAC (3:2)	--
9	CA PCL(Core-shell)	17% 16%	Acetone:DMAC (3:2) Acetone:DMAC (3:2)	+ -
10	CA PCL(Core-shell)	15% 16%	Acetone:DMAC (3:2) Acetone:DMAC (3:2)	--
11	CA PCL(Core-shell)	17% 14%	Acetone:DMAC (3:2) Acetone:DMAC (7:3)	++
12	CA PCL(Mix)	15% 10%	Acetone:DMF (2:1) DMF:CHF (1:9)	--
13	CA PCL(Mix)	17% 14%	Acetone:DMF (2:1) DMF:CHF (1:9)	++

The core-shell structure of the optimum coaxial fiber in run 11 (using 17% CA in Aceton:DMAC (3:2) and 14% PCL in Acetone:DMAC (7:3) was evaluated using JEOL JEM-F200 transmission electron microscope (TEM). The TEM images in Figure 4.3 shows a clear distinction between

phases, which is generated by electron beam diffraction. The dark regions represent the core phase, while the bright regions indicate the shell of the nanofiber. A lower wall thickness of the core-shell fibers was observed with change in the flow rate of the syringe in coaxial electrospinning.

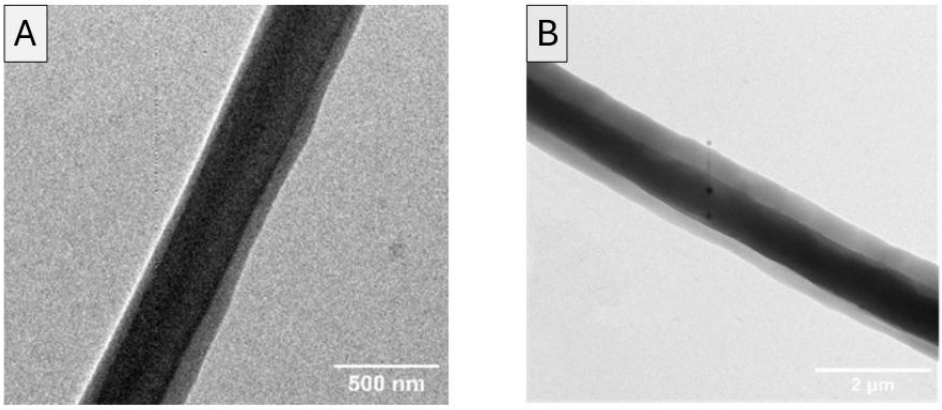

Figure 4.3 TEM images of core-shell structured electrospun nanofibers with CA as the shell and PCL as the core, displaying distinct core-shell boundaries: (A) core-shell fiber: lower shell flow rate and (B) core-shell fiber: higher shell flow rate

4.4.1 Rheological Measurements

The rheological properties of PCL and CA solutions were evaluated to understand their flow behavior within the needles during the electrospinning process. by assuming the solutions behave as newtonian fluids, The existing shear rate at the needle walls was estimated using equation below [188, 189]:

$$\dot{\gamma} = \frac{4Q}{\pi R^3} \qquad Equation\ (4.4)$$

where $\dot{\gamma}$ shows shear rate at the needle wall, Q is the volumetric flow rate, and R is the radius of the needle.

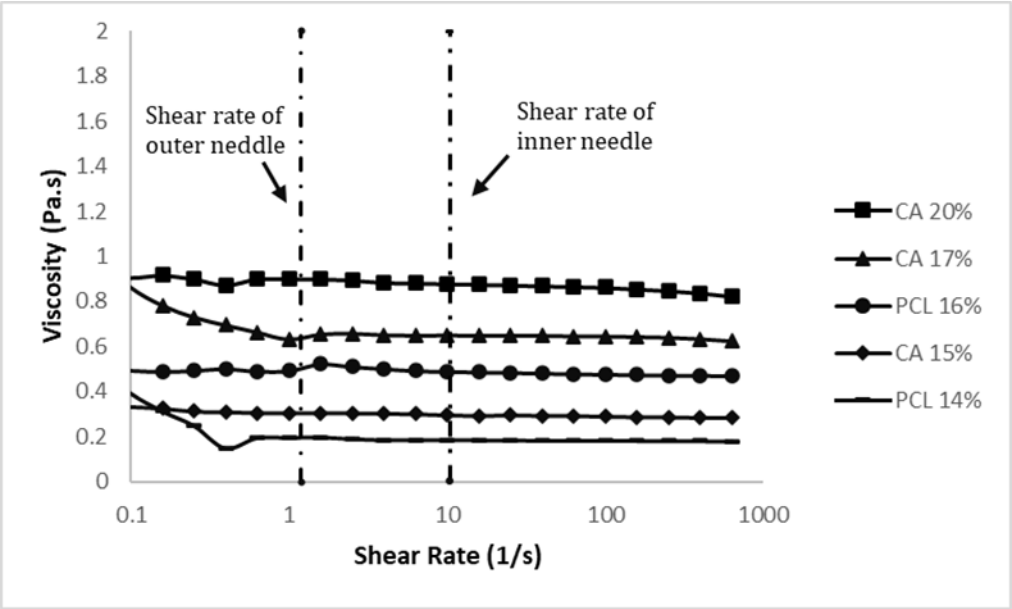

Figure 4.4 Dependence of viscosity on shear rate for CA and PCL solutions

Figure 4.4 is showing the results of rheological measurement in terms of viscosity vs shear rate for pure component. As expected, the viscosity is rising by increasing the solution concentration. For flow rate of 0.5 mL/h and needles with 21 gauge (approximately 514 μm inner diameter) and 16 gauge (approximately 1,372 μm outer diameter), shear rates of 10.3 s^{-1} and 1.2 s^{-1} were obtained, respectively, as indicated by the dotted lines in Figure 4.4. Based on the calculated shear rates, the operation is expected to be in Newtonian region, and no shear-thinning behavior should be happening in coaxial electrospinning.

As seen in Table 4.3, the fiber formation did not occur with PCL 16% and CA 15% (run 10) which is in align with rheological measurements results. At these concentrations, the viscosity of the shell was lower than that of the core, resulting in core breakage through the shell which made it nonsufficient to fabricate the fibers. Furthermore, when the viscosities of the core and shell were almost similar, such as with PCL 14% and CA 15% (run 8), or PCL 16% and CA 17% (run 9) (viscosity ratio less than 1.5), an unstable fiber structure was observed. This occurs because the viscosity of the shell solution requires to be sufficiently high to stabilize the compound Taylor cone

(the conical shape at the end of the nozzle) and maintain the coaxial structure of the solution jet from the needle until complete solidification [125, 190].

4.4.2 Solvents Properties and Boiling Point Determinations

Observations of the jet behavior and Taylor cone formation showed that using a mixture of chloroform and methanol as the core solvent, and acetone and dioxane as the shell solvent, prevented continuous fiber formation, and caused blockage and clogging at the spinneret tip (run 7). This problem was primarily due to the low boiling point of the core solvent mixture, which reduced the wrapping ability of the shell solution and inhibited effective fiber formation. As indicated in Table 4.4, the shell solvent mixture (acetone: dioxane) has a boiling point of around 65°C, while the core solvent mixture (chloroform: methanol) has a boiling point of 56°C. Consequently, the core solvent mixture evaporated faster from the charged jet, considerably reducing the jet's stability and Taylor cone formation [191].

In contrast, using a mixture of acetone and DMAC for both core and shell with different volume ratios provided suitable boiling points, resulting in a more stable jet during coaxial electrospinning Because of the suitable boiling points of the mixture. The boiling point of the acetone: DMAC mixture with a 3:2 volume ratio was estimated to be 68°C, and for the shell solution with a 7:3 ratio, it was 64°C. Therefore, no change in condition were needed for the volatility of the spinning solutions. In coaxial electrospinning, a higher boiling point of the core solvent is particularly vital, as rapid evaporation of core solvent can destabilize the jet and destroys the core–shell fiber structure.

Table 4.4 Boiling point of solvent mixtures

Solvent mixtures(C)	Volume ratio	BP (°C)
Acetone:DMAC	3:2	68
Acetone:DMAC	7:3	64
Chloroform:methanol	9:1	56
Acetone:dioxane	1:2	65

4.4.3 Solvent Extraction Analysis for Assessing Fiber Morphology

To confirm the presence of CA in the shell and PCL in the core during coaxial electrospinning, solvent extraction analysis was performed, and followed with the SEM characterization, the results are shown in Figure 4.5. As seen in Figure 4.5 (A), CA-PCL fibers with a core-shell structure (PCL in the core and CA in the shell) maintain their smooth structure when placed in acetone. This happens because the surface of the fiber, consisting of CA, dissolves in the solvent, while the core layer persists as does not dissolve in acetone at room temperature. However, in fibers formed from a mixed polymer solution (CA/PCL), placing them in the solvent dissolves the cellulose acetate within the fiber, leading to the destruction of the fiber structure due to the absence of a portion of the fiber (Figure 4.5 (B)). These results confirm the core-shell formation in the fibers during coaxial electrospinning.

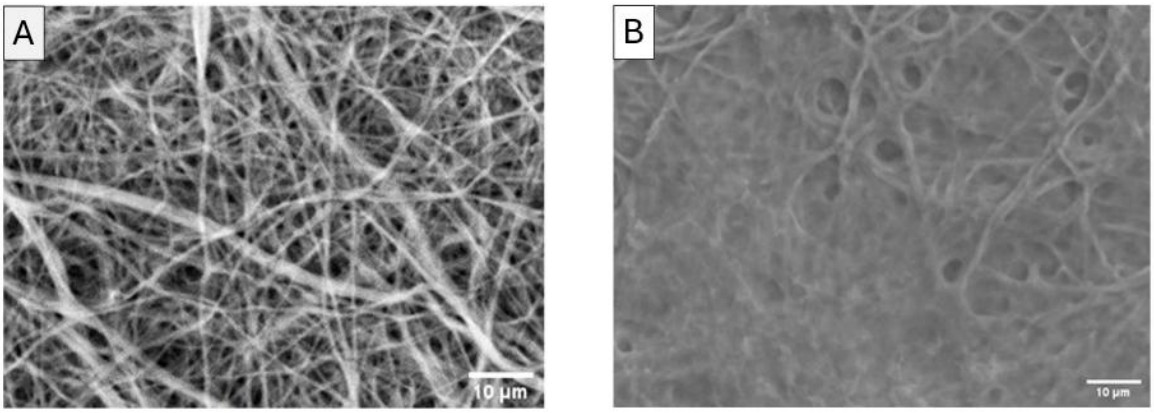

Figure 4.5 SEM images of (A) core-shell fiber and (B) mixed fiber morphology after solvent extraction analysis

4.4.4 Thermal Analysis

To assess the percentage of CA and PCL in each sample (coaxial and single electrospinning) and study their thermal degradation behavior, the fabricated mats were examined through TGA analysis. Fig 4.6 (A) presents the derivative thermogravimetric (DTG) profiles for pure CA and PCL, as well as both CA-PCL and CA/PCL samples (B). The DTG curve of CA demonstrates a main degradation phase beginning around 300°C and continuing until 400°C. PCL exhibited higher thermal stability, with degradation starting at approximately 350°C and concluding around 450°C. These stages related to weight losses of approximately 52% for CA and 48% for PCL in the coaxial fibers, and 57% for CA and 43% for PCL in the blend fibers.

Moreover, a slight shift to lower degradation temperatures for CA and PCL in the mixed fibers was observed, likely because of interactions of different types of polymers (CA and PCL). in the blended fibers may PCL crystallinity reduce and disrupt chain packing, causing decreased thermal stability.

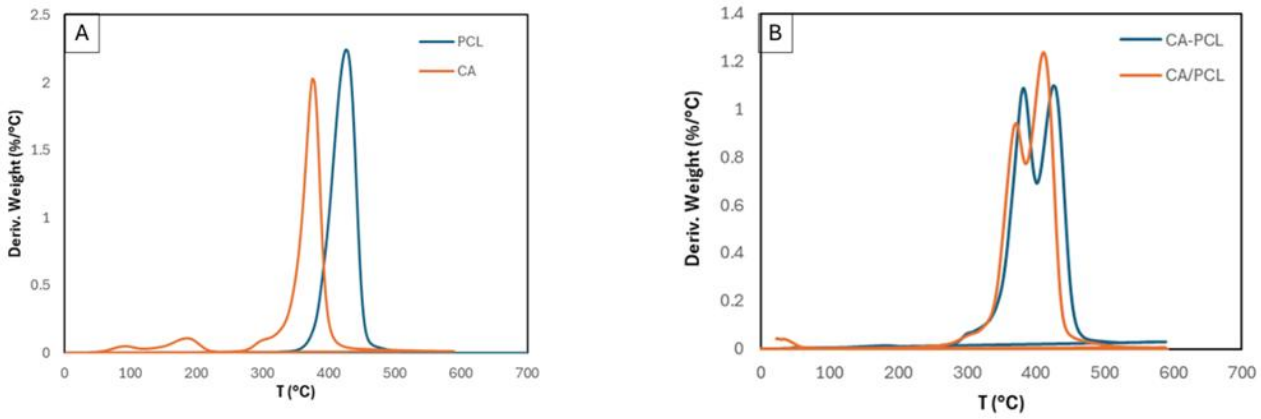

Figure 4.6 (A) first-order derivative of CA and PCL electrospun mat, (B) first-order derivative of CA/PCL (mixed) and CA-PCL (core-shell) electrospun mat

4.4.5 Mechanical Performance

The effect of electrospinning method (single or coaxial) and the presence of PCL in the samples on their mechanical properties was assessed using a tensile testing. Pure PCL mat showed higher tensile strength and elongation at break in comparison to CA fibers. The incorporation of PCL in both the CA-PCL blend and the coaxial electrospun mats considerably improved the mechanical performance of the mats. As shown in the Figure 4.7, the breaking strength approximately doubled in the core-shell fiber compared to CA. However, for CA/PCL blend, the results indicated just a slight increase in the strength at break.

Additionally, the stiffness of the blend fibers is lower than that of the coaxial fibers, this is mainly because of the well-defined interface between the two polymers in the coaxial fibers. In contrast, the polymers in the blend fibers may not form distinct structures as seen in the core-shell configuration.

There are some factors that noticeably impact both the breaking load and stiffness of the samples such as size, thickness, and orientation of fibers among the samples. In this test, we tried to ensure similar size and orientation in the electrospun mats to minimize errors.

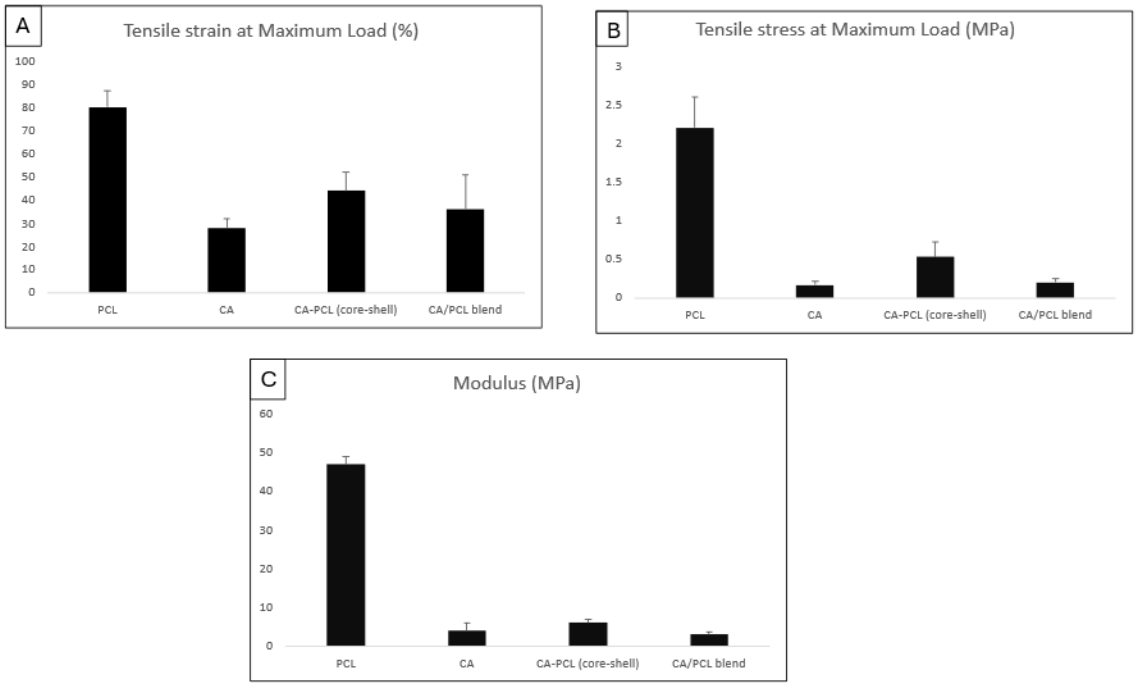

Figure 4.7 Effect of tensile load on various mat. (A) Tensile strain at Maximum Load (MPa). (B) Tensile stress at Maximum Load (%). (C) Modulus (MPa)

4.4.6 Wettability and Degree of Swelling

Water contact angle measurements were made on PCL, CA, CA/PCL, PCL-CA (Fig 4.8). The results indicated an average contact angle of around 89° for CA mat and 90° for PCL-CA (core-shell) mat, showing their close wettability. It reveled the successful presence of CA in the fiber's shell in coaxial electrospinning which is a desirable property for the final application.

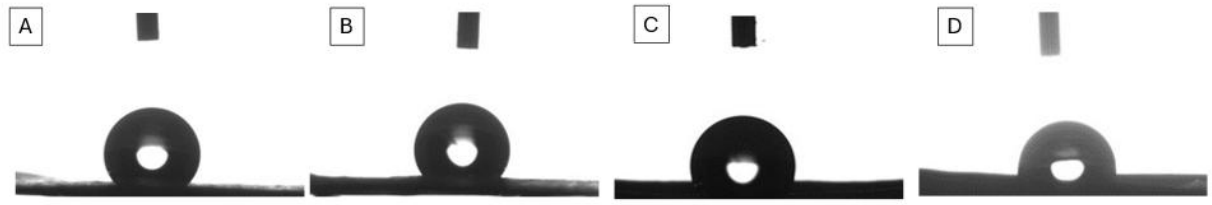

Figure 4.8 Water contact angles of electrospun nanofibers: (A) PCL mat, (B) CA/PCL mat, (C) CA-PCL, and (D) CA

The contact angle of the blend of CA and PCL mat was measured at 120°, which is approximately close to the single PCL mat with contact angle of 130°. This data indicates the presence of PCL in the CA-PCL mixture structure, resulting to increased hydrophobic properties of the mat.

The swelling degree of the mats was assessed by measuring weight before and after being exposed in an environment of 95% relative humidity (RH) at 35°C. The CA mat showed higher absorption of water molecules lead to more increasing weight (3.7 ± 0.3%) among all samples. This measurement shows the wettability of the mats which is reflecting their ability to absorb and retain water molecules from the moisture condition or generated through respiratory activities. Therefore, CA fibers can swell significantly during mask usage, resulting the comfort of the face mask during prolonged wear. In comparison to single CA mat, both CA/PCL, CA-PCL mat showed lower swelling degrees, 2.4 ± 0.3% and 2.8 ± 0.2%, respectively. This result is an advantageous as it is helpful to maintain the pore size of the mat during face mask usage because of lower swelling of fibers. Hence, the existence of PCL either in the core or blended with CA can limit excessive swelling in fibers. This is crucial in face mask applications because an increased fiber diameter may cause reduction of pores between fibers [167], thereby affecting the breathability of the electrospun mat, which is not desirable.

Table 4.5 Degree of swelling determinations for CA, CA/PCL, CA-PCL, and PCL electrospun mats

Mats	Degree of Swelling (%)	Contact Angle
PCL	0.2 ± 0.1%	130°
CA/PCL	2.4 ± 0.3%	120°
CA-PCL	2.8 ± 0.2%	90°
CA	3.7 ± 0.3%	89°

4.4.7 Antibacterial Activity

The antibacterial and antiviral properties of electrospun mats containing CPC is important for their application in advanced antimicrobial masks. In this test, the biocidal effectiveness of CPC-loaded mat was studied through S. aureus and E. coli bacteria strain, which are gram-positive and gram-negative bacterial strains, respectively. Generally, results indicated that CPC can reduced S. aureus activity more significantly compared to E. coli strain. This is mainly because of that the Gram-negative bacteria have two cell membranes, and the presence of this second membrane reduces the efficacy of CPC in targeting the membrane [115].

Regarding S. aureus, all samples in different contact time led to a reduction in viable bacterial colonies. In detail, within 1 h of contact time, a 1.5 to 2 log reduction was measured. After 3 h of contact time, the inoculum of 5 log bacteria was reduced to 3.2, while after 24 hours, S. aureus growth was approximately totally inhibited.

E. coli showed greater persistent to CPC as antibacterial agent. After 1 hour, bacteria reduced by 1.3 log, while the results showed approximately the same results after 3 hours. However, increasing the contact time to 24 h caused further reduction in colony numbers by around of 0.5 log.

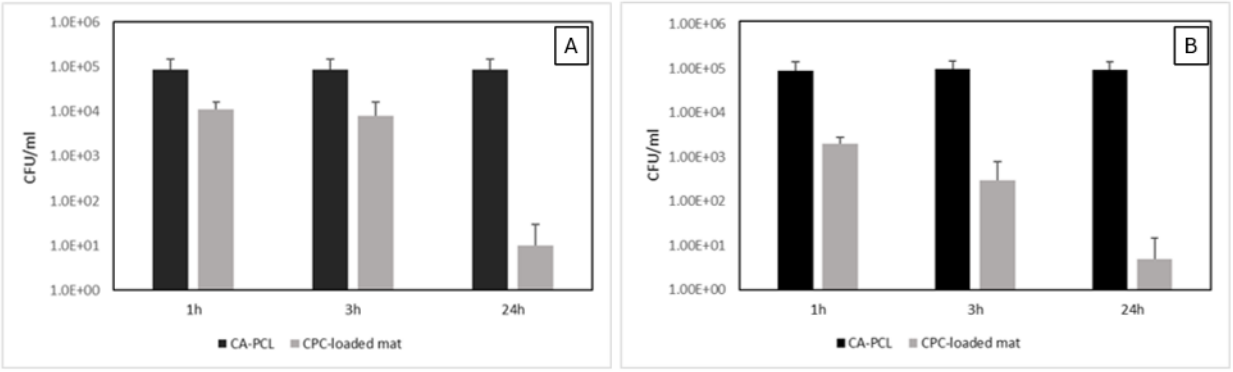

Figure 4.9 (A) Antibacterial efficacy of CPC- loaded mat against E. coli (B) Antibacterial efficacy of CPC-loaded mat against S. aureus

4.4.8 Antiviral Test

The antiviral effectiveness of CPC in electrospun mat was evaluated using the human coronavirus 229E (HcoV-229E). The results in Figures 4.10, shows viral titers after a short time (30 min) and extended (2 h) contact time to verify the virucidal efficacy of electrospun mat containing CPC.

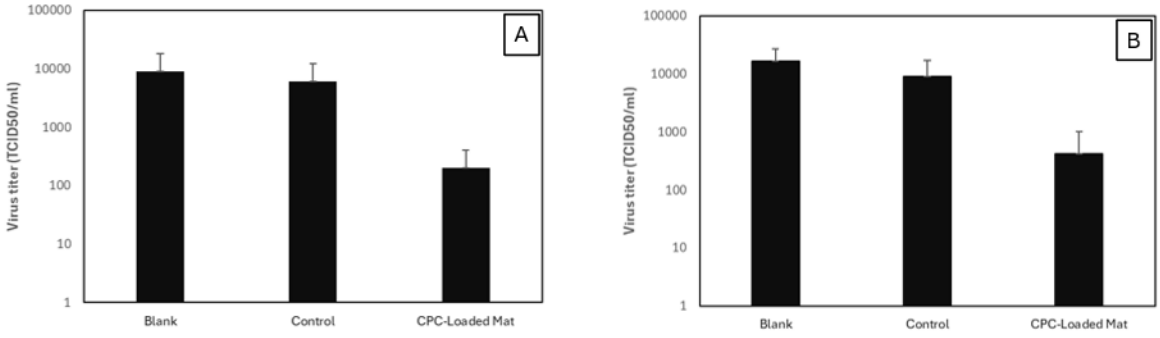

Figure 4.10 (A) Antiviral efficacy of CA-CPC mat against HCoV-229E with a 30 min contact time, (B) Antiviral efficacy of CA-CPC mat against HCoV-229E with a 2-hour contact time

The electrospun mats incorporating CPC showed different antiviral activities due to varying contact times. CPC-loaded mat achieved a 1.8 log reduction against human coronavirus with a 2-hour

contact time, while its antiviral activity against human coronavirus with a shorter contact time (30 minutes) was not significant (1.4 log reduction). The results confirm that CPC needs longer contact times to be more effective [192].

4.5 Conclusion

In this work, biodegradable antimicrobial CA-PCL/CPC electrospun membranes were produced for facemask applications. Different concentrations and solvents were used for solution preparation to achieve uniform fibers in coaxial electrospinning. To this aim, a mixture of acetone and DMAC was chosen as the appropriate solvent for the core and shell solutions.

CA-PCL mat showed enhanced mechanical properties in comparison to pure cellulose acetate, resulting the mat to withstand higher loads or forces before breaking and to maintain their form, which is an appropriate property for the face mask. Such mechanical strength and flexibility are vital for face mask filter application, as in this way the mat can resist handling stresses, airflow-induced deformation during breathing, and repeated mechanical loading during use by users, while preserving comfort and fit. These properties support maintaining pore structure, filtration efficiency, and breathability during of mask usage, making them appropriate characteristics for face mask.

With core shell structure of fibers, the membrane preserves its high level of hydrophilicity, similar to cellulose acetate. This hydrophilic character is important for face mask filters, as it provides absorption and retention of exhaled respiratory droplets containing pathogenic microorganisms, thereby reducing the risk of pathogen transmission. Meanwhile, the presence of PCL in the core structure significantly reduces high swelling occur in high-humidity conditions.

The electrospun mats loaded with CPC exhibited an inhibitory effect against S. aureus and E. coli. However, the antibacterial activity against Gram-negative bacteria was lower during shorter contact times compared to Gram-positive bacteria. Moreover, the mat containing CPC demonstrated ability to inhibit viral activity. In short contact time, the antiviral properties of the CPC-loaded mats were limited against human coronavirus, showing the need for further investigation to enhance virus inhibition mechanisms over shorter periods.

CHAPTER 5 ARTICLE 2: DEVELOPMENT OF ELECTROSPUN FIBERS EMBEDDING ANTIMICROBIAL COMPOUNDS WITH SYNERGISTIC EFFECTS FOR RAPID ACTION AND CONTROLLED RELEASE

Sheyda Kordjazi [a], Abdellah Ajji [a], Zahra Kordjazi [a]

[a] Department of Chemical Engineering, École Polytechnique de Montréal, Montréal, Québec H3T 1J4, Canada.

Submitted to Biomaterials Advances on October 6, 2025

5.1 Abstract

The increasing demand for the use of personal protective equipment, especially during pandemics, has determined the need for the development of products with rapid action against microorganisms and sustained antimicrobial effectiveness. In this study, biodegradable core-shell electrospun mats were developed, incorporating eucalyptus essential oil (EEO) and cetylpyridinium chloride (CPC). Different fiber structures, including single fibers of cellulose acetate (CA), polycaprolactone (PCL), CA/PCL blend, and coaxially spun core-shell fibers loaded with EEO and CPC, were fabricated and characterized. The results showed that EEO release over a 30-day period from electrospun mats was different depending on the fiber structure: single fibers indicated a burst release, while core-shell structures provided the most controllable and sustainable release. Moreover, the synergistic antimicrobial effects of combining two different antimicrobial agents, EEO and CPC, was investigated to assess their antimicrobial efficiency. The antibacterial and antiviral activities of the mats containing both antimicrobial agents (EEO and CPC) demonstrated a significant reduction in bacterial colonies and effective antiviral activity, particularly for short contact times. These findings suggest that incorporating eucalyptus essential oil in the core of core–shell structure provide controllable release during product usage and confirmed that presence of CPC in combination of EEO improve both antiviral activity and antibacterial protection at short contact time.

Keywords: Electrospun mats, Core–shell fibers, Cellulose acetate, Polycaprolactone, Essential oil, Cetylpyridinium chloride, Sustained release, Antimicrobial activity, Antiviral activity, Synergistic effect

5.2 Introduction

Throughout the pandemic, the use of personal protective equipment (PPE) has been proven effective significantly in reducing the rapid spread of pathogens. Among different types of PPE, face masks have been the most commonly used in public. However, it was shown that some infections, such as SARS-CoV-2, can survive and remain on the surfaces of masks for at least five days at room temperature, depending on the material [34, 193]. This presence of pathogens could increase the risk of infection. One way to solve this issue is incorporating antimicrobial materials in final products, which can kill or deactivate microorganisms that come into contact with the mask's surface. This approach not only enhances the mask's efficiency during use but also helps maintaining its protective properties over prolonged usage.

Quaternary ammonium compounds (QACs) are some of the effective antimicrobial agents and were the first biocides used before phenolic and nitrogen-based products. Their structure formed one or more quaternary ammonium ions, each attached to four lateral substituents [178]. QACs are membrane-active agents that interact with the cytoplasmic membrane of bacteria. Due to hydrophobic properties of them, they are effective against lipid-containing viruses, and based on the product formulation, they can also be effective against non-lipid-containing viruses [81]. In QACs, the hydrophobic lateral chains play an important role through penetrating into the membrane and disrupting its structure. Chains with lengths ranging from C12 to C16 show the highest level of activity [81, 178]. Between various types of QACs, cetylpyridinium chloride (CPC) is one of the most effective agents. CPC appears as a beige-colored salt. It consists of a positively charged pyridinium group acting as a hydrophilic headgroup, combined with a hexadecyl (C16) alkyl chain as a lipophilic tail. Having this molecular structure, CPC is categorized as a cationic surfactant [83, 158, 194]. However, this group of antimicrobial agents is less effective in short contact times and needs more time to be active against pathogens [192].

Another well-known class of antimicrobial agent is natural oil extracts, which have antimicrobial activity, are low-cost, and environmentally friendly [99, 170]. Essential oils (EOs) are generally complex mixtures of nonpolar and semipolar lipophilic components with low molecular weight. These oils are derived from different part of plants such as roots, fruits, wood, herbs, bark, twigs, leaves, seeds, buds, rhizomes, peels, flowers, and entire plants of specific botanical species [195-197]. Essential oils (EOs) prevent bacterial growth and the production of harmful bacterial metabolites. Their hydrophobic nature disrupts bacterial cell structure, leading to increased permeability and leakages. This disruption bring negative impact on microorganisms, including disturbances in energy balance and energy transfer processes associated with the cell membrane, solute transport, and metabolic regulation [198, 199]. Essential oils are also popular for their antiviral activities. Along with their constituent phytochemicals, disrupt viral replication and benefit the host respiratory system by promoting mucus lysis and bronchodilation [195].

Despite the promising antimicrobial activities of essential oils (EOs) their practical use is often limited. The main reason is lack of sustainability and uncontrollable release because of sensitivity to external factors such as temperature, light, and oxygen, as well as their volatile nature; which restricts their practical use [174, 200].

One way to resolve this issue and protect them from external factors is their encapsulation. In this method, the active material is placed in the core and coated with another material or a mix of materials as shell [201].

Recently, coaxial electrospinning as an effective encapsulation method has gained attention for its ability to control and preserve active materials due to core shell structure of fibers. Coaxial electrospinning is similar to the traditional electrospinning process, with a key difference: in coaxial electrospinning, two coaxial nozzles are connected to a high voltage source instead of one nozzle like single electrospinning. Two different solutions (core and shell materials) are pumped through the nozzles, fabricating in a core–sheath fiber morphology. In this method, the solutions keep separated until the final step in the tip of needle [128].

In this study, we focused first on the encapsulation of EEO and fabrication of core-shell fibers using coaxial electrospinning, with polycaprolactone (PCL) as the core and cellulose acetate (CA) as the shell. Eucalyptus essential oil (EEO) was mixed into the core solution in order to control the release behaviour. The results obtained with the core-shell structure were compared to those

obtained using single-fiber mats of CA and PCL, as well as a blend of CA and PCL loaded with EEO. All fabricated mats were characterized in terms of morphology, fiber diameter, EEO release behavior and related physical properties. Moreover, the antibacterial and antiviral activity of mats incorporating with CPC and EEO was assessed, and the synergistic effect of the combination of both agents was considered to analyze antibacterial and antiviral performance.

5.3 Materials and Methods

5.3.1 Materials

Cellulose acetate (CA, 30 kDa) and polycaprolactone (PCL, 80 kDa) were used, along with chloroform (CHL), dimethylformamide (DMF), acetone (99.9%), N,N-dimethylacetamide (DMAC), powdered cetylpyridinium chloride (CPC), eucalyptus essential oil (EEO) provided by Sigma-Aldrich. Beef extract powder, peptone powder, minimum essential medium eagle (EMEM), and fetal bovine serum (FBS) were all purchased from Sigma (Canada, ON). Escherichia coli (E. coli) ATCC 11229 were acquired from ATCC, USA.

5.3.2 Preparation of Polymer Solutions for Electrospinning

For the single fiber, CA (17% w/v) was dissolved in a mixture of acetone and DMAC at a ratio of 2:1 (v:v) at room temperature using a magnetic stirrer. Similarly, PCL (15% w/v) was first dissolved in CHF at 35°C, and after 3 hours, DMF was added to the solution, with a final solvent ratio of CHF/DMF at 4:1 (v:v).

For the blend, CA (17% w/v) and PCL (14% w/v) solutions were mixed at a 1:1 ratio, and the resulting mixture was stirred for 24 hours before electrospinning. A DMF/CHF mixture (1:9, v:v) was used for the PCL solution, while an acetone/DMF mixture (2:1, v:v) was prepared for the CA solution.

For coaxial electrospinning, a mixture of acetone and DMAC was chosen as the solvent for both CA and PCL, but with different ratios. For the CA solution, the ratio was 3:2 (v:v), while for the PCL solution, it was 7:3 (v:v). Concentrations of 14% (w/v) and 17% (w/v) were used for CA and PCL, respectively.

EEO concentrations of 4% and 8% with respect to the polymer were used to provide antibacterial and antiviral activity in the electrospun mats, along with CPC at a concentration of 0.5%, which was added to the electrospinning solution.

5.3.3 Electrospinning

A vertical electrospinning setup (Tong Li Tech Co., Ltd., Shenzhen, China) with adjustable electric power and flow rate was used for both single and coaxial electrospinning. The solution was poured into a 10 mL syringe and connected to the needle through a plastic tube. The voltage was set between 12-20 kV, and the flow rate ranged from 0.5 to 1 mL/h. Electrospun fibers were collected on aluminum foil attached to the collector.

5.3.4 Surface Morphology

To evaluate the morphology of the electrospun fibers scanning electron microscopy (SEM) was employed. The fibers were collected on aluminum foil for 2 hours, then the mat separated from the foil and attached to carbon tape. SEM images were captured using a high-resolution microscope (SEM, Hitachi TM3030Plus) operated at 15 kV. Fiber diameters were measured using the ImageJ processing software. For each sample, assessments were performed three times, with 100 fibers analyzed in each trial.

5.3.5 Detection of EOs Loading

Encapsulation efficiency (EE), defined as the ratio of the amount of EO that remained in the fabricated fibers after electrospinning to the initial amount, was measured. For this aim, mats containing essential oil (EO), including single fibers of CA, PCL, CA and PCL blend and core-shell CA/PCL fibers, were submerged in 4 mL of solvent (ethanol) and mixed at 150 rpm at room temperature for 6 hours. After that, a specific volume of the solution was collected and transferred to a cuvette for absorbance measurements in the 200–500 nm range using a UV-1800 spectrophotometer (Tecan Infinite® 200 PRO, Switzerland). Ethanol was chosen as the extraction solvent because of its high solubility for EO and also it is safe to work with it. An immersion time of 6 h was selected to allow enough diffusion of the extractable EO into the solvent. After 6 hours, the released amount reached a stable plateau with no significant increase with more immersion. The percentage of essential oils within the mats was calculated based on the absorbance data. A calibration curve was established using different EO solutions with various concentrations. A wavelength of 274 nm was used to establish a standard calibration curve. The encapsulation efficiency (EE) was calculated from the following equation [110]:

$$EE(\%) = \frac{Amount\ of\ oil\ content\ entrapped\ in\ the\ fibers}{Theoretical\ total\ amount\ of\ oil} * 100 \qquad Equation\ (5.1)$$

5.3.6 Quantification of EO Released

The release study of EOs was measured by headspace (HS) extraction method through transferring the vapor phase above the sample matrix into a syringe containing 3 mL of ethanol. The syringe containing solvent and EO vapor was shaken to ensure complete dissolution of the essential oils in ethanol. The samples were then transferred into a cuvette, and absorbance measurements were assessed using a UV-Visible spectrophotometer. The range of 200–500 nm considered for

absorbance measurements, with each sample tested three times. For calibration, a series of diluted EO solutions in ethanol were prepared, and the relevant peaks were identified.

To calculate the EO concentration, the Beer–Lambert law was applied [202, 203]:

$$[EO](M) = \frac{A}{L * \varepsilon} \qquad Equation\ (5.2)$$

where A is the absorbance at 274 nm, L is the path length of the cuvette, and ε is the molar absorptivity of the essential oil.

5.3.7 Wettability Measurements and Swelling Degree

To measure hydrophilic properties of fabricated mats, water contact angle assessments were conducted using Contact Angle measurement equipment (OCA, Dataphysics). In this test, a 10 µL droplet of distilled water was placed on samples, which was cut into a 2 cm rectangular shape. Measurements were recorded immediately after the droplet contacted the surface. The experiment was repeated five times for each sample to ensure accuracy. The degree of swelling (DS) in the mats was measured by comparing the sample weights before and after exposure in a climate chamber, set at 95% relative humidity and a temperature of 35 °C. The exposure period was 4 hours.

$$DS = \frac{(W_{wet} - W_{dry})}{W_{dry}} \times 100\% \qquad Equation\ (5.3)$$

where W_{wet} (mg) is the weight of the wet mat, W_{dry} (mg) is the weight of the dry mat [174].

5.3.8 Antibacterial Activity

The antimicrobial effectiveness of developed mats, two types of bacteria, Gram-positive (Staphylococcus aureus) and Gram-negative (Escherichia coli), were used, following the ISO 20743:2021 guidelines (Textiles-Determination of the antibacterial activity of textile products). A total of five samples were assessed, including electrospun mats containing 4% EO, 8% EO, 4% EO combined with CPC, and a control sample without any antimicrobial agent. The procedure was repeated three times for each sample to validate the findings, and the average values were reported.

Before testing, all samples were sterilized using UV light and then immersed in a bacterial solution. First, to prepare the bacterial suspension, 5 µL of bacteria preserved at −80°C was transferred into 5 mL LB medium and incubated at at 200 rpm, 37°C for 18 hours. The bacteria concentration adjustment performed by setting OD600 to be equivalent to 1. For dilution, nutrient broth (NB) was used to achieve a final concentration of 10^5 CFU/mL. Next, 5 µL of the prepared bacterial suspension was deposited onto the sample surface, followed by the addition of NB to the vials containing the samples. All test vials, along with the control group, were incubated for different contact times (1 hr, 3 hr, and 24 hr) at 37°C and 90% relative humidity. After incubation, serial dilutions were performed by adding 100 µl of the vortexed mixture into 900 µl of phosphate-buffered saline (PBS). Finally, 100 µL of the diluted solution was plated onto agar and incubated for another 24 hours at 37°C. The antibacterial activity was determined by counting the number of bacterial colonies on the Petri dishes [204].

5.3.9 Antiviral Tests

For antiviral testing, the procedure followed the ISO 18184:2019 protocol titled "Textiles — Determination of the Antiviral Activity of Textile Products." The antiviral activity of the samples was evaluated using virus 229E (ATCC® VR-740™) and human cell line MRC-5 (ATCC CCL-171™) was used and the method employed in this study is the Median Tissue Culture Infectious Dose ($TCID_{50}$) technique [187].

First, samples measuring 3×3 cm^2 were sterilized by using UV lamps for 20 minutes. In accordance with ISO, essential control tests were conducted to confirm the absence of cytotoxic effects, preservation of cell sensitivity to the virus.

Samples placed into a container and a volume of 100 µL of virus solution, with a concentration of 3×10^5 $TCID_{50}$/mL, was applied directly onto the sample surfaces. After the specified contact time (tested at two different contact times: 30 minutes and 2 hours), the virus was collected by adding 5 ml of the neutralizing solution and vortex the mixture for 5 seconds in 5 cycles. In this step, serially diluted was performed with EMEM by a factor of 10. From each dilution, 100 µL was transferred to a 96-well plate containing a monolayer of MRC-5 cells. The 96-well plate contained MRC-5 cells were with a confluency of around 60%. The plates were incubated for 1 hour at 35°C under 5% CO_2, after which the virus solution was removed, the cells were washed with PBS, and fresh EMEM supplemented with 2% FBS was added to the infected cells to support infected cell growth. The plates were incubated for 5 days at 37°C, and cytopathic effects (CPE) were observed under a microscope [186].The viral titer ($TCID_{50}$) was calculated, and antiviral activity was determined using ISO 18184:2019 [187].

5.4 Results and Discussion

5.4.1 Electrospun Mats Morphology

Samples from each experimental run, prepared with different EEO concentrations and the addition of CPC, were analyzed by SEM to assess fiber morphology and spinnability. Table 5.1 summarizes the information about the electrospun mats containing different concentrations of antimicrobial agents. The fiber evaluation in this table is based on morphological observations, where '++' indicates uniform, bead-less fibers and '+-' shows fibers containing beads.

Table 5.1 Summary of compositions utilized to produce electrospun membranes. Fiber as bead-less fibers (++), fiber with beads (+-)

Fiber type	Run	Polymer	Essential oil content	0.5% CPC content	Boiling point of solvents(°C) [205]	Average fiber diameter(nm)	Fiber evaluation
Single Fiber	(1)	CA	0%	-	Acetone: 56 DMAC: 165	720 ± 80	+-
Single Fiber	(2)	CA	4%	+	Acetone: 56 DMAC: 165	820 ± 60	++
Single Fiber	(3)	CA	8%	+	Acetone: 56 DMAC: 165	860 ± 30	++
Single Fiber	(4)	PCL	0%	-	DMF: 153 CHF: 61	780 ± 40	+-
Single Fiber	(5)	PCL	4%	+	DMF: 153 CHF: 61	860 ± 90	++
Single Fiber	6)	PCL	8%	+	DMF: 153 CHF: 61	900 ± 70	++
Shell Core	(7)	CA PCL	0%	-	Acetone: 56 DMAC: 165	790 ± 110	+-
Shell Core	(8)	CA PCL	4%	+	Acetone: 56 DMAC: 165	870 ± 85	++
Shell Core	(9)	CA PCL	8%	+	Acetone: 56 DMAC: 165	910 ± 65	++
Blend	(10)	CA PCL	0%	-	Acetone: 56 DMAC: 165 CHF: 61	770 ± 125	+-
Blend	(11)	CA PCL	4%	+	Acetone: 56 DMAC: 165 CHF: 61	850 ± 95	++
Blend	(12)	CA PCL	8%	+	Acetone: 56 DMAC: 165 CHF: 61	890 ± 75	++

As seen in the SEM images in Figure 5.1, increasing the concentration of essential oil in the polymer solution from 4% to 8% increased the average fiber diameter in all samples. This result

can be attributed to the lower conductivity due to the higher essential oil content. In fact, lower electrical conductivity of solution reduces the charge density of the jet [206], and consequently, the reduced amount of charge reduces the stretching force under the electric field in the process of electrospinning, causing to the formation of fibers with higher diameters. These results are in agreement with finding reported by other researchers in this field [207, 208].

Additionally, the results showed that the addition of CPC surfactant has positive impact on fabrication of more uniform and bead-free fibers. In fact, the presence of CPC in the solution as surfactant decreased surface tension, which led to reduced bead formation and slightly increased fiber diameters [209]. This effect occurs because lower surface tension stabilizes the electrospinning jet, allowing continuous stretching and preventing droplet formation [210]. It is noticeable that CPC as a quaternary ammonium salt, can be dissolved in acetone which is a polar aprotic solvent.

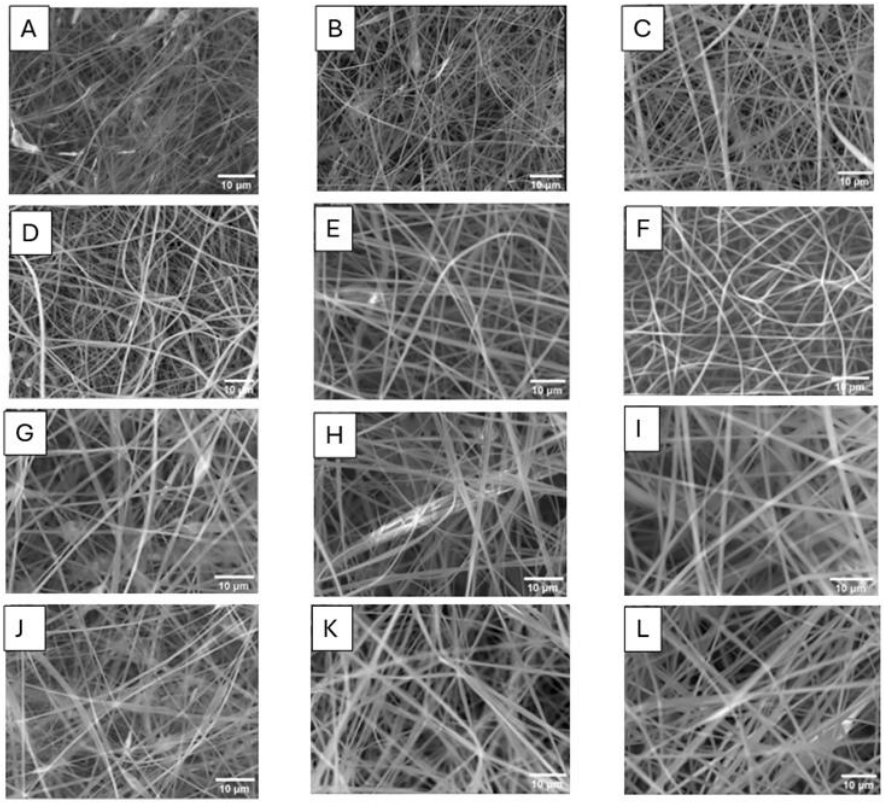

Figure 5.1 Scanning electron micrographs of single and coaxial fibers with different concentartion of EEO and CPC based on table 1: (A) run order 1, (B) run order 2, (c) run order 3, (D) run order 4, (E) run order 5, (F) run order 6, (G) run order 7, (H) run order 8, (I) run order 9, (J) run order 10, (K) run order 11, (L) run order 12

5.4.2 Encapsulation Efficiency (EE)

Encapsulation efficiency (EE) is an important factor for assessing the amount of essential oil trapped within electrospun fibers after electrospinning process. As observed in Figure 5.2, the EE of CA fibers is lower than other single fibers used in this study including PCL and the CA/PCL blend. During the electrospinning process, fiber formation happens when the polymer jet solidifies because of solvent evaporation [211]. Solvents with lower boiling points promote faster solidification, thereby enhancing the entrapment of essential oils within the fiber matrix. In the

case of the CA and PCL solutions, boiling points of the solvent mixtures were measured using reference tables and Raoult's law [183, 184]. For the CA solution the estimated boiling point of the solvent system is estimated to be around 92 °C, considering the individual solvent boiling points provided in Table 5.1. Boiling point of the CA solution is more than boiling point of the PCL solution with an estimated temperature of around 79 °C, leading to delayed solidification and lower EE.

Furthermore, the release mechanism of EO is significantly influenced by the hydrophilicity of the polymer [212]. In fact, hydrophobic interactions between the hydrophobic polymer matrix and the essential oil contributed to a slower release rate of EO, and as result, improving its encapsulation efficiency [213]. In hydrophilic materials like cellulose acetate (CA), fiber swelling occurs because of water absorption, which simplify the diffusion of encapsulated essential oils and allowing them to diffuse out more easily [214]. As CA easily absorbs moisture, it provides appropriate condition for swelling and migration of active agent from the fiber matrix, resulting in a faster release and lower EE, around 55% compared to more hydrophobic polymers like PCL which showed more than 60% EE.

As expected, the EE of the CA/PCL blend is approximately 60%, which is between the values observed for the single CA and PCL mats. However, the core–shell structure produced by coaxial electrospinning showed a significantly improved performance for encapsulation of active agent, with EE exceeding 80%. This result showed that coaxial electrospinning helps in controlling release and protecting EO during electrospinning. The higher EE observed for the coaxial electrospun fibers is related to the formation of a well-defined core–shell structure, in which the essential oil is limited within the PCL core and completely surrounded by the CA shell. In this study, CA was deliberately chosen as the shell material to provide a hydrophilic fiber surface appropriate for face-mask applications, where surface wettability is needed to absorb respiratory droplets containing pathogens and to prevent transmission risk. PCL was not used as the shell because of its hydrophobic nature, which does not meet these functional requirements. The CA shell provides an effective physical barrier that limits essential oil evaporation during electrospinning, and reduces exposure to ambient air. Based on this barrier effect, the coaxial core-shell architecture, regardless of polymer sequence, plays an important role in enhancing EE, and

that even a reversed core-shell configuration would be expected to exhibit higher encapsulation efficiency compared to the single-fluid electrospun fibers.

Based on these findings, the core-shell structure is promising approach for essential oil encapsulation, reducing loss during processing.

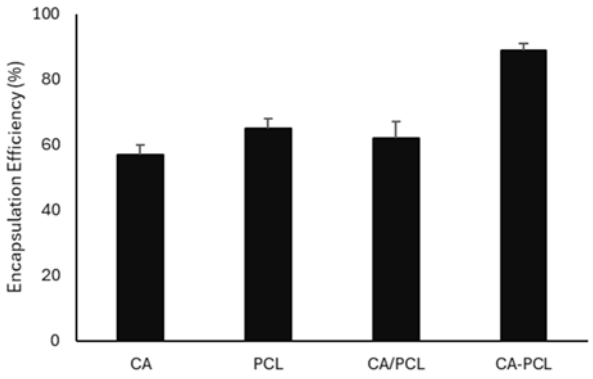

Figure 5.2 Encapsulation efficiency (EE) of eucalyptus oil loaded into different electrospun mats

5.4.3 Wettability Measurements and Swelling Degree

Water contact angle measurements were performed on electrospun mats including CA, PCL, CA/PCL blends, and CA–PCL core–shell structures, with and without essential oil (EO) incorporation (Table 5.2). The results showed that the presence of EO caused an increase in the average contact angle for all samples. Specifically, the contact angle of CA mats increased from 89° to 110°, CA/PCL from 120° to 135°, and PCL from 130° to 137° after EO incorporation. This is mainly because of the hydrophobic and lipophilic properties of Eucalyptus essential oil [215]. In the case of core–shell fibers (CA–PCL), the contact angle stayed relatively stable after EO incorporation, with small changes from 90° to 95°. This result shows that the formation of a shell layer in the structure of the fiber preserved the surface hydrophilicity of the fibers due to the presence of CA and the EO encapsulated in the core had minimal impact on the surface wettability. As contact angle records were performed immediately after droplet placement, the impact on the core-loaded EO for the shell surface properties was negligible. Moreover, the degree of swelling

reduced for all EO-loaded samples. The swelling degree for CA mats decreased from 3.7 ± 0.3% to 3.3 ± 0.1%, and the blend of CA/PCL mats also showed a slight decrease, from 2.4 ± 0.3% to 2.3 ± 0.3%. These results confirm that the incorporation of EO increased the hydrophobicity of the mats and reduced their moisture absorption capacity.

Table 5.2 Degree of swelling determinations for CA, CA/PCL, CA-PCL, and PCL electrospun mats, both with and without essential oils (EOs)

Mats	Degree of Swelling (%)	Contact Angle
CA	3.7 ± 0.3%	89°
CA-EO	3.3± 0.1%	110°
CA/PCL	2.4 ± 0.3%	120°
CA/PCL-EO	2.3 ± 0.3%	135°
CA-PCL	2.8 ± 0.2%	90°
CA-PCL-EO	2.6 ± 0.4%	95°
PCL	0.2 ± 0.1%	130°
PCL-EO	0.2 ±0.2 %	137°

5.4.4 Antibacterial Test

The antibacterial activity of coaxial mats containing 4% and 8% essential oil (EO), with or without CPC as a second antimicrobial agent, as well as mats containing 0.5% CPC, was assessed against

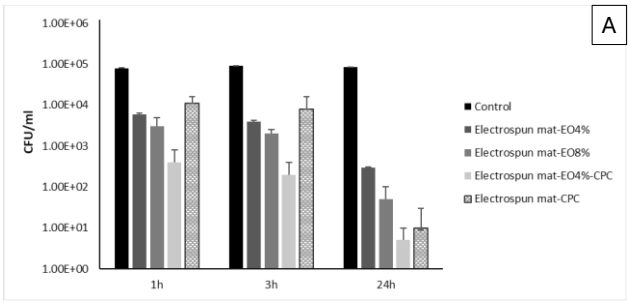

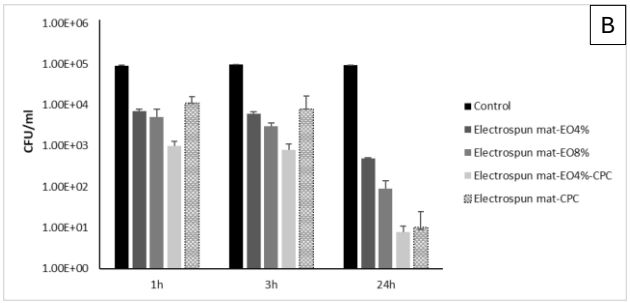

two bacterial strains: Staphylococcus aureus (Gram-positive) and Escherichia coli (Gram-negative). Generally, S. aureus showed higher sensitivity to the antibacterial agents in comparison to E. coli. The main reason is the additional outer membrane layer in Gram-negative bacteria, which offers a protective barrier and limits the permeability of antimicrobial agents [94].

In the case of 1 hour of contact time, mats containing 4% EO indicated around a 1.5-log reduction in E. coli and slightly lower reduction against S. aureus. With increasing the EO concentration to 8%, a modest improvement was observed in reduction of bacterial colonies, achieving to an approximately 1.8-log reduction. However, the most significant antibacterial effect was observed in the sample with CPC added to 4% EO in electrospun mat, reaching about a 2.5-log reduction for both S. aureus and E. coli within 1 hour, which is a short contact time. The mats containing CPC showed less than a 2 log reduction against S. aureus and E. coli at 1 hour.

At 3 hours contact time, bacterial reduction decreased slightly across all groups compared to 1 hour contact time as the samples placed in contact with antimicrobial agents in the mats, but the overall trend stayed similar to the 1-hour results. At 24 hours, almost complete bacterial colonies elimination happened, specifically in the mats incorporating combined CPC and EO, for both S. aureus and E. coli bacteria compared to the control group. These results indicate that increasing the EO concentration from 4% to 8% causes a slight improvement in antibacterial activity of the mats specially in short contact time (1 hour and 3 hours) but combining EO with CPC provide a much stronger antibacterial effect in short contact time, which is required in personal protective equipment.

The main reason of the synergistic effect and significant improvement in antibacterial efficiency, when the mats contain both CPC and essential oil (EO), is attributed to the different structures and mechanisms of action of CPC and EO against bacteria. The lipophilic nature of EO components provide a condition that they can interact with the fatty acids in bacterial membranes, disrupting membrane integrity and increasing permeability in different types of bacteria [216]. At the same time, the positively charged CPC attributed to nitrogen binds to the bacterial surface, and its alkyl chains start penetrating the cell wall, disrupting ion and material exchange, which causes problems in membrane function and leads to bacterial death [217].

5.4.5 Antiviral Test

The antiviral activity of the electrospun mats was tested by assessing virus titers ($TCID_{50}$/mL) in different contact time (after 30 minutes and 2 hours of contact time). The highest reduction in viral titer among different samples including mats loaded with 4% and 8% EO, 0.5% CPC and CPC-4% EO-loaded mat was observed for the CPC-4% EO-loaded mat, showing approximately a 2.5-log reduction in comparison to the control group. Mats loaded with 4% and 8% EO without adding CPC also indicated small reduction in viral titer, around 1.5 logs, but they were less effective than the sample incorporating the combination of EO and CPC. Notably, the results indicated there is no significant difference between samples which tested in the two contact times, showing that most of the antiviral activity happened rapidly within the first 30 minutes.

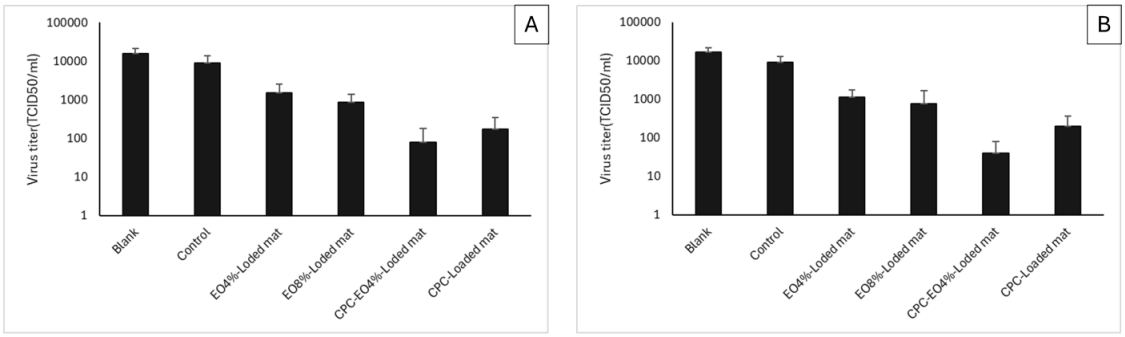

Figure 5.4 (A) Antiviral efficacy of electrospun mats containing 4% essential oil, 8% essential oil, 0.5% CPC and 4% essential oil combined with CPC after 30 minutes of contact time, (B) after 2 hours of contact time

5.4.6 Quantification of EO Release

The essential oil (EO) release profiles indicate different behaviors among electrospun mats with various structures and materials. A significant burst release was observed in the CA-EO mat during the first 5 days that the EO concentration rapidly increased from approximately 4 mg/L to nearly 9 mg/L. This rapid release is mainly attributed lack of a strong barrier, volatility and low binding

affinity and also the hydrophilic properties of cellulose acetate (CA), which provides penetration of water molecules to the fiber structure, and as result accelerating EO diffusion. After this initial burst, the release graph for CA-EO reach to plateau around 10–11 mg/L. In comparison, the PCL-EO mat exhibited a slower and more controlled release. At first the EO concentration was around 3 mg/L, this amount gradually increased to around 9–10 mg/L over 20 days. This behavior reflects the hydrophobic and semi-crystalline nature of polycaprolactone (PCL), which slows down EO diffusion through the fiber matrix. The CA/PCL blend mat showed intermediate behavior between CA and PCL. Its release profile climbed steadily from around 3.5 mg/L to approximately 9.5 mg/L, combining the water-penetration properties of CA with the barrier effect of PCL, resulting in a moderately controlled release without a sharp initial burst. However, in all single-fiber samples, including CA-EO, PCL-EO, and CA/PCL-EO, the absence of an encapsulating layer for controlling EO release caused an initial burst release and reaching to plateau in the release profile that was reached after around 20 days.

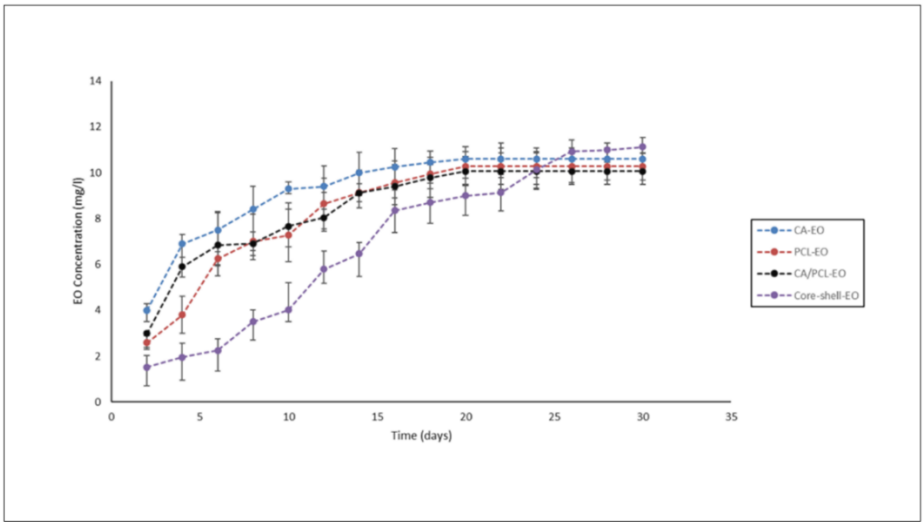

Figure 5.5 Evaluation of the release profile of essential oil (EO) encapsulated in single electrospun fibers of CA, PCL, CA/PCL blend, and in the core of core–shell CA-PCL fibers

Notably, the core-shell EO mat indicated the highest controllable release profile. In the start of assessment, the amount of EO was about 2 mg/L, the EO concentration increased slowly and persistently, approaching to 9–10 mg/L after 25–30 days. In this configuration of the fiber, the essential oil is encapsulated inside a core material, covered by a protective shell layer. The shell

acts as an efficient diffusion barrier, considerably decreasing burst release and providing a gradual, sustained delivery of EO over a longer period.

5.5 Conclusion

In this research, we successfully developed biodegradable electrospun mats incorporating eucalyptus essential oil (EEO) and cetylpyridinium chloride (CPC) as antibacterial and antiviral agents through single fibers of cellulose acetate (CA), polycaprolactone (PCL), CA/PCL blend, and core-shell configuration of fibers. Among the different fiber structures, core–shell fibers showed the highest encapsulation efficiency (EE) and demonstrated the most controllable release profile due to the presence of the shell layer in preserving the active agent. Antibacterial and antiviral tests showed that mats embedding both EO and CPC provided fast and considerable reductions in bacterial colonies (approximately a 2.5-log reduction against Staphylococcus aureus, Escherichia coli), and Human Coronavirus 229E within short contact times which is a critical factor in personal protective equipment. Furthermore, the incorporation of CPC as second antimicrobial agent in the fabricated mats provided the lower EO concentrations which is needed for antimicrobial performance. Additionally, core–shell fibers maintained surface hydrophilicity because of CA shell layer, while controlling EO diffusion over time. Overall, these results confirm that synergistic effect of EO encapsulation within a core–shell configuration with CPC as a promising approach for providing antimicrobial activity of mats in short contact time as well as prolonged release of EO which improved user comfort, making them suitable for protective and biomedical applications.

CHAPTER 6 ARTICLE 3: ENHANCED STABILITY AND CONTROLLED RELEASE OF EUCALYPTUS ESSENTIAL OIL VIA HALLOYSITE NANOTUBE ENCAPSULATION IN ELECTROSPUN MATS

Sheyda Kordjazi [a], Abdellah Ajji [a], Zahra Kordjazi [a]

[a] Department of Chemical Engineering, École Polytechnique de Montréal, Montréal, Québec H3T 1J4, Canada.

Submitted to *Applied Clay Science* on October 6, 2025

6.1 Abstract

This article studied the encapsulating of eucalyptus essential oil (EEO) into halloysite nanotubes (HNTs) to enhance stability of EEO and provide a controllable release. Electrospun cellulose acetate (CA) mats were fabricated through electrospinning method, incorporating free EEO (CA/EO) and EEO encapsulated in HNTs (CA/EO-HNT). The study assessed the impact of modification of HNTs on loading efficiency, EEO release from CA/EO and CA/EO-HNT mat, as well as antibacterial and antiviral efficacy of mats containing EEO. The results showed that modification of HNT considerably increased the EEO loading efficiency and improved the dispersion stability of HNTs in solution of electrospinning. The CA/EO-HNT mat provided a more controllable release of essential oil compared to the CA/EO mat, prolonged storage time and more controllable release during usage. Moreover, CA/EO-HNT mats demonstrated antibacterial and antiviral activity. These findings demonstrate that encapsulation of EEO into HNTs can effectively prolong the release of EO as antimicrobial agent from mats, proving their potential use for healthcare applications.

Keywords: Halloysite clay nanotubes; electrospun fibers; essential oil encapsulation; antibacterial and antiviral activity; biodegradable polymers; controlled release.

6.2 Introduction

The encapsulation of active agents has gained significant attention in recent years. Encapsulation includes designing systems that stabilize active compounds while preserving their chemical, physical, and biological characteristics. Generally, in the encapsulation technique, the active material (core material) is coated with one or a mixture of materials (shell materials). These processes are considered to control the release or delivery of the active compounds under determined conditions. Encapsulation methods have great potential to improve the efficiency, stability, and effectiveness of a wide range of products and applications [201, 218].

Generally, encapsulation techniques are classified into two main classes: physical and chemical encapsulation [201]. The physical methods including Vacuum-assisted loading [219] spray-drying [220] and freeze-drying [221, 222] which are the most popular techniques. Chemical encapsulation methods, on the other hand, include methods such as molecular inclusion [223], and co-crystallization [224].

Encapsulation process is widely applied in biology field [225, 226], food industry [226, 227], pharmaceuticals [221, 228], and agriculture [229], providing protection, stability, and controlled release of various active materials.

Among the different sensitive agents targeted for encapsulation, essential oils (EOs) have been significantly investigated. EOs are natural material, volatile liquids extracted from various parts of plants, including complex combination of lipophilic compounds [230, 231]. Due to their significant antimicrobial activity, essential oils are considered as promising alternatives approach to conventional antibiotics and chemical preservatives in industries [231]. However, there is a limitation that essential oils are sensitive to degradation when exposed to environmental factors such as light, oxygen, temperature fluctuations, and humidity [232], which prevent their direct use in productions [232]. Therefore, encapsulation strategies are considerably used to preserve the functional and biological properties of essential oils as well as to provide controlled release profiles [212].

Several studies have investigated the impact of encapsulation in enhancing the antimicrobial activity of active agents. For example, Amina L. Mohamed and colleagues encapsulated lemon oil and metal nanoparticles within a biopolymer matrix, significantly improving the antibacterial

performance of cellulosic fabrics against common pathogens [233]. In another study, Natsorn Watcharadulyarat et al. developed dextran-based nanoparticles for the encapsulation of ciprofloxacin (CIP), developing the stability of drug and achieving controlled release while keeping strong antimicrobial activity against oral pathogens and good biocompatibility with dental stem cells [234].

Among the different carriers employed for encapsulation, halloysite nanotubes (HNTs) have been introduced as an attractive material because of their biocompatibility [235], unique tubular structure [136, 236] and also low cost [155].

Halloysite nanotubes are naturally occurring nanoclays that include hydrous aluminosilicate with the general chemical formula $Al_2(OH)_4Si_2O_5 \cdot nH_2O$ [237]. They generally show tube lengths ranging from 0.2 to 1.5 μm, with inner diameters of 10–30 nm and outer diameters of 50–100 nm. The outer surface of HNTs is comprised of silica, while the inner lumen is formed predominantly of alumina [155, 238].

To improve their loading capacity, different modifications have been characterized, including alterations to the lumen surface functional groups [239], improving pore volume and surface area [240], and adjustments of surface charge [154]. For example, Cavallaro et al. modified the inner lumen of HNTs through adsorbing a perfluorinated anionic surfactant, resulting in a hydrophobic internal surface that improved the encapsulation efficiency and release of nonpolar compounds in aqueous environments [241]. In another study, Giuseppe Cavallaro and his team functionalized the outer surface of HNTs by employing cationic surfactant cetyltrimethylammonium bromide (CTAB), providing the selective loading of hydrophilic guest molecules into the lumen [242].

According to the literature, antimicrobial agent which is loaded to halloysite nanotubes (HNTs), providing controllable antimicrobial activity. For instance, cinnamon essential oil-loaded HNTs have been added into biodegradable films to improve active packaging systems [243]. In another study, erythromycin-loaded HNTs were incorporated into electrospun polycaprolactone (PCL) nanofibers, significantly enhancing antibacterial activity and improving the mechanical strength of the fibers [244].

In this study, we investigated the effect of halloysite nanotube (HNT) modification with an anionic surfactant on the loading efficiency of eucalyptus essential oil and its controlled release behavior in normal and under humid condition. The essential oil-loaded HNTs were subsequently

incorporated into electrospun CA mats, and the antibacterial and antiviral activities of the resulting mats were evaluated.

6.3 Materials and Methods

6.3.1 Materials

Sodium dodecyl sulfate (SDS) also known as sodium lauryl sulfate (SLS), cellulose acetate (CA; average molecular weight ~30 kDa), acetone (≥99.9%), N,N-dimethylacetamide (DMAC), ethyl alcohol anhydrous, eucalyptus essential oil, halloysite nanoclay (HNT), were purchased from Sigma-Aldrich. Beef extract powder, peptone powder, minimum essential medium eagle (EMEM), and fetal bovine serum (FBS) were all purchased from Sigma (Canada, ON).

6.3.2 Preparation of Eucalyptus-loaded Carrier

Vacuum pulling treatment was employed to load EEO into the HNT [245, 246]. Approximately, 5 mL of eucalyptus essential oil (EEO) was completely mixed with 15 mL of anhydrous ethanol by a vortex mixer. Subsequently, 1 gram of halloysite nano clay were added to the EEO solution and dispersed by sonication method using an ultrasonic instrument. The resulting suspension was placed to vacuum evacuation for 30 minutes at 25 °C, and then, return to atmospheric pressure. This vacuum cycle was repeated three times. After the final cycle, the EEO-loaded halloysite was washed with ethanol to remove any unencapsulated oil.

6.3.3 Preparation of Functionalized Nanotubes with Surfactant

Aqueous surfactant solutions were prepared by dissolving 5 g of surfactant (SDS) in 250 mL of deionized water. Subsequently, 5 g of halloysite nanotubes (HNTs) were added to the solution, and

the resulting dispersion was magnetically stirred at room temperature. After stirring, the functionalized HNTs were recovered and washed to remove any unbound surfactant from HNT, providing complete purification of the modified material [247]. The figure 6.1 shows the chemical structure of SDS and its interaction with the inner groups of HNTs during the functionalization process.

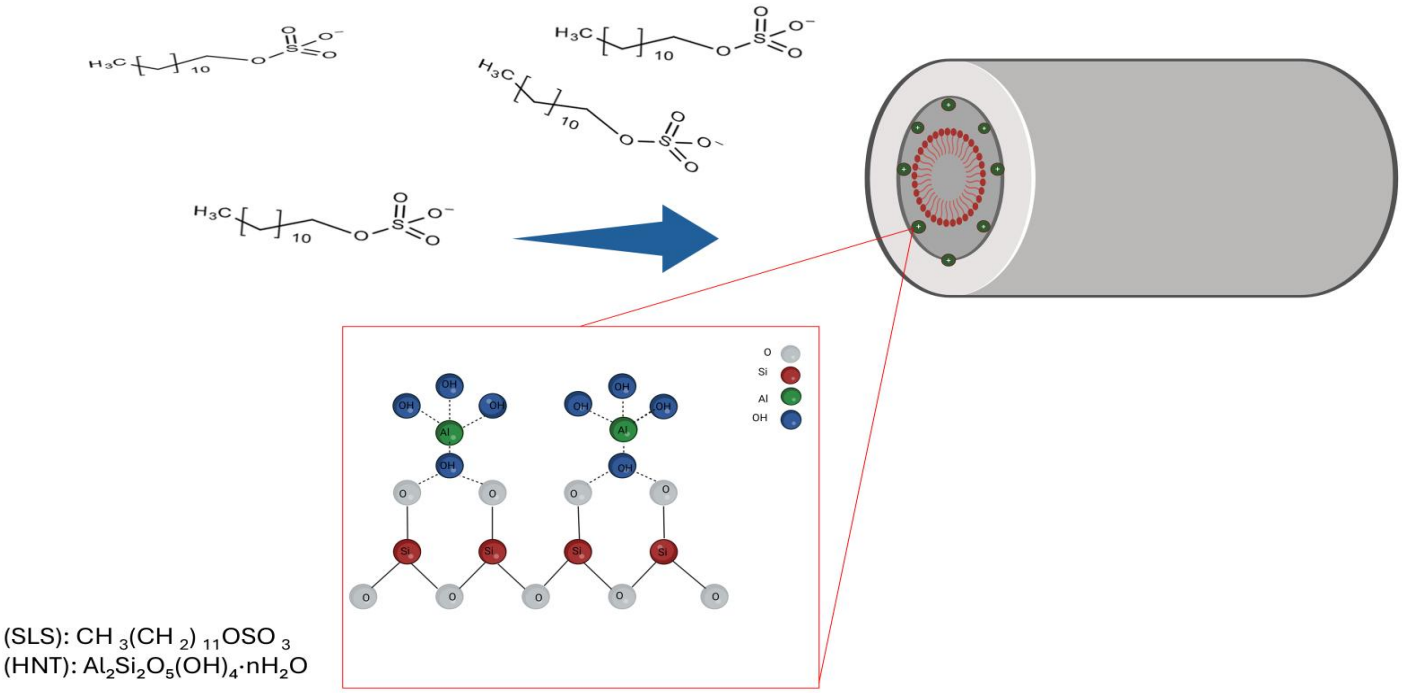

Figure 6.1 Schematic of SLS electrostatic interaction with halloysite nanotube (HNT)

6.3.4 FT-IR Analysis

To confirm that the modification of HNTs occurred and to identify the characteristic functional groups of SDS, FTIR spectroscopy was conducted. Spectra were recorded using a PerkinElmer spectrometer (Waltham, MA) with a resolution of 4 cm^{-1} and an accumulation of 32 scans, over a wavenumber range of 400–4000 cm^{-1}.

6.3.5 Thermal Analysis

To determine loading efficiency of the EEO before and after modification, thermogravimetric analysis (TGA) was employed by a thermogravimetric analyzer (TGA, Q-500, USA) under a nitrogen atmosphere with a constant flow rate of 50 mL/min. Approximately 8 mg of each material, including HNT, SLS, EO, and HNT loaded with EO and SLS, was heated from room temperature to 400°C at a steady heating rate of 20°C per minute. The weight loss of pure SLS, HNT, EO, and the HNT-loaded EO and SLS samples was measured from the thermogravimetric data.

6.3.6 Release Behavior in Ambient and High Moisture Condition

To quantify the release of essential oil (EEO) from HNT in different condition, ultraviolet-visible (UV-Vis) spectrophotometry was employed (using Tecan Infinite® 200 PRO, Switzerland) as an indirect technique. This test was performed under different humidity conditions; samples were exposed to 1) high humidity environments and 2) ambient condition. For the high humidity setup, a small volume of water was placed at the bottom of container, and the sample were placed on a stand above the water, ensuring they were only encounter by moisture and not direct contact with water.

At specific time, the samples were collected and mixed in ethanol under stirring in order that essential oil dissolve into the solvent completely. The ethanol solution including EEO were then transferred to a UV-Vis cuvette, and the absorbance was measured at the selected wavelength. Through a calibration curve, the concentration of essential oil in the solvent was calculated [243, 248].

6.3.7 Electrospinning of Fibers Incorporating EO-Loaded HNT

Cellulose acetate (CA) was dissolved in a solvent mixture of acetone and N,N-dimethylacetamide (DMAC) at a 2:1 (v/v) ratio to prepare a 17% (w/v) polymer solution. HNTs loaded Eucalyptus essential oil were then added to the polymer solution at a concentration of 10% relative to CA. Additionally, a sample composed of 17 wt% cellulose acetate (CA) and that 4 % essential oil with

respect to the polymer directly added to the electrospinning solution, was prepared to use as a comparative sample for evaluating the effect of encapsulation of EEO loading into HNTs. The resulting mixture was used for single electrospinning.

Table 6.1 Electrospinning solution compositions of CA-based fibers with varying EO and HNT content

Run	Polymer	Polymer Concentration%	EO-loaded HNTs %	Free EO %	Solvent System (v/v)	Purpose
R1	Cellulose Acetate (CA)	17	10	0	Acetone/DMAC (2:1)	Test sample with EO-loaded HNTs
R2	Cellulose Acetate (CA)	17	0	4	Acetone/DMAC (2:1)	Test sample with free EO (no HNTs)
R3	Cellulose Acetate (CA)	20	0	0	Acetone/DMAC (2:1)	Pure CA control (no EO or HNTs)

A vertical electrospinning setup (Tong Li Tech Co., Ltd., Shenzhen, China) was employed, and nanofibers were collected on a rotating drum covered with aluminum foil. Electrospinning was performed at a flow rate of 0.8 mL/h and 18 kV voltage was applied. The process was conducted under ambient conditions, with the air temperature maintained at 22 °C and relative humidity at approximately 50%.

6.3.8 Morphological Characterization

To investigate the morphology of electrospun fibers, with and without addition of halloysite nanotubes (HNTs), scanning electron microscopy (SEM) was employed. Fibers were collected on aluminum foil for 4 hours, then carefully removed and attached to carbon tape for imaging. SEM

analysis was performed using a high resolution microscope (Hitachi, Ltd., Tokyo, Japan) operated at an accelerating voltage of 15 kV.

In addition, transmission electron microscopy (TEM) was conducted using a JEOL JEM-F200 microscope to evaluate bead formation within the fibers and to determine the size of HNT. For TEM analysis, fibers were directly produced onto a copper mesh grid with a short time electrospinning of 3 seconds.

6.3.9 EEO Stability during Storage

To measure stability of EEO during storage, retention test was performed [248]. For this aim, mats containing EEO kept in open tubes and placed in the desiccator. Every 4 days, mats containing EEO (free EEO and EEO loaded into HNT in electruspun mat) cut into rectangular shape and were stirred in 10 mL of solvent (ethanol) and mixed at 150 rpm at room temperature for 6 hours. Then, a specific volume of the solution was collected and transferred to a cuvette for absorbance measurements in the 200–500 nm range using a UV-1800 spectrophotometer (Tecan Infinite® 200 PRO, Switzerland). The initial EEO content of the electrospun mats was first determined immediately after fabrication. The percentage of essential oils within the mats was calculated according to the absorbance data. A calibration curve was established using different EO solutions with various concentrations. A wavelength of 274 nm was determined to establish a standard calibration curve.

6.3.10 Antibacterial Efficacy Characterization

The antibacterial test was conducted according to the ISO 20743:2021 guidelines (Textiles — Determination of the antibacterial activity of textile products). To evaluate the antibacterial activity of samples including CA/EO and CA/EO-loaded HNTs, two types of bacteria, gram-positive (S. aureus) and gram-negative (E. coli), were used. The mats were cut and then were sterilized using UV light before immersing in bacterial solution. For bacteria solution, 5 µL of bacteria were added to 5 mL of LB medium and incubated at 200 rpm and 37°C for 18 hours. The bacterial solution

was adjusted to a concentration of 3-5 × 10^5 CFU/mL employing a spectrophotometer by setting OD600 to be equivalent to 1. To reach final concentration, Nutrient broth (NB) was used for dilution. After that, 5 µL of the prepared bacterial inoculum was poured onto the sample surface and 5 mL of NB was added to the vials containing samples. vials were incubated for 24 hours at 37°C and 90% relative humidity. After the incubation time, 500 µL of the solutions in the vials were added to 9.5 mL of Neutralizing Broth (D/E) and serial dilutions were conducted by adding 100 µL of the previous step's solution into 900 µL of phosphate-buffered saline (PBS). For counting bacterial colonies in Petri dishes, 100 µL of the diluted solution placed on agar plate and incubated for 24 h at 37 °C [186]. The experiment was repeated three times, and the average values were reported.

6.3.11 Antiviral Test

For antiviral testing, the procedure followed the ISO 18184:2019 protocol titled "Textiles — Determination of the Antiviral Activity of Textile Products." The antiviral activity of the samples was evaluated using Human Coronavirus 229E (HCoV-229E) and the MRC-5 human lung cell line and the method used in this study is the Median Tissue Culture Infectious Dose ($TCID_{50}$) technique [187]. Samples were sterilized by exposure to UV lamps for 20 minutes and placed into tubes. A volume of 100 µL of virus solution, with a concentration of 3 × 10^5 $TCID_{50}$/mL, was applied directly onto the sample surfaces. After the specified contact time (at 25°C and 2 hours contact time), a neutralizing solution was added and the solution vortexed, and the obtained solution was then serially diluted ten-fold using EMEM (Eagle's Minimum Essential Medium).

From each dilution, 100 µL was transferred to a 96-well plate containing a monolayer of MRC-5 cells which was prepared previously. The plates were incubated for 1 hour at 35°C under 5% CO_2, after that the virus solution was removed, the cells were washed, and fresh EMEM supplemented was added to support infected cell growth. The plates were incubated for 5 days at 37°C, and cytopathic effects (CPE) were observed under a microscope [186]. The viral titer ($TCID_{50}$) was calculated, and antiviral activity was determined through ISO 18184:2019 [187].

6.4 Results and Discussion

6.4.1 FT-IR Analysis

The FTIR spectra (Figure 6.2) confirms the successful modification of HNTs with SLS due to the appearance of absorption bands related to SLS functional groups. particularly, the peaks observed near 2920 cm^{-1} and 2850 cm^{-1} are attributed to the asymmetric and symmetric stretching vibrations of the $–CH_2$ groups from the long alkyl chains of SLS [249]. Additionally, the band at approximately 1220 cm^{-1} is related to the S=O stretching vibration of the sulfate groups present in SLS [250]. These characteristic signals do not exit in the pure HNT spectrum, but obviously appear in the HNT modified by SLS, showing the presence of SLS on the modified nanotubes.

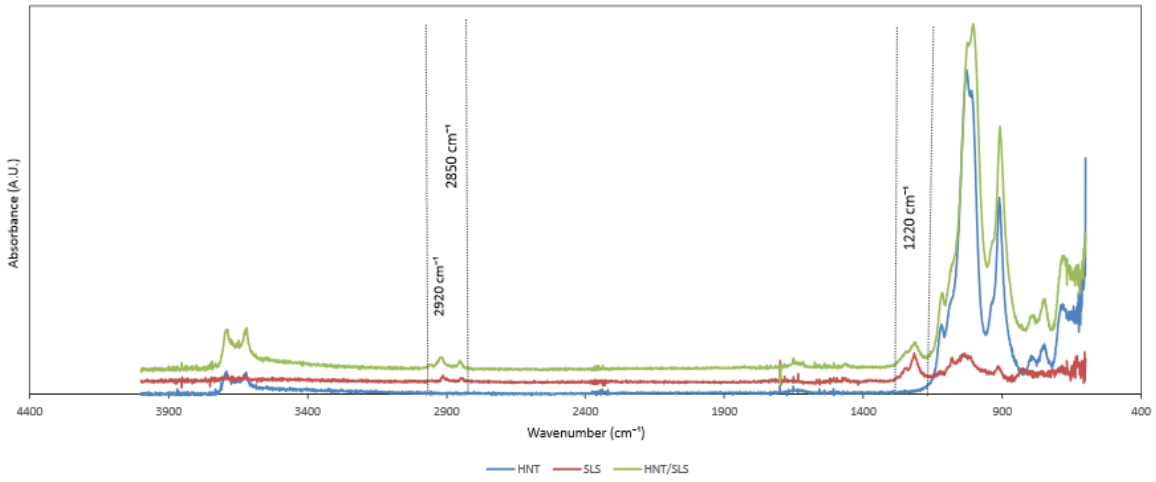

Figure 6.2 FTIR spectra of the HNT, SLS and HNT loaded SLS collected between 4000–400 cm-1

6.4.2 Thermogravimetric Analysis (TGA)

The TGA analysis (Figure 6.3) demonstrated considerable differences in the weight loss profiles of HNTs loading EO before and after modification with the anionic surfactant. HNTs before modification demonstrated minimal weight loss (around ~6%) below 200°C, reporting limited EO loading. This low loading efficiency can be related to two main factors: the capillary forces in HNT

that weakly hold guest molecules within the lumen and also the naturally hydrophilic property of the halloysite lumen, which reduces the affinity for hydrophobic compounds such as EO [155, 251, 252]. In contrast, SLS-modified HNTs exhibited significantly higher weight loss (~11%) over the same temperature range that confirmed that functionalization of HNT with SLS improved EO loading. This improvement is due to the surfactant's ability to provide a hydrophobic inner environment, effectively transforming the nanotube into a sponge-like structure that can absorb and retains hydrophobic EO molecules.

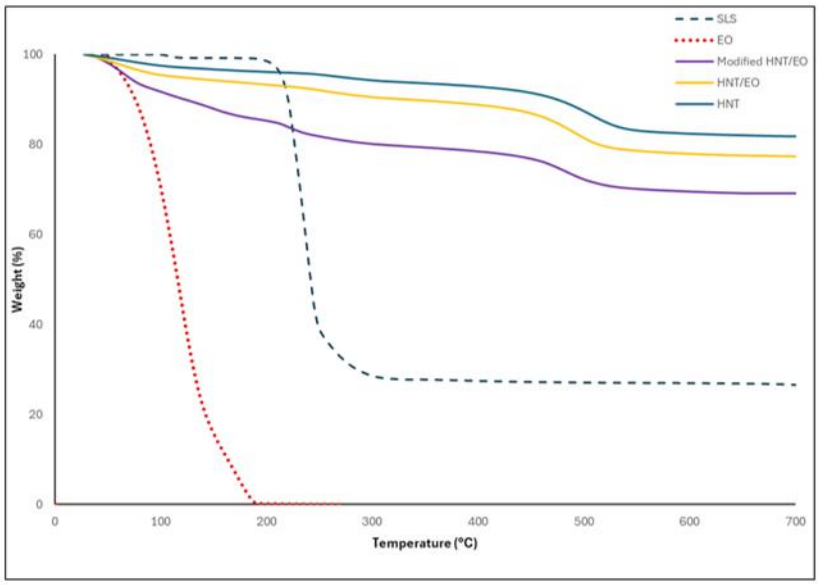

Figure 6.3 Thermogravimetric analysis (TGA) curves of pure HNT, HNT loaded EO, modified HNT loaded EO, EO and SLS surfactant

6.4.3 Morphological Characterization of Halloysite Nanotubes (HNTs)

To determine physical properties of selected carrier, Transmission electron microscopy (TEM) was conducted to measure and observe the physical properties of HNT. The measured characteristics, including the average length and diameter of HNTs, are summarized in Table 6.2.

Table 6.2 Summary of physical properties of halloysite nanotubes (HNTs)

Material	Average length	Average diameter	Linear Formula
Halloysite nanoclay (HNT)	400 ± 50 nm	70 ± 10 nm	$Al_2Si_2O_5(OH)_4 \cdot 2\ H_2O$

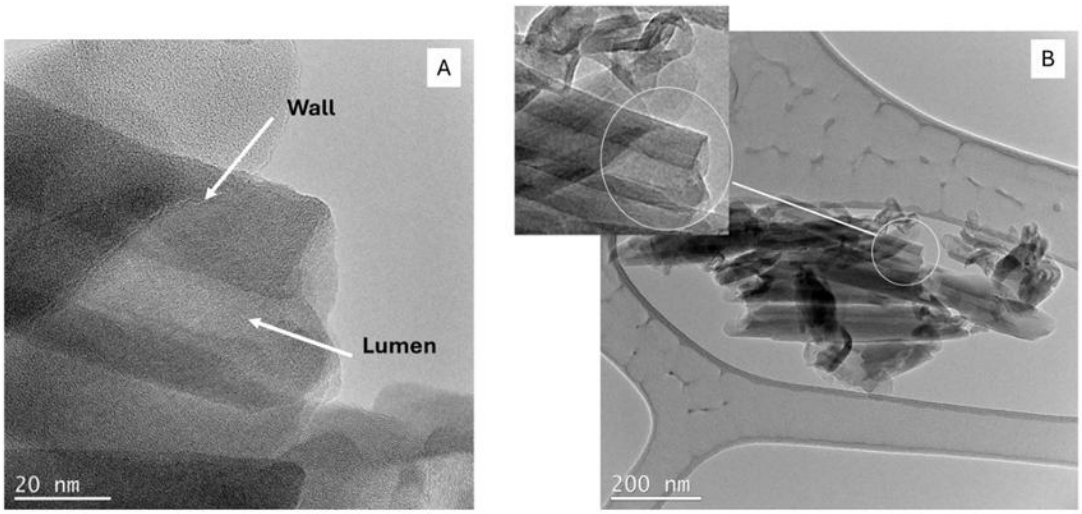

Figure 6.4 TEM images of halloysite nanotubes (HNTs): (A) high-magnification image (tubular structure with a visible lumen and wall); (B) overall view of HNTs morphology

Figure 6.4 (TEM imaging) clearly demonstrates the tubular structure of the halloysite nanotubes, with visible and intact lumens. These images confirms that the nanotubes maintain their structural integrity, providing their potential for effectively encapsulating essential oils during processing.

6.4.4 Morphological Characterization of Electrospun CA/HNT Fibers

Figure 6.5 shows SEM images of electrospun cellulose acetate (CA) fibers incorporating halloysite nanotubes, before and after surface modification of the HNTs. In the image A, several dark spots

observed within the fiber in the mat, which were likely formed because of the aggregation of HNTs during electrospinning. These accumulations showed poor dispersion ability of the nanotubes in the solution. However, after surface modification of the HNTs and their incorporation into the electrospinning solution, these dark spots are significantly reduced, as seen in image B. This improvement is mainly attributed to introducing electrostatic repulsive forces by the SLS which functionalized HNTs, and reduces the tendency of the nanotubes to aggregate [253]. As a result, the HNTs are more uniformly dispersed within the fiber structure, developing the overall quality of the electrospun mat. Uniform dispersion is important for filtration application, as HNT agglomeration can cause structural defects and block pores. Therefore, these blocking points negatively affecting breathability and filtration performance. Moreover, homogeneous dispersion of EO-loaded HNTs provides a controlled and sustained release of EO across the entire mat surface, that ensure consistent antimicrobial activity. This feature is important factor for face mask applications, where sustained protection is needed.

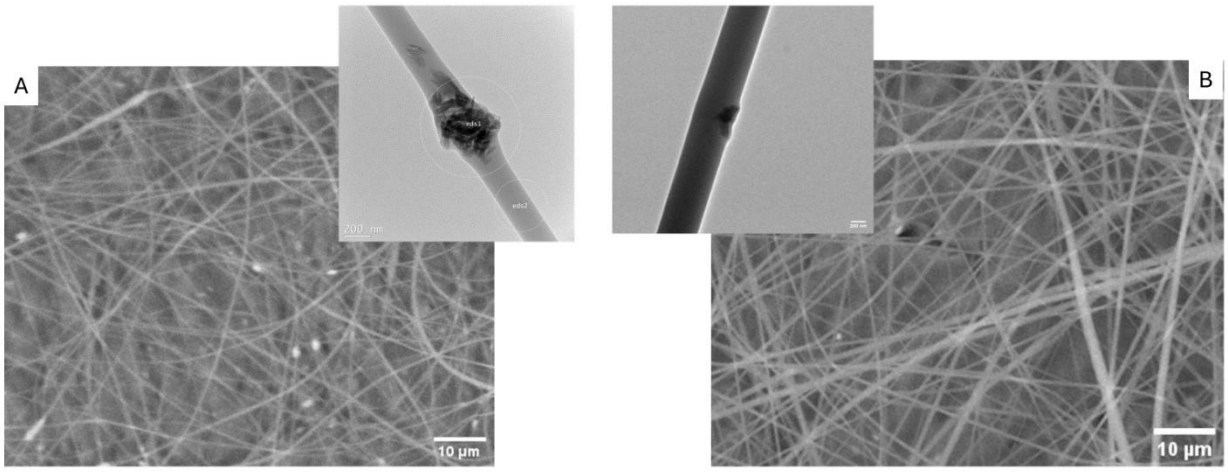

Figure 6.5 . SEM images of electrospun CA fibers containing (A) unmodified HNTs and (B) modified HNTs added to the spinning solution.

To confirm that the observed dark spots in the electrospun fibers SEM images were not polymeric beads and they were HNT accumulations, TEM-EDS characterization was conducted. Although

the accumulation of HNT is obvious in TEM image, the EDS spectra confirmed their presence. As shown in the Figure 6.6, EDS spectra were taken from two distinct regions: the dark spot (EDS1) and the surrounding fiber (EDS2). The EDS1 spectrum demonstrates clear peaks for aluminum (Al) and silicon (Si), which are characteristic elements of HNT. In contrast, EDS2 did not show an Al peak, showing that the surrounding fiber is free of HNTs. These results verify that the dark spots correspond to HNT agglomerates embedded within the fibers rather than bead defects from the electrospinning process.

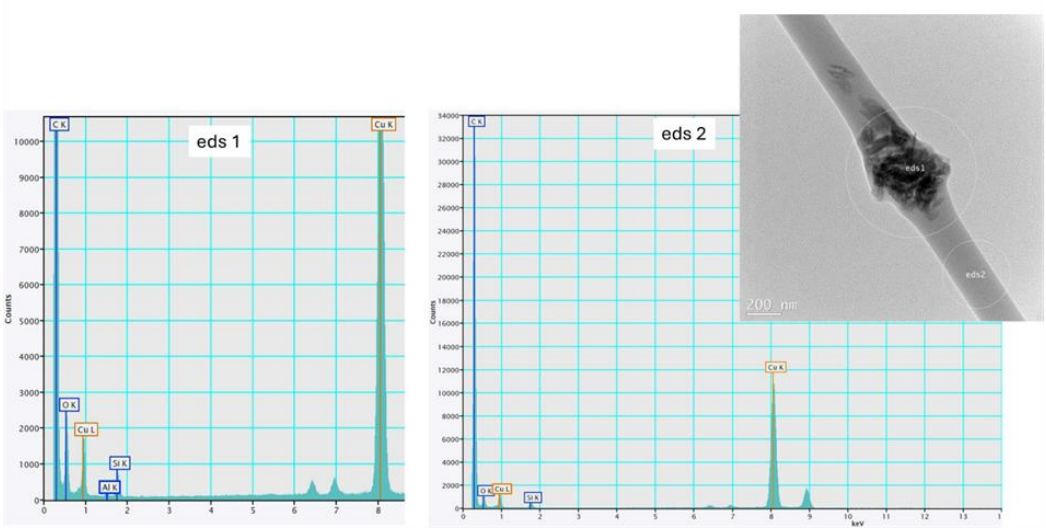

Figure 6.6 TEM image and EDS spectra of electrospun fiber

6.4.5 Release Behavior of EO in Ambient and High Moisture Condition

Figure 6.7 demonstrate the indirect study of the release behavior of encapsulated EEO from HNTs under two different conditions: humid and ambient. Over a period of 60 hours, the remaining amount of EEO in HNT was higher in ambient conditions compare to HNT in humid condition, indicating slower release of EEO from the nanotube in ambient condition compared to the humid environment. In humid conditions, the EEO concentration in the HNT decreased significantly over time, from approximately 29 mg/L to 6 mg/L, showing faster release. In contrast, under ambient

conditions, the EEO concentration decreased more gradually, from about 30 mg/L to 13 mg/L due to the fact that HNTs can preserve EEO more efficiently in less humid environments.

This behavior is regarding to the adsorption of water molecules into the HNT lumen and interact with the inner surface through hydrogen bonding. These interactions reduce the EEO attachment inside the nanotube and increase the release [254]. In applications such as face masks, where antimicrobial activity of EEO is needed in high moisture condition, because of exhalation, this property can be considered a positive property, as HNTs can provide a greater amount of EEO under this condition.

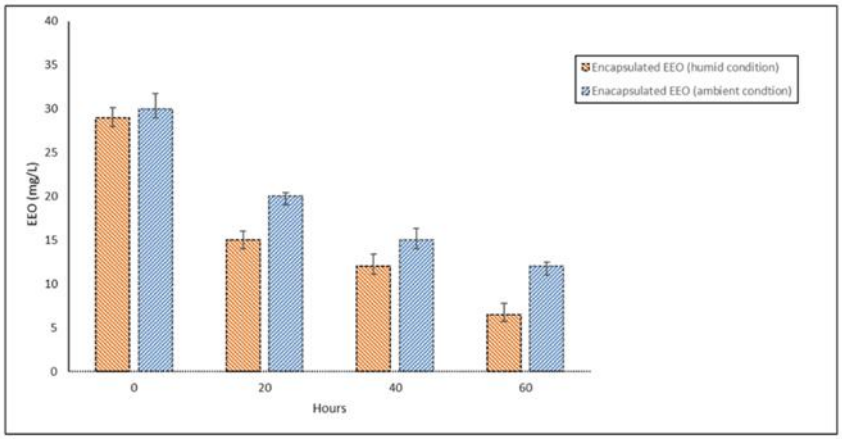

Figure 6.7 Release Behavior of Encapsulated Eucalyptus Essential Oil (EEO) from HNT under Different Humidity Conditions

6.4.6 EEO Stability during Storage

Figure 6.8 demonstrates the release profile of eucalyptus essential oil over a 28-day period for two sample groups: CA/EO and CA/EO-loaded HNTs. According to the graph there is an obvious difference in release behavior between the two groups of samples over time.

As shown in the graph, the CA/EO sample demonstrated a rapid release of essential oil. The remaining EO in the electrospun mat reduced to near 60% by day 3, 45% by day 7, and dropping below 10% by day 28. This sharp decline shows the high volatility and limited stability of the essential oil when directly added to the electrospinning solution.

In contrast, the CA/EO-loaded HNTs demonstrated a higher controllable release rate. After 3 days, EO retention percentage was around 70, and by day 10 approximately 55% of EO detected in the sample. By the end of the 28-day period, 20 % of essential oil remained in the CA mat. This sustained release behavior confirms that halloysite nanotubes are effective in providing controllable release of essential oils over time.

These results show that encapsulating EEO in HNTs improved its retention, providing a more controlled and extended release profile; however, both methods, encapsulation in HNT and adding essential oil in electrospinning solution, successfully prolonged EO retention, as essential oils generally show rapid evaporation when not encapsulated.

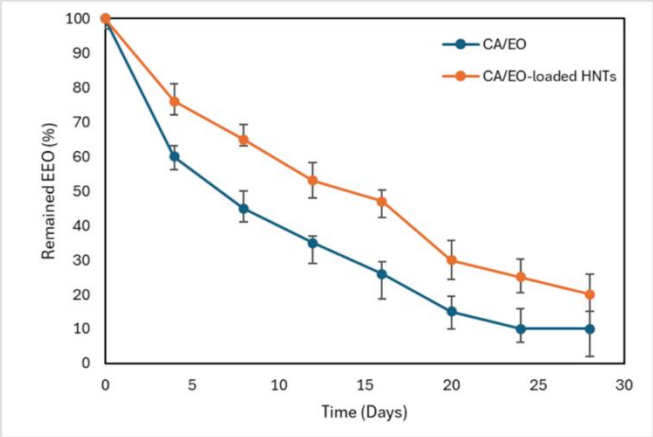

Figure 6.8 EO retention over 28 days comparing CA/EO-loaded HNTs with CA/EO

6.4.7 Determination of Antimicrobial Effect of Electrospinning Mat

The antibacterial activity of the CA/EEO mat and the CA/EEO-loaded HNTs mat against Escherichia coli and Staphylococcus aureus was evaluated, and the results are presented in the Figure 6.9.

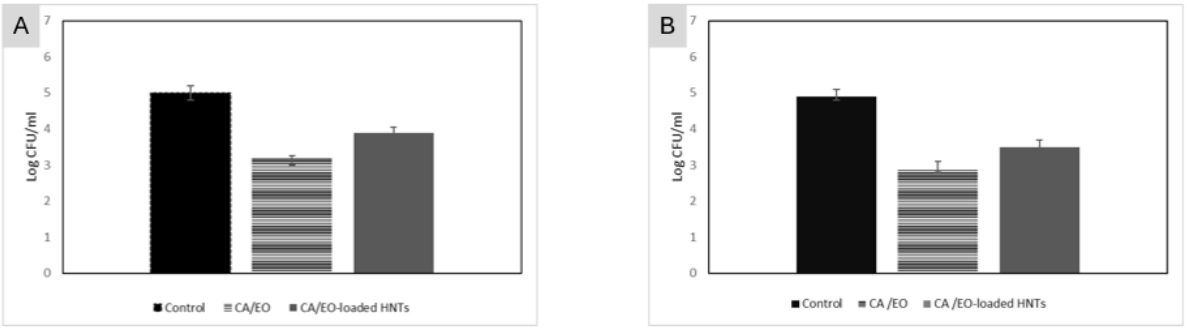

Figure 6.9 Antibacterial efficacy of CA/EO and CA/EO-loaded HNTs against (A) E. coli and (B) S. aureus

Based on the results, the control samples showed the highest bacterial counts, showing no inherent antibacterial activity. In comparison, the CA/EO samples reduced bacterial growth, providing near 2-log reduction for S. aureus and E. coli.

The CA/EO-loaded HNTs samples also illustrated antibacterial activity, showing approximately a 1–1.5 log reduction for E. coli (A) and S. aureus (B). However, their antibacterial effect was lower than that of the CA/EO mats, mainly because of the smaller amount of essential oil exist in the samples. It could be suggested that improving the antibacterial activity of CA/EO-loaded HNTs by combining this method with a second antimicrobial agent may create a synergistic effect, achieving more than a 2-log reduction in bacterial count.

6.4.8 Antiviral Evaluation

The antiviral efficacy of the samples including CA/EO and CA/EO-loaded HNTs was assessed, and the results are presented in Figure 6.10.

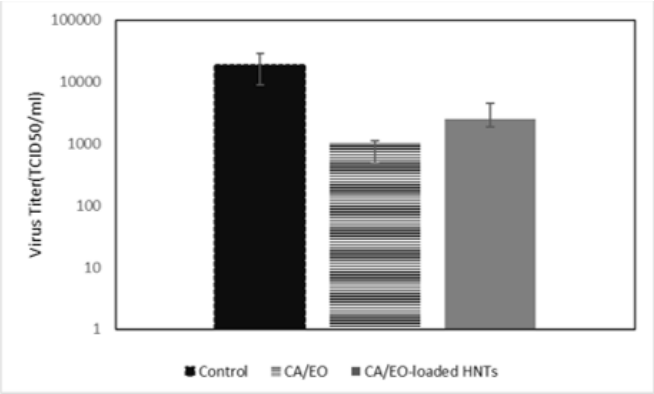

Figure 6.10 Antiviral efficacy of electrospun mats including CA/EO and CA/EO-loaded HNTs

According to the results, both samples, including sample that EO directly added to the solution and those where EO was encapsulated in HNTs and then incorporated into the solution, showed antiviral activity. CA/EO provided approximately 1.5-log reduction, while CA/EO-loaded HNTs were less effective in comparison, achieving near a 1-log reduction. The antiviral activity of essential oils is mainly due to their ability to disrupt the viral envelope, damage the capsid, and prevent the virus from attaching to host cell receptors. Additionally, they can interfere with the viral replication process [255]. Although adding HNTs containing EO can offer slight antiviral activity against human coronavirus 229E (HCoV-229E), suggesting the need for incorporating a second antimicrobial agent to enhance the antimicrobial properties of the mat.

6.5 Conclusion

The results of this article show that encapsulating eucalyptus essential oil (EEO) in halloysite nanotubes (HNTs) is an effective strategy to control the release of EEO and prolong the storage period of electrospun cellulose acetate (CA) mats. Surface modification of HNTs with sodium dodecyl sulfate (SDS), an anionic surfactant, improved EO loading by approximately 6%. This improvement is regarded to the hydrophobic tail of SDS, which form a condition in the lumen of

the nanotubes, developing EEO absorption as hydrophobic compound. Additionally, the modification increased dispersion stability behaviour of HNT, which is crucial property for maintaining a uniform electrospinning solution and preventing nozzle blockage during fiber formation.

Release tests showed that EEO release from HNTs was accelerated under high humidity conditions. This characteristic is particularly appropriate for applications such as face masks, where high moisture from exhalation can trigger increased EO release during usage. Antibacterial and antiviral evaluations showed that while mats containing EO-loaded HNTs provided lower antibacterial and antiviral activity compared to mats with EO directly added but it can be effective in prolonged release. Therefore, they can be considered as secondary antimicrobial agents for synergistic effects. These findings demonstrate the importance of encapsulation of sensitive agents like essential oil in preserving the long-term functionality, supporting their application in different fields such as personal protective equipment, medical textiles, and active packaging.

CHAPTER 7 GENERAL DISCUSSION

This study developed and evaluated advanced cellulose acetate (CA)-based electrospun mats incorporated with antimicrobial agents for face mask applications, with the main objective of enhancing antimicrobial properties and prolonging the usability of face masks. The design of the mats focused on three key factors: the processability of coaxial fibers, the synergistic effects enabling rapid antibacterial and antiviral activity, and the controlled release of essential oil as antimicrobial agents through encapsulation method. The processability of coaxial electrospun mats encompassed four major aspects: (i) fabrication of core–shell configurations using a solution coaxial electrospinning method, (ii) maintaining the hydrophilic properties of the mat while controlling the degree of swelling under high-moisture conditions, (iii) improving the mechanical properties of the mat, and (iv) achieving controlled release of essential oils during processing, storage, and use. Assessing the synergistic effects involved in using two different antimicrobial agents, CPC and essential oils (EOs), which have different mechanisms for microorganism deactivation and structural destruction and differ in molecular size. The antimicrobial activity was assessed when each agent was used individually and together at different contact times to analyze whether their combined use could decrease the time needed for deactivation. In addition, controlled release was investigated, with the final objective of assessing EO encapsulation within halloysite nanotubes (HNTs) and assessing the effect of HNT modification on increasing encapsulation efficiency and release behavior.

Our initial investigations involved developing core–shell fibers fabricated by cellulose acetate (CA) as the shell and polycaprolactone (PCL) as the core. This design provides appropriate hydrophilic properties, which are necessary for the final application as a filtration mat in the middle layer of a face mask. With these hydrophilic properties, the mat can absorb droplets from exhalation that may contain bacteria and viruses. Moreover, because of the presence of PCL with hydrophobic properties, the design provides a controllable degree of swelling when exposed to high-moisture conditions. In this design, we have both a hydrophilic surface of the mat and controllable swelling, which helps maintain the structure of the mat in real situations. In this way, the structure of the mat remains stable in high-humidity environments. Some studies have reported that the application of

filtration mats is reduced by excessive hydrophilicity, which reduces their filtration performance under humid conditions [39].

We identified key factors influencing core–shell fabrication, including the polymer concentration in the solution and solvent evaporation rate. Particularly, the mechanical properties of the coaxial electrospun mat improved with the presence of PCL in the core, and the degree of swelling was reduced compared to pure cellulose acetate mat. Interestingly, contact angle measurements of pure CA mats and coaxial mats revealed similar values, which was attributed to the presence of the CA shell layer. In addition, the results of this study confirmed that incorporating cetylpyridinium chloride (CPC) into the mat provided antimicrobial activity; however, at short contact times, the performance was limited to approximately a one-log reduction. This limitation is highly debatable and should be considered in face-mask applications. It should be addressed, as it is vital that the mask provides antimicrobial properties and protects users from harmful microorganisms from the moment it is worn, where rapid deactivation of bacteria and viruses is required.

The second phase of the research aimed to reduce the contact time required for antimicrobial agents to effectively inactivate bacteria and viruses by incorporating two different agents: eucalyptus essential oil (EEO) and CPC. This investigation provided critical insights into the relationship between contact time and antimicrobial activity of the mat. The synergistic effect of combining EEO and CPC reduced the required contact time to achieve a two-log reduction in antibacterial and antiviral test. The reason behind choosing these types of antimicrobial agents was their different mechanisms of action. CPC has a positive charge that can be attracted to the negatively charged phospholipids of bacteria and viruses; upon penetration of the alkyl chain, it disrupts and destroys the bacterial or viral membrane. In contrast, essential oils consist of smaller molecules and, due to their hydrophobic structure, can penetrate the hydrophobic phase of bacteria and virus. Together, these mechanisms are likely to reduce the contact time required for microbial deactivation. Moreover, the core–shell structure provided more controlled release of EEO compared to cellulose acetate fibers or CA/PCL blends over a period of 30 days as the shell layer protect essential oil and reduce the speed of evaporation of EO. The encapsulation efficiency of EEO during the electrospinning process was significantly higher in coaxial mats, reaching approximately 80%, which is much higher than in single electrospun fibers. This confirmed that incorporating EEO into

the core in core-shell fibers resulted in a more efficient and stable active electrospun mat compared to single electrospinning fiber.

The third phase of this study focused on the investigation of an encapsulation method to load EEO into halloysite nanotubes (HNTs). This strategy allowed us to study the impact of encapsulation on the release behavior of EEO in different humidity condition and its impact on increasing storage period. Moreover, the effect of HNT modification with an anionic surfactant, sodium lauryl sulfate (SLS), was evaluated. With modification of HNTs, the loading efficiency of EO doubled, as SLS with an anionic charge adsorbed inside the lumen, which has a positive charge, and provided a hydrophobic environment, similar to a sponge, for improved absorption of EO, which has a hydrophobic structure. The results confirmed that encapsulation of EEO in HNTs provided a controllable release profile for up to 30 days that humidity increased the release rate of EEO. Furthermore, modification of HNTs, enhanced dispersion stability of HNTs in the electrospinning solution, which is vital for the electrospinning process and uniform incorporation of HNTs in the mat. In this way, blocking points that might be created due to HNT agglomeration are reduced, which can increase breathability, as no significant blocking exists within the fiber structure.

In summary, these investigations demonstrated that a hydrophilic mat with a controllable degree of swelling was achieved by strategically using CA and PCL in a coaxial fiber structure. Existence of a shell layer and the encapsulation of essential oils in HNTs allowed adjustment of the release rate, with environmental conditions playing a crucial role. For example, high humidity was found to increase the release of EEO from HNTs. The relationship between EEO release and relative humidity is specifically important for the face mask application, as it can trigger release of antimicrobial agents only during mask use. Furthermore, this study confirmed the synergistic effect of combining EEO and CPC against Escherichia coli, Staphylococcus aureus, and coronavirus at short contact time. The presence of both agents resulted in more than a two-log reduction within a short exposure time, showing the efficacy of this approach in enhancing antimicrobial properties for mask wearers.

A significant advantage of this research is its holistic approach, which addresses not only the fundamental aspects of desired physical and antimicrobial properties of the mat required for face mask applications, but also contributes to resolving environmental challenges. By utilizing

biodegradable polymers and increasing the effective usage period of face masks, this study presents a positive step toward reducing waste generated by the use of personal protective masks.

CHAPTER 8 CONCLUSION AND RECOMMENDATIONS

8.1 Conclusion

This study successfully developed a novel core–shell electrospun mat fabricated from cellulose acetate (CA) as the shell and polycaprolactone (PCL) as the core, as well as incorporating cetylpyridinium chloride (CPC) and eucalyptus essential oil (EEO) as antibacterial and antiviral agents. The fabricated mat provided ideal properties for face mask applications, such as low degree of swelling in high moisture condition, enhanced mechanical properties, controllable release of EEO, and effective antibacterial and antiviral activity with considering short contact times. The study was conducted through three main categories, and the key findings are summarized below.

The first study investigated the feasibility of fabricating core-shell fibers through coaxial electrospinning, cellulose acetate (CA) as the shell and polycaprolactone (PCL) as the core. Different solvents and polymer concentrations were tested for their impact on spinnability and fiber morphology. CPC (cetylpyridinium chloride) was incorporated as an antibacterial and antiviral agent into the fiber. Key findings are below:

- Core-shell fiber formation was successfully achieved employing biodegradable polymers (CA and PCL) with appropriate solvents (acetone and DMAC), which provided optimum viscosity and balanced evaporation rates.
- The fabricated fibers demonstrated moisture resistance in high humidity condition because of the hydrophobic nature of PCL in the core, simultaneously the fibers keeping their hydrophilic surface characteristic attributed to presence of CA in the shell.
- The using of PCL in the core of the fiber enhanced the mechanical properties of the mats, improving tensile strength and elongation at break which is important factor for prolonged mask usage.
- CPC-loaded mats demonstrated antibacterial activity against both Gram-positive and Gram-negative strains, as well as antiviral performance; however, the antimicrobial activity was limited during short contact time.

The second study investigated the effect of combining eucalyptus essential oil (EEO) and CPC, as a secondary antimicrobial agent into the mat. The study evaluated antimicrobial properties of CPC and EEO in various contact times and also assessed EEO release behavior in different methods including, single electrospinning (CA, PCL, and their blend) and coaxial electrospinning. Important results:

- Core-shell fibers showed the most sustained EEO release profile, because of the shell layer in the structure of fiber, providing a slow release of agent up to 30 days.
- Combining two different types of antimicrobial agents, CPC and EEO, demonstrated a strong synergistic effect, with more than a 2-log reduction in bacterial and viral activity within short contact times.

The final step of the study focused on encapsulating EEO into halloysite nanotubes (HNTs) as a carrier for improving stability and controlled release of EEO. Key findings included:

- Mats incorporating EEO-loaded HNTs provide more controllable release in longer storage period in comparison to the mat where EEO was added directly to the spinning solution.
- Loading efficiency of EEO into HNT and dispersion stability of nanotubes was significantly increased through HNTs modification using an anionic surfactant.
- EEO release from HNTs increased under high moisture conditions, showing moisture can trigger release of EEO during mask usage which the humidity is high due to exhalation.

In conclusion, this research suggests a novel way for designing biodegradable electrospun mats with improved antimicrobial performance, developed mechanical properties, and moisture resistance characteristics. The findings confirm the advantageous of using different kind of antimicrobial agents (CPC and EEO), controlled release systems (core-shell fiber configuration and HNT encapsulation), and moisture-responsive functionality. These insights not only improve our approach for providing antimicrobial activity of mats which are active in short contact time but also offer a practical framework for developing antimicrobial face masks for prolonged usage. Moreover, using biodegradable polymers for fabrication of coaxial fibers in this study, contributes valuable knowledge toward reducing environmental impact while developing product performance.

8.2 Recommendations

While this research offered a comprehensive study for developing biodegradable coaxial fibers for face mask application with synergistic antibacterial and antiviral properties, further work is recommended to extend and deepen the findings and results:

- Investigate the effect of different ratio of CA (shell) to PCL (core) on the release rate of EEO and mechanical performance, particularly under high moisture condition.

- Develop a predictive model for EEO release from core-shell mats based on different factors including humidity, temperature, thickness of the wall, to give information for different applications.

- Perform trials employing needleless or multi-jet electrospinning process to assess the scalability of producing uniform, high quality mats in commercial scale.

- Compare HNTs with other nano carriers in terms of loading efficiency of agents into carriers, release profile, and compatibility with electrospinning

- Investigate the effect of other essential oils such as thymol or combinations of EOs for synergic effect of antibacterial and antiviral activity

- Investigate the biodegradability of the developed electrospun mats in relevant environmental and physiological conditions to better assess their environmental impact and suitability for disposable face mask applications

REFERENCES

1. Pullangott, G., et al., *A comprehensive review on antimicrobial face masks: an emerging weapon in fighting pandemics.* 2021. **11**(12): p. 6544-6576.
2. Rahman, M.Z., et al., *Face masks to combat coronavirus (covid-19)—processing, roles, requirements, efficacy, risk and Sustainability.* 2022. **14**(7): p. 1296.
3. *XinhuaNet. China's daily mask output exceeds 110 million units. Beijing:*

Xinhua News Agency; 2020. 2020.

4. Ajaj, R., et al., *Understanding the environmental impacts of facemasks: a review on the facemask industry and existing life cycle assessment studies.* 2023. **33**(1): p. 1-19.
5. Tuñón-Molina, A., et al., *Protective face masks: current status and future trends.* 2021. **13**(48): p. 56725-56751.
6. Wang, A.-B., et al., *A review of filtration performance of protective masks.* 2023. **20**(3): p. 2346.
7. Chatterjee, P., et al., *Healthcare workers & SARS-CoV-2 infection in India: A case-control investigation in the time of COVID-19.* 2020. **151**(5): p. 459-467.
8. Soleman, S.R., et al., *Efficacy of personal protective equipment to prevent environmental infection of COVID-19 among healthcare workers: a systematic review.* 2023. **28**: p. 1-1.
9. Liang, M., et al., *Efficacy of face mask in preventing respiratory virus transmission: A systematic review and meta-analysis.* 2020. **36**: p. 101751.
10. Abboah-Offei, M., et al., *A rapid review of the use of face mask in preventing the spread of COVID-19.* 2021. **3**: p. 100013.
11. Mukhopadhyay, A.J.T.P., *Pulse-jet filtration: An effective way to control industrial pollution Part II: Process characterization and evaluation of filter media.* 2010. **42**(1): p. 1-97.
12. Adanur, S. and A.J.J.o.I.T. Jayswal, *Filtration mechanisms and manufacturing methods of face masks: An overview.* 2022. **51**(3_suppl): p. 3683S-3717S.
13. Tcharkhtchi, A., et al., *An overview of filtration efficiency through the masks: Mechanisms of the aerosols penetration.* 2021. **6**(1): p. 106-122.
14. Lee, K., B.J.A.S. Liu, and Technology, *Theoretical study of aerosol filtration by fibrous filters.* 1982. **1**(2): p. 147-161.
15. Mao, X. and A.E.J.P.R.F. Hosoi, *Estimating the filtration efficacy of cloth masks.* 2021. **6**(11): p. 114201.
16. Cho, H.-w., et al., *Comparison of pressure drop and filtration efficiency of particulate respirators using welding fumes and sodium chloride.* 2011. **55**(6): p. 666-680.
17. Adanur, S., *Wellington Sears handbook of industrial textiles*. 2017: Routledge.
18. Seidi, F., et al., *Functionalized masks: powerful materials against COVID-19 and future pandemics.* 2021. **17**(42): p. 2102453.

19. Wibisono, Y., et al., *Facile approaches of polymeric face masks reuse and reinforcements for micro-aerosol droplets and viruses filtration: A review.* 2020. **12**(11): p. 2516.

20. Adomavičiūtė, E. and R.J.F.T.E.E. Milašius, *The influence of applied voltage on poly (vinyl alcohol)(PVA) nanofibre diameter.* 2007. **15**(5-6): p. 63.

21. Bhardwaj, N. and S.C. Kundu, *Electrospinning: A fascinating fiber fabrication technique.* Biotechnology Advances, 2010. **28**(3): p. 325-347.

22. Avossa, J., et al., *Electrospinning based on benign solvents: current definitions, implications and strategies.* 2022. **24**(6): p. 2347-2375.

23. Song, J., M. Kim, and H.J.P. Lee, *Recent Advances on nanofiber fabrications: Unconventional state-of-the-art spinning techniques.* 2020. **12**(6): p. 1386.

24. Maduna, L. and A.J.P. Patnaik, *Challenges associated with the production of nanofibers.* 2024. **12**(10): p. 2100.

25. Zhang, K., et al., *A new magnetic melt spinning device for patterned nanofiber.* 2021. **11**(1): p. 8895.

26. Khandaker, M., et al., *Use of polycaprolactone electrospun nanofiber mesh in a face mask.* 2021. **14**(15): p. 4272.

27. Hutten, I.M., *Handbook of nonwoven filter media*. 2007: Elsevier.

28. Bandi, M.J.P.o.t.R.S.A., *Electrocharged facepiece respirator fabrics using common materials.* 2020. **476**(2243): p. 20200469.

29. Lee, S.J., et al., *The use of thermal treatments to enhance the mechanical properties of electrospun poly (ε-caprolactone) scaffolds.* 2008. **29**(10): p. 1422-1430.

30. Midha, V., A.J.J.o.t.e. Dakuri, and f. technology, *Spun bonding technology and fabric properties: a review.* 2017. **1**(4): p. 1-9.

31. Agarwal, S., J.H. Wendorff, and A.J.P. Greiner, *Use of electrospinning technique for biomedical applications.* 2008. **49**(26): p. 5603-5621.

32. Naragund, V.S. and P.J.E.m. Panda, *Electrospun nanofiber-based respiratory face masks—A review.* 2022. **5**(2): p. 261-278.

33. Fadare, O.O. and E.D.J.T.S.o.t.t.e. Okoffo, *Covid-19 face masks: A potential source of microplastic fibers in the environment.* 2020. **737**: p. 140279.

34. Shanmugam, V., et al., *Potential natural polymer-based nanofibres for the development of facemasks in countering viral outbreaks.* 2021. **138**(27): p. 50658.

35. Kai, D., et al., *Biodegradable polymers for electrospinning: Towards biomedical applications.* 2014. **45**: p. 659-670.

36. MOL, Ġ.Y., et al., *ELECTROSPINNING OF ANTIBACTERIAL CELLULOSE ACETATE NANOFIBERS.*

37. Kadam, V., et al., *Gelatin/β–Cyclodextrin Bio–Nanofibers as respiratory filter media for filtration of aerosols and volatile organic compounds at low air resistance.* 2021. **403**: p. 123841.

38. Wang, Z., et al., *A versatile Silk Fibroin based filtration membrane with enhanced mechanical property, disinfection and biodegradability.* 2021. **426**: p. 131947.

39. Ferreira, C.A., et al., *Advanced Face Mask Filters Based on PCL Electrospun Meshes Dopped with Antimicrobial MgO and CuO Nanoparticles.* 2022. **14**(16): p. 3329.

40. Geetha, K., et al., *Electrospun nanofibrous ZnO/PVA/PVP composite films for efficient antimicrobial face masks.* 2022. **48**(19): p. 29197-29204.

41. Wang, L., et al., *Biodegradable and high-performance multiscale structured nanofiber membrane as mask filter media via poly (lactic acid) electrospinning.* 2022. **606**: p. 961-970.

42. Lou, C.-W., et al., *Preparation of Needleless Electrospinning Polyvinyl Alcohol/Water-Soluble Chitosan Nanofibrous Membranes: Antibacterial Property and Filter Efficiency.* 2022. **14**(5): p. 1054.

43. Wang, C., et al., *Quaternary ammonium chitosan/polyvinyl alcohol composites prepared by electrospinning with high antibacterial properties and filtration efficiency.* 2019. **54**: p. 12522-12532.

44. Zepnik, S., et al., *Extensional flow properties of externally plasticized cellulose acetate: influence of plasticizer content.* 2013. **5**(3): p. 873-889.

45. Seong, O.H., et al., *Electrospinning of cellulose acetate nanofibers using a mixed solvent of acetic acid/water: Effects of solvent composition on the fiber diameter.* 2008. **62**(4-5): p. 759-762.

46. Nicosia, A., et al., *Cellulose acetate nanofiber electrospun on nylon substrate as novel composite matrix for efficient, heat-resistant, air filters.* 2016. **153**: p. 284-294.

47. Liu, X., et al., *Antimicrobial electrospun nanofibers of cellulose acetate and polyester urethane composite for wound dressing.* 2012. **100**(6): p. 1556-1565.

48. Omollo, E., et al., *Electrospinning cellulose acetate nanofibers and a study of their possible use in high-efficiency filtration.* 2016. **45**(5): p. 716-729.

49. Zhijiang, C., et al., *Poly (hydroxybutyrate)/cellulose acetate blend nanofiber scaffolds: Preparation, characterization and cytocompatibility.* 2016. **58**: p. 757-767.

50. Wsoo, M.A., et al., *A review on the properties of electrospun cellulose acetate and its application in drug delivery systems: A new perspective.* 2020. **491**: p. 107978.

51. Nair, L.S. and C.T.J.P.i.p.s. Laurencin, *Biodegradable polymers as biomaterials.* 2007. **32**(8-9): p. 762-798.

52. Khan, M.T., et al., *Effect of different solvent systems on fiber morphology and property of electrospun PCL nano fibers.* 2021. **28**(122): p. 61-76.

53. Yoshimoto, H., et al., *A biodegradable nanofiber scaffold by electrospinning and its potential for bone tissue engineering.* 2003. **24**(12): p. 2077-2082.

54. Can-Herrera, L., et al., *Morphological and mechanical properties of electrospun polycaprolactone scaffolds: Effect of applied voltage.* 2021. **13**(4): p. 662.

55. de Oliveira, A.E., et al., *Applying different techniques for evaluating the resistance to moisture of electrospun PVA nanofibers.* 2021. **7**(3): p. 12938-01-10e.

56. Hua, T., et al., *Stable low resistance air filter under high humidity endowed by self-emission far-infrared for effective PM2. 5 capture.* 2017. **6**: p. 29-33.

57. Zhao, X., et al., *Cleanable air filter transferring moisture and effectively capturing PM2. 5.* 2017. **13**(11): p. 1603306.

58. Wu, R., S. Shanbhag, and P.R.J.M. Selvaganapathy, *Efficient, Breathable, and Compostable Multilayer Air Filter Material Prepared from Plant-Derived Biopolymers.* 2023. **13**(4): p. 380.

59. Chua, M.H., et al., *Face masks in the new COVID-19 normal: materials, testing, and perspectives.* 2020. **2020**.

60. Arnold, W.A., et al., *Quaternary ammonium compounds: a chemical class of emerging concern.* 2023. **57**(20): p. 7645-7665.

61. https://health.ec.europa.eu/publications/revision-opinion-cetylpyridinium-chloride-submission-ii-p97_en, *Public Health*

62. Osimitz, T., W.J.J.o.T. Droege, and P.B. Environmental Health, *Perspectives on safety of quaternary ammonium compounds (QACs).* 2025: p. 1-26.

63. Ali, B., et al., *Essential oils used in aromatherapy: A systemic review.* 2015. **5**(8): p. 601-611.

64. Ramsey, J.T., et al., *Essential oils and health.* 2020. **93**(2): p. 291.

65. Svoboda, K.P. and S.G. Deans. *Biological activities of essential oils from selected aromatic plants*. in *Internat. Symposium on Medicinal and Aromatic Plants 390*. 1994.

66. Jimbo, D., et al., *Effect of aromatherapy on patients with Alzheimer's disease.* 2009. **9**(4): p. 173-179.

67. Hwang, E., S.J.T.J.o.A. Shin, and C. Medicine, *The effects of aromatherapy on sleep improvement: a systematic literature review and meta-analysis.* 2015. **21**(2): p. 61-68.

68. Smith, C.A., et al., *Aromatherapy for pain management in labour.* 1996. **2011**(8).

69. Diaz, A., et al., *Prepubertal gynecomastia and chronic lavender exposure: report of three cases.* 2016. **29**(1): p. 103-107.

70. Ramsey, J.T., et al., *Lavender products associated with premature thelarche and prepubertal gynecomastia: case reports and endocrine-disrupting chemical activities.* 2019. **104**(11): p. 5393-5405.

71. Tisserand, R. and R. Young, *Essential oil safety: a guide for health care professionals*. 2013: Elsevier Health Sciences.

72. Ali, A., et al., *Safety assessment of nanomaterials for antimicrobial applications.* 2020. **33**(5): p. 1082-1109.

73. Dizaj, S.M., et al., *Antimicrobial activity of the metals and metal oxide nanoparticles.* 2014. **44**: p. 278-284.

74. Gupta, R., H.J.J.o.E.P. Xie, Toxicology, and Oncology, *Nanoparticles in daily life: applications, toxicity and regulations.* 2018. **37**(3).

75. Egbuna, C., et al., *Toxicity of nanoparticles in biomedical application: nanotoxicology.* 2021. **2021**(1): p. 9954443.

76. Theodorou, I.G., et al., *Inhalation of silver nanomaterials—Seeing the risks.* 2014. **15**(12): p. 23936-23974.

77. Hussain, S.M. and J.J.J.T.s. Schlager, *Safety evaluation of silver nanoparticles: inhalation model for chronic exposure.* 2009. **108**(2): p. 223-224.

78. https://www.cdc.gov/niosh/docs/2021-112/.

79. Simoncic, B. and B.J.T.R.J. Tomsic, *Structures of novel antimicrobial agents for textiles-a review.* 2010. **80**(16): p. 1721-1737.

80. Lacasse, K. and W. Baumann, *Textile Chemicals: Environmental data and facts*. 2012: Springer Science & Business Media.

81. Gerba, C.P.J.A. and e. microbiology, *Quaternary ammonium biocides: efficacy in application.* 2015. **81**(2): p. 464-469.

82. Vereshchagin, A.N., et al., *Quaternary ammonium compounds (QACs) and ionic liquids (ILs) as biocides: From simple antiseptics to tunable antimicrobials.* 2021. **22**(13): p. 6793.

83. Mao, X., et al., *Cetylpyridinium chloride: mechanism of action, antimicrobial efficacy in biofilms, and potential risks of resistance.* 2020. **64**(8): p. 10.1128/aac. 00576-20.

84. Block, S.S., *Disinfection, sterilization, and preservation*. 2001: Lippincott Williams & Wilkins.

85. Zhou, C., et al., *Selective antimicrobial activities and action mechanism of micelles self-assembled by cationic oligomeric surfactants.* 2016. **8**(6): p. 4242-4249.

86. Zhao, X., et al., *Antibacterial Mechanism of Octamethylene-1, 8-Bis (Dodecyldimethylammonium Bromide) Against E. coli.* 2017. **20**(3): p. 717-723.

87. Ioannou, C.J., et al., *Action of disinfectant quaternary ammonium compounds against Staphylococcus aureus.* 2007. **51**(1): p. 296-306.

88. Zhang, S., et al., *Antibacterial activity, in vitro cytotoxicity, and cell cycle arrest of gemini quaternary ammonium surfactants.* 2015. **31**(44): p. 12161-12169.

89. Fedorowicz, J. and J.J.I.J.o.M.S. Sączewski, *Advances in the Synthesis of biologically active quaternary ammonium compounds.* 2024. **25**(9): p. 4649.

90. Tseng, C.-C., et al., *Application of a quaternary ammonium agent on surgical face masks before use for pre-decontamination of nosocomial infection-related bioaerosols.* 2016. **50**(3): p. 199-210.

91. Friedle, A., et al. *Determination of quaternary ammonium compounds (QAC) in food products*. in *9th European Pesticide Residue Workshop, Vienna, Austria*. 2012.

92. Kim, Y., et al., *Potential use of 3-(trimethoxysilyl) propyldimethyl octadecyl ammonium chloride as an antimicrobial and antiviral agent for the disinfection of personal protective equipment.* 2020. **9**(2): p. 174.

93. Okamoto, N., et al., *Virucidal activity and mechanism of action of cetylpyridinium chloride against SARS-CoV-2.* 2022. **34**(6): p. 800-804.

94. Jennings, M.C., K.P. Minbiole, and W.M.J.A.i.d. Wuest, *Quaternary ammonium compounds: an antimicrobial mainstay and platform for innovation to address bacterial resistance.* 2015. **1**(7): p. 288-303.

95. Merianos, J.J.J.D., sterilization, and preservation, *Surface-active agents.* 2001. **5**.

96. Lainioti, G.C. and D.J.I.J.o.M.S. Druvari, *Designing Antibacterial-Based Quaternary Ammonium Coatings (Surfaces) or Films for Biomedical Applications: Recent Advances.* 2024. **25**(22): p. 12264.

97. El-Deeb, M., et al., *Evaluation of antibacterial activity of an experimental dental adhesive containing synthesized quaternary ammonium compound: in vitro study.* 2024. **6**(3): p. 120.

98. Hwang, G.B., et al., *Antimicrobial air filters using natural Euscaphis japonica nanoparticles.* 2015. **10**(5): p. e0126481.

99. Woo, C.G., et al., *Treatment of air filters using the antimicrobial natural products propolis and grapefruit seed extract for deactivation of bioaerosols.* 2015. **49**(8): p. 611-619.

100. Murbach Teles Andrade, B.F., et al., *Antimicrobial activity of essential oils.* 2014. **26**(1): p. 34-40.

101. Sikkema, J., J.A. de Bont, and B.J.M.r. Poolman, *Mechanisms of membrane toxicity of hydrocarbons.* 1995. **59**(2): p. 201-222.

102. de Sousa, D.P., et al., *Essential oils: Chemistry and pharmacological activities.* 2023. **13**(7): p. 1144.

103. Wang, X., et al., *Antibacterial activity and mechanism of ginger essential oil against Escherichia coli and Staphylococcus aureus.* 2020. **25**(17): p. 3955.

104. Rao, J., et al., *Improving the efficacy of essential oils as antimicrobials in foods: Mechanisms of action.* 2019. **10**(1): p. 365-387.

105. Rehman, A., et al., *Development of active food packaging via incorporation of biopolymeric nanocarriers containing essential oils.* 2020. **101**: p. 106-121.

106. Silva, H.D., M.Â. Cerqueira, and A.A. Vicente, *Nanoemulsions for Food Applications: Development and Characterization.* Food and Bioprocess Technology, 2012. **5**(3): p. 854-867.

107. Daewoo, H., *Selective pH-Responsive Core–Sheath Nanofiber Membranes for Chem/Bio/Med Applications: Targeted Delivery of Functional Molecules.* 2017.

108. Liao, I.-C., et al., *Sustained viral gene delivery through core-shell fibers.* 2009. **139**(1): p. 48-55.

109. Yarin, A.J.P.f.A.T., *Coaxial electrospinning and emulsion electrospinning of core–shell fibers.* 2011. **22**(3): p. 310-317.

110. Yao, Z.C., et al., *Essential oil bioactive fibrous membranes prepared via coaxial electrospinning.* 2017. **82**(6): p. 1412-1422.

111. Sung, Y.K., et al., *Magnetic nanofibers with core (Fe3O4 nanoparticle suspension)/sheath (poly ethylene terephthalate) structure fabricated by coaxial electrospinning.* 2012. **324**(6): p. 916-922.

112. Ji, W., et al., *Fibrous scaffolds loaded with protein prepared by blend or coaxial electrospinning.* 2010. **6**(11): p. 4199-4207.

113. Rajabifar, N., et al., *Wound Dressing with Electrospun Core-Shell Nanofibers: From Material Selection to Synthesis.* 2024. **16**(17): p. 2526.

114. Wang, C., et al., *Biodegradable core/shell fibers by coaxial electrospinning: processing, fiber characterization, and its application in sustained drug release.* 2010. **43**(15): p. 6389-6397.

115. He, J., et al., *Lavender Essential Oil-Loaded Composite Fiber Membrane Prepared by Coaxial Electrospinning for High-Performance, Antibacterial, and Lasting-Fragrance Air Filtration.* 2025. **142**(23): p. e57000.

116. Asli, M.M., B. Pourdeyhimi, and E.G.J.M.b. Loboa, *Release Profiles of Tricalcium Phosphate Nanoparticles from Poly (L-lactic acid) Electrospun Scaffolds with Single Component, Core–Sheath, or Porous Fiber Morphologies: Effects on hASC Viability and Osteogenic Differentiation.* 2012. **12**(7): p. 893-900.

117. He, P., et al., *Dual drug loaded coaxial electrospun PLGA/PVP fiber for guided tissue regeneration under control of infection.* 2018. **90**: p. 549-556.

118. He, M., et al., *Fibrous guided tissue regeneration membrane loaded with anti-inflammatory agent prepared by coaxial electrospinning for the purpose of controlled release.* 2015. **335**: p. 121-129.

119. Kiatyongchai, T., S. Wongsasulak, and T.J.J.o.A.P.S. Yoovidhya, *Coaxial electrospinning and release characteristics of cellulose acetate–gelatin blend encapsulating a model drug.* 2014. **131**(8).

120. Sohrabi, A., et al., *Sustained drug release and antibacterial activity of ampicillin incorporated poly (methyl methacrylate)–nylon6 core/shell nanofibers.* 2013. **54**(11): p. 2699-2705.

121. Deitzel, J.M., et al., *The effect of processing variables on the morphology of electrospun nanofibers and textiles.* 2001. **42**(1): p. 261-272.

122. Gupta, P., et al., *Electrospinning of linear homopolymers of poly (methyl methacrylate): exploring relationships between fiber formation, viscosity, molecular weight and concentration in a good solvent.* 2005. **46**(13): p. 4799-4810.

123. Tiwari, S.K., S.S.J.M.S. Venkatraman, and E. C, *Importance of viscosity parameters in electrospinning: Of monolithic and core–shell fibers.* 2012. **32**(5): p. 1037-1042.

124. Yoon, J., et al., *Recent progress in coaxial electrospinning: New parameters, various structures, and wide applications.* 2018. **30**(42): p. 1704765.

125. Kaerkitcha, N., et al., *Influence of the viscosity ratio of polyacrylonitrile/poly (methyl methacrylate) solutions on core–shell fibers prepared by coaxial electrospinning.* 2017. **49**(6): p. 497-502.

126. Halaui, R., et al., *Polymeric microtubes for water filtration by co-axial electrospinning technique.* 2017. **28**(5): p. 570-582.

127. Yu, D.G., et al., *Improving Polymer Nanofiber Quality Using a Modified Co-axial Electrospinning Process.* 2011. **32**(9-10): p. 744-750.

128. Nikmaram, N., et al., *Emulsion-based systems for fabrication of electrospun nanofibers: Food, pharmaceutical and biomedical applications.* 2017. **7**(46): p. 28951-28964.

129. Sy, J.C., A.S. Klemm, and V.P.J.A.M. Shastri, *Emulsion as a means of controlling electrospinning of polymers.* 2009. **21**(18): p. 1814-1819.

130. Xu, X., et al., *Ultrafine medicated fibers electrospun from W/O emulsions.* 2005. **108**(1): p. 33-42.

131. Yang, Y., et al., *Core–sheath structured fibers with pDNA polyplex loadings for the optimal release profile and transfection efficiency as potential tissue engineering scaffolds.* 2011. **7**(6): p. 2533-2543.

132. Wu, Y.-P., et al., *In vitro and in vivo toxicity evaluation of halloysite nanotubes.* 2018.

133. Liu, M., et al., *Recent advance in research on halloysite nanotubes-polymer nanocomposite.* 2014. **39**(8): p. 1498-1525.

134. Lvov, Y. and E.J.P.i.P.S. Abdullayev, *Functional polymer–clay nanotube composites with sustained release of chemical agents.* 2013. **38**(10-11): p. 1690-1719.

135. Stavitskaya, A., et al., *Antimicrobial applications of clay nanotube-based composites.* 2019. **9**(5): p. 708.

136. Vergaro, V., et al., *Cytocompatibility and uptake of halloysite clay nanotubes.* 2010. **11**(3): p. 820-826.

137. Long, Z., et al., *In vitro and in vivo toxicity evaluation of halloysite nanotubes.* 2018. **6**(44): p. 7204-7216.

138. Arruebo, M.J.W.I.R.N. and Nanobiotechnology, *Drug delivery from structured porous inorganic materials.* 2012. **4**(1): p. 16-30.

139. Cao, J., X. Li, and H.J.C.m.c. Tian, *Metal-organic framework (MOF)-based drug delivery.* 2020. **27**(35): p. 5949-5969.

140. Wu, M.X. and Y.W.J.A.M. Yang, *Metal–organic framework (MOF)-based drug/cargo delivery and cancer therapy.* 2017. **29**(23): p. 1606134.

141. Wang, Y., et al., *Mesoporous silica nanoparticles in drug delivery and biomedical applications.* 2015. **11**(2): p. 313-327.

142. Li, Y., et al., *Manipulation of halloysite clay nanotube lumen for environmental remediation: A review.* 2022.

143. Asgar, H., et al., *Contrasting thermally-induced structural and microstructural evolution of alumino-silicates with tubular and planar arrangements: Case study of halloysite and kaolinite.* 2021. **613**: p. 126106.

144. Yuan, P., et al., *Changes in structure, morphology, porosity, and surface activity of mesoporous halloysite nanotubes under heating.* 2012. **60**(6): p. 561-573.

145. White, R.D., D.V. Bavykin, and F.C.J.N. Walsh, *The stability of halloysite nanotubes in acidic and alkaline aqueous suspensions.* 2012. **23**(6): p. 065705.

146. Abdullayev, E., et al., *Enlargement of halloysite clay nanotube lumen by selective etching of aluminum oxide.* 2012. **6**(8): p. 7216-7226.

147. Belkassa, K., et al., *Physicochemical and adsorptive properties of a heat-treated and acid-leached Algerian halloysite.* 2013. **421**: p. 26-33.

148. Belver, C., M.A. Bañares Muñoz, and M.A.J.C.o.m. Vicente, *Chemical activation of a kaolinite under acid and alkaline conditions.* 2002. **14**(5): p. 2033-2043.

149. Zhang, A.-B., et al., *Effects of acid treatment on the physico-chemical and pore characteristics of halloysite.* 2012. **396**: p. 182-188.

150. Peixoto, A.F., et al., *Physicochemical characterization of organosilylated halloysite clay nanotubes.* 2016. **219**: p. 145-154.

151. Yuan, P., et al., *Functionalization of halloysite clay nanotubes by grafting with γ-aminopropyltriethoxysilane.* 2008. **112**(40): p. 15742-15751.

152. Xing, X., et al., *Influence of acid treatment on the loading and release behavior of halloysite with 2-mercaptobenzothiazole.* 2019. **19**(11): p. 7178-7184.

153. Cavallaro, G., et al., *Halloysite nanotube with fluorinated lumen: Non-foaming nanocontainer for storage and controlled release of oxygen in aqueous media.* Journal of Colloid and Interface Science, 2014. **417**: p. 66-71.

154. Cavallaro, G., et al., *Modified halloysite nanotubes: nanoarchitectures for enhancing the capture of oils from vapor and liquid phases.* 2014. **6**(1): p. 606-612.

155. Li, Y., et al., *Manipulation of the halloysite clay nanotube lumen for environmental remediation: a review.* 2022. **9**(3): p. 841-866.

156. Chen, X., et al., *Antibacterial coatings on orthopedic implants.* 2023. **19**: p. 100586.

157. Gerba Charles, P., *Quaternary Ammonium Biocides: Efficacy in Application.* Applied and Environmental Microbiology, 2015. **81**(2): p. 464-469.

158. Teng, F., et al., *Cetylpyridinium chloride mouth rinses alleviate experimental gingivitis by inhibiting dental plaque maturation.* International Journal of Oral Science, 2016. **8**(3): p. 182-190.

159. Tebyetekerwa, M., et al., *Electrospun nanofibers-based face masks.* 2020. **2**(3): p. 161-166.

160. Costa, S.M., et al., *Antibacterial and biodegradable electrospun filtering membranes for facemasks: An attempt to reduce disposable masks use.* 2021. **12**(1): p. 67.

161. Yin, X., et al., *Ultra-fine electrospun nanofibrous membranes for multicomponent wastewater treatment: Filtration and adsorption.* 2020. **242**: p. 116794.

162. Zhang, Z., et al., *Electrospun ultrafine fibers for advanced face masks.* 2021. **143**: p. 100594.

163. Gunn, J. and M.J.T.i.b. Zhang, *Polyblend nanofibers for biomedical applications: perspectives and challenges.* 2010. **28**(4): p. 189-197.

164. Mol, İ.Y., et al., *Electrospinning of Antibacterial Cellulose Acetate Nanofibers.* 2023. **57**: p. 1-2.

165. Baek, W.-I., et al., *Effect of adhesive on the morphology and mechanical properties of electrospun fibrous mat of cellulose acetate.* 2011. **346**(13): p. 1956-1961.

166. Ding, B., et al., *Fabrication of blend biodegradable nanofibrous nonwoven mats via multi-jet electrospinning.* 2004. **45**(6): p. 1895-1902.

167. Cimadoro, J. and S.J.J.o.P.S. Goyanes, *Reversible swelling as a strategy in the development of smart membranes from electrospun polyvinyl alcohol nanofiber mats.* 2020. **58**(5): p. 737-746.

168. Francavilla, P., et al., *Smart fibrous structures produced by electrospinning using the combined effect of pcl/graphene nanoplatelets.* 2021. **11**(3): p. 1124.

169. Cipitria, A., et al., *Design, fabrication and characterization of PCL electrospun scaffolds—a review.* 2011. **21**(26): p. 9419-9453.

170. Chua, M.H., et al., *Face masks in the new COVID-19 normal: materials, testing, and perspectives.* 2020.

171. Li, D., et al., *Fabrication and applications of multi-fluidic electrospinning multi-structure hollow and core–shell nanofibers.* 2022. **13**: p. 116-127.

172. Rahimi, M. and J.J.J.o.I.T. Mokhtari, *Fabrication of thermo-regulating hexadecane-polyurethane core-shell composite nanofibrous mat as advanced technical layer: Effect of coaxial nozzle geometry.* 2018. **47**(6): p. 1134-1151.

173. Kamperman, M., et al., *Nanomanufacturing of continuous composite nanofibers with confinement-induced morphologies.* 2010. **1**(7): p. 1001-1004.

174. Domingues, J.M., et al., *Inhibition of Escherichia virus MS2, surrogate of SARS-CoV-2, via essential oils-loaded electrospun fibrous mats: Increasing the multifunctionality of antivirus protection masks.* 2022. **14**(2): p. 303.

175. Ma, S., et al., *Multifunctional cellulose-based air filters with high loadings of metal–organic frameworks prepared by in situ growth method for gas adsorption and antibacterial applications.* 2018. **25**: p. 5999-6010.

176. Burdușel, A.-C., et al., *Biomedical applications of silver nanoparticles: an up-to-date overview.* 2018. **8**(9): p. 681.

177. Huang, L., et al., *Self-reporting and photothermally enhanced rapid bacterial killing on a laser-induced graphene mask.* 2020. **14**(9): p. 12045-12053.

178. Peyneau, M., et al., *Quaternary ammonium compounds in hypersensitivity reactions.* 2022. **4**: p. 973680.

179. Gilbert, P. and L.J.J.o.a.m. Moore, *Cationic antiseptics: diversity of action under a common epithet.* 2005. **99**(4): p. 703-715.

180. McDonnell, G. and A.D.J.C.m.r. Russell, *Antiseptics and disinfectants: activity, action, and resistance.* 1999. **12**(1): p. 147-179.

181. Riveira-Muñoz, E., et al., *Cetylpyridinium Chloride-Containing Mouthwashes Show Virucidal Activity against Herpes Simplex Virus Type 1.* 2023. **15**(7): p. 1433.

182. Lide, D.R., *CRC handbook of chemistry and physics*. Vol. 85. 2004: CRC press.

183. Huang, J., et al., *A Simple and Practical Theoretical Model for Interpreting Binary Azeotropes.* 2021.

184. Zhang, D., et al., *An empirical model to evaluate the effects of environmental humidity on the formation of wrinkled, creased and porous fibre morphology from electrospinning.* 2020. **10**(1): p. 18783.

185. Roberge, R.J., J.-H. Kim, and A.J.A.o.o.h. Coca, *Protective facemask impact on human thermoregulation: an overview.* 2012. **56**(1): p. 102-112.

186. Heli, B., et al., *Synthesis and Characterization of Antimicrobial Bacterial Cellulose Crosslinked with Branched Polyethylenimine.* 2024. **7**: p. 100457.

187. Standard, I.J.I., *18184: 2019. Textiles—Determination of antiviral activity of textile products.* 2019. **6**.

188. Darby, R., *Chemical engineering fluid mechanics, revised and expanded*. 2017: CRC Press.

189. Pakravan, M., M.-C. Heuzey, and A.J.B. Ajji, *Core–shell structured PEO-chitosan nanofibers by coaxial electrospinning.* 2012. **13**(2): p. 412-421.

190. Li, D. and Y.J.N.l. Xia, *Direct fabrication of composite and ceramic hollow nanofibers by electrospinning.* 2004. **4**(5): p. 933-938.

191. Khalf, A., et al., *Influence of solvent characteristics in triaxial electrospun fiber formation.* 2015. **90**: p. 36-46.

192. Pullangott, G., et al., *A comprehensive review on antimicrobial face masks: an emerging weapon in fighting pandemics.* 2021. **11**(12): p. 6544-6576.

193. Perkins, D.J., et al., *COVID-19 global pandemic planning: Dry heat incubation and ambient temperature fail to consistently inactivate SARS-CoV-2 on N95 respirators.* 2021. **246**(8): p. 952-959.

194. Gilbert, P. and L.E. Moore, *Cationic antiseptics: diversity of action under a common epithet.* Journal of Applied Microbiology, 2005. **99**(4): p. 703-715.

195. Wani, A.R., et al., *An updated and comprehensive review of the antiviral potential of essential oils and their chemical constituents with special focus on their mechanism of action against various influenza and coronaviruses.* 2021. **152**: p. 104620.

196. Masango, P.J.J.o.C.P., *Cleaner production of essential oils by steam distillation.* 2005. **13**(8): p. 833-839.

197. Kumari, S., et al., *EssOilDB: a database of essential oils reflecting terpene composition and variability in the plant kingdom.* 2014. **2014**: p. bau120.

198. Trumpower, B.L. and R.B.J.A.r.o.b. Gennis, *Energy transduction by cytochrome complexes in mitochondrial and bacterial respiration: the enzymology of coupling electron transfer reactions to transmembrane proton translocation.* 1994. **63**(1): p. 675-716.

199. Nazzaro, F., et al., *Effect of essential oils on pathogenic bacteria.* 2013. **6**(12): p. 1451-1474.

200. Sana, S.S., et al., *Recent advances in essential oils-based metal nanoparticles: A review on recent developments and biopharmaceutical applications.* 2021. **333**: p. 115951.

201. Sonawane, S.H., et al., *Current overview of encapsulation.* 2020: p. 1-8.

202. Sadeghi, K., et al., *A polymeric chlorine dioxide self-releasing sheet to prolong postharvest life of cherry tomatoes.* 2020. **161**: p. 111040.

203. KÖrtvÉlyesi, Z. and G.J.J.A.W.W.A. Gordon, *Chlorite ion interference in the spectrophotometric measurement of chlorine dioxide.* 2004. **96**(9): p. 81-87.

204. Heli, B., et al., *Synthesis and Characterization of Antimicrobial Bacterial Cellulose Crosslinked with Branched Polyethylenimine.* 2024: p. 100457.

205. Joshi, D.R. and N.J.J.P.R.I. Adhikari, *An overview on common organic solvents and their toxicity.* 2019. **28**(3): p. 1-18.

206. Hosseini, F., et al., *Encapsulation of rosemary essential oil in zein by electrospinning technique.* 2021. **86**(9): p. 4070-4086.

207. Teilaghi, S., et al., *Preparation as well as evaluation of the nanofiber membrane loaded with Nigella sativa extract using the electrospinning method.* 2020. **28**: p. 1614-1625.

208. Tavassoli-Kafrani, E., et al., *Encapsulation of orange essential oil using cross-linked electrospun gelatin nanofibers.* 2018. **11**: p. 427-434.

209. de Almeida, D.S., et al., *Development and characterization of electrospun cellulose acetate nanofibers modified by cationic surfactant.* 2020. **81**: p. 106206.

210. Lin, T., et al., *The charge effect of cationic surfactants on the elimination of fibre beads in theelectrospinning of polystyrene.* 2004. **15**(9): p. 1375.

211. Xue, J., et al., *Electrospinning and Electrospun Nanofibers: Methods, Materials, and Applications.* Chemical Reviews, 2019. **119**(8): p. 5298-5415.

212. Yammine, J., et al., *Advances in essential oils encapsulation: Development, characterization and release mechanisms.* 2024. **81**(5): p. 3837-3882.

213. Ulici, A.M., et al., *Nanoencapsulation of citrus essential oils in systematic modified chitosan-based nanofibers.* 2024. **141**(45): p. e56176.

214. Chacha, J.S., et al., *Essential oil-based active polymer-based packaging system: A review of its effect on the antimicrobial, antioxidant, and sensory properties of beef and chicken meat.* 2022. **46**(11): p. e16933.

215. Yip, S.C., et al., *Chemical composition and bioactivities of Eucalyptus essential oils from selected pure and hybrid species: A review.* 2024. **222**: p. 120118.

216. Rai, M., et al., *Synergistic antimicrobial potential of essential oils in combination with nanoparticles: Emerging trends and future perspectives.* 2017. **519**(1-2): p. 67-78.

217. Wang, S., et al., *Quaternary ammonium antimicrobial agents and their application in antifouling coatings: a review.* 2024. **21**(1): p. 87-103.

218. Silva, H.D., et al., *Nanoemulsions for food applications: development and characterization.* 2012. **5**: p. 854-867.

219. Zheng, H., et al., *Preparation and characterization of carvacrol essential oil-loaded halloysite nanotubes and their application in antibacterial packaging.* 2022. **34**: p. 100972.

220. Anandharamakrishnan, C., *Spray drying techniques for food ingredient encapsulation*. 2015: John Wiley & Sons.

221. Klojdová, I., et al., *Encapsulation: a strategy to deliver therapeutics and bioactive compounds?* 2023. **16**(3): p. 362.

222. Rezvankhah, A., Z. Emam-Djomeh, and G.J.D.T. Askari, *Encapsulation and delivery of bioactive compounds using spray and freeze-drying techniques: A review.* 2020. **38**(1-2): p. 235-258.

223. Piletti, R., et al., *Microencapsulation of garlic oil by β-cyclodextrin as a thermal protection method for antibacterial action.* 2019. **94**: p. 139-149.

224. Chezanoglou, E., A.M.J.T.i.f.s. Goula, and technology, *Co-crystallization in sucrose: A promising method for encapsulation of food bioactive components.* 2021. **114**: p. 262-274.

225. Chen, S., et al., *Encapsulation technology to improve biological resource recovery: recent advancements and research opportunities.* 2021. **7**(1): p. 16-23.

226. Valdivia-Rivera, S., et al., *Encapsulation of microorganisms for bioremediation: Techniques and carriers.* 2021. **20**(3): p. 815-838.

227. Estevinho, B.N. and A.J.F. López-Rubio, *Recent Advances in Encapsulation for Food Applications.* 2024. **13**(4): p. 579.

228. Farasati Far, B., et al., *Hydrogel Encapsulation Techniques and Its Clinical Applications in Drug Delivery and Regenerative Medicine: A Systematic Review.* 2024. **9**(27): p. 29139-29158.

229. Yanovska, A., et al., *Encapsulated organic–mineral fertilizers with nanoporous structure.* 2022. **12**(4): p. 1275-1283.

230. Benchaar, C., H.J.A.F.S. Greathead, and Technology, *Essential oils and opportunities to mitigate enteric methane emissions from ruminants.* 2011. **166**: p. 338-355.

231. Sousa, V.I., et al., *Microencapsulation of essential oils: A review.* 2022. **14**(9): p. 1730.

232. De Billerbeck, V.-G.J.P., *Huiles essentielles et bactéries résistantes aux antibiotiques.* 2007. **5**(5): p. 249-253.

233. Mohamed, A.L., et al., *Encapsulated lemon oil and metal nanoparticles in biopolymer for multifunctional finishing of cotton and wool fabrics.* 2023. **204**: p. 117373.

234. Watcharadulyarat, N., et al. *Dextran-Based Nanoparticles for Encapsulation of Ciprofloxacin*. in *Journal of Physics: Conference Series*. 2022. IOP Publishing.

235. Satish, S., M. Tharmavaram, and D.J.N. Rawtani, *Halloysite nanotubes as a nature's boon for biomedical applications.* 2019. **6**: p. 1849543519863625.

236. Stodolak-Zych, E., et al., *Functionalized halloysite nanotubes as potential drug carriers.* 2023. **14**(3): p. 167.

237. Fahimizadeh, M., et al., *Halloysite clay nanotubes: Innovative applications by smart systems.* 2024. **251**: p. 107319.

238. Xue, J., et al., *Electrospun microfiber membranes embedded with drug-loaded clay nanotubes for sustained antimicrobial protection.* 2015. **9**(2): p. 1600-1612.

239. Ouyang, J., et al., *High morphological stability and structural transition of halloysite (Hunan, China) in heat treatment.* 2014. **101**: p. 16-22.

240. Bessaha, F., et al., *Characterization and application of heat-treated and acid-leached halloysites in the removal of malachite green: adsorption, desorption, and regeneration studies.* 2016. **57**(31): p. 14609-14621.

241. Cavallaro, G., et al., *Halloysite nanotube with fluorinated lumen: Non-foaming nanocontainer for storage and controlled release of oxygen in aqueous media.* 2014. **417**: p. 66-71.

242. Cavallaro, G., et al., *Nanohydrogel formation within the halloysite lumen for triggered and sustained release.* 2018. **10**(9): p. 8265-8273.

243. Zhou, M., et al., *Cinnamon Essential Oil-Loaded Halloysite Nanotubes Applied in Degradable Film: Characterization and Non-Contact Antimicrobial Activity.* 2025. **17**(9): p. 1144.

244. Khunová, V., et al., *Antibacterial Electrospun Polycaprolactone Nanofibers Reinforced by Halloysite Nanotubes for Tissue Engineering.* 2022. **14**(4): p. 746.

245. Abdullayev, E., et al., *Halloysite Tubes as Nanocontainers for Anticorrosion Coating with Benzotriazole.* ACS Applied Materials & Interfaces, 2009. **1**(7): p. 1437-1443.

246. Zhou, M., et al. *Cinnamon Essential Oil-Loaded Halloysite Nanotubes Applied in Degradable Film: Characterization and Non-Contact Antimicrobial Activity*. Polymers, 2025. **17**, DOI: 10.3390/polym17091144.

247. Cavallaro, G., et al., *Structure of Hybrid Materials Based on Halloysite Nanotubes Filled with Anionic Surfactants.* The Journal of Physical Chemistry C, 2016. **120**(25): p. 13492-13502.

248. Khezri, Z., et al., *Stability enhancement of garlic essential oil using new opopanax gum/gelatin nanofibres.* 2021. **56**(5): p. 2255-2263.

249. Jafta, N., et al., *Effect of sodium lauryl sulfate (SLS)/carbon nanotubes on the properties of cellulose membrane isolated from maize stalk.* 2022. **56**(5-6): p. 549-558.

250. Elsayed, A., et al., *Chitosan–sodium lauryl sulfate nanoparticles as a carrier system for the in vivo delivery of oral insulin.* 2011. **12**: p. 958-964.

251. Aguzzi, C., et al., *Halloysite-doped zinc oxide for enhanced sunscreening performance.* 2019. **2**(10): p. 6575-6584.

252. Ouyang, J., et al., *Radical guided selective loading of silver nanoparticles at interior lumen and out surface of halloysite nanotubes.* 2016. **110**: p. 169-178.

253. Cavallaro, G., G. Lazzara, and S.J.T.J.o.P.C.C. Milioto, *Exploiting the colloidal stability and solubilization ability of clay nanotubes/ionic surfactant hybrid nanomaterials.* 2012. **116**(41): p. 21932-21938.

254. Rozza, R. and F.J.A.C.S. Ferrante, *Computational study of water adsorption on halloysite nanotube in different pH environments.* 2020. **190**: p. 105589.

255. De Sousa, D., et al., *Essential oils: chemistry and pharmacological activities. Biomolecules. 2023; 13: 1144*. 2023.